

AD-755 378

FLOW DECAY

C. C. Addison

Nottingham University

Prepared for:

Air Force Rocket Propulsion Laboratory
European Office of Aerospace Research

30 June 1972

DISTRIBUTED BY:



National Technical Information Service
U. S. DEPARTMENT OF COMMERCE
5285 Port Royal Road, Springfield Va. 22151

AD 755978

UNCLASSIFIED

Security Classification

DOCUMENT CONTROL DATA - R & D

(Security classification of title, body of abstract and indexing annotation must be entered when the overall report is classified)

1. ORIGINATING ACTIVITY (Corporate author)		2a. REPORT SECURITY CLASSIFICATION
Department of Chemistry University of Nottingham Nottingham NG7 2RD, England		Unclassified
3. REPORT TITLE		2b. GROUP
FLOW DECAY		
4. DESCRIPTIVE NOTES (Type of report and inclusive dates)		
Scientific. Final.		
5. AUTHOR(S) (First name, middle initial, last name)		
C. C. Addison		
6. REPORT DATE	7a. TOTAL NO. OF PAGES	7b. NO. OF REFS
30 June 1972	152	42
8a. CONTRACT OR GRANT NO.	9a. ORIGINATOR'S REPORT NUMBER(S)	
Contract F61052-70-C-0035		
8b. PROJECT NO.	9b. OTHER REPORT NO(S) (Any other numbers that may be assigned this report)	
3148	AFRPL-TR-72-84	
c. 62302F		
d. 669800		
10. DISTRIBUTION STATEMENT		
Approved for public release; distribution unlimited.		
11. SUPPLEMENTARY NOTES	12. SPONSORING MILITARY ACTIVITY	
Tech, other	Details of illustrations in this document may be better studied on microfiche	Air Force Rocket Propulsion Laboratory/LKDP Edwards, California 93523
13. ABSTRACT		
<p>An investigation of N_2O_4 adducts of $Fe(NO_3)_3$ was carried out, since the compound $Fe(NO_3)_3 \cdot N_2O_4$ was claimed to be responsible for flow decay of liquid propellant N_2O_4 in steel systems. Equilibrium vapour pressures of the system $Fe(NO_3)_3 \cdot nN_2O_4$ were measured at 10°C for values of n between 6.0 and 1.0. The compound $Fe(NO_3)_3 \cdot 1.5N_2O_4$ is now recognised as the solid phase in equilibrium with liquid N_2O_4. The presence of HNO_3 in N_2O_4 influences the physical and chemical nature of the flow-decay deposit. The behaviour of $Fe(NO_3)_3 \cdot nN_2O_4$ ($n = 1.0$ to 1.5) in 100% HNO_3 and in HNO_3/N_2O_4 and H_2O/N_2O_4 mixtures was therefore studied. A flow apparatus for liquid N_2O_4 was constructed, and the flow-decay material which was isolated (in a mild steel needle valve, from N_2O_4 containing 0.1 wt.% "H₂O") was identified as $Fe(NO_3)_3 \cdot 1.5N_2O_4$. The influence of temperature differential on the rate of flow decay was also investigated. The corrosion of steels by pure liquid N_2O_4 or by samples containing small known amounts of $NOCl$, HNO_3 or NO was studied by scanning electron microscopy. Corrosion was found to follow the sequence $HNO_3 < NO < NOCl$. The stability of several potential flow decay prevention additives, in contact with liquid N_2O_4, was assessed by ¹H nmr.</p>		

Security Classification

14 KEY WORDS	LINK A		LINK B		LINK C	
	ROLE	WT	ROLE	WT	ROLE	WT
Iron nitrate Dinitrogen tetroxide Liquid propellant Dinitrogen tetroxide adducts Flow decay deposit Corrosion						

II

Security Classification

AFRPL - TR - 72 - 84

30th June 1972

FINAL SCIENTIFIC REPORT

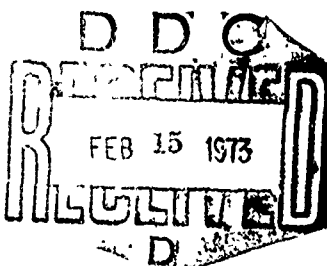
TITLE: FLOW DECAY

Covering 1st July 1970

to 30th June 1972

Author: Professor C. C. Addison

Department of Inorganic Chemistry,
The University, Nottingham NG7 2RD.



This document has been approved for public release and sale;
its distribution is unlimited.

This research has been sponsored in part by the Air Force
Rocket Propulsion Laboratory through the European Office of
Aerospace Research, OAR, United States Air Force, Under
Contract F61052-70-C-0035.

III

FINAL SCIENTIFIC REPORT

TABLE OF CONTENTS

ABSTRACT

SUMMARY

LIST OF TABLES

LIST OF FIGURES

NOMENCLATURE

	Page
1. <u>INTRODUCTION</u>	1
2. <u>PRELIMINARY INVESTIGATIONS ON THE NATURE OF THE ADDUCTS</u>	5
<u>BETWEEN $\text{Fe}(\text{NO}_3)_3$ AND N_2O_4.</u>	
2.1 <u>Methods of preparation and purification</u>	
(a) $\text{Fe}(\text{CO})_5/\text{N}_2\text{O}_4$	5
(b) $\text{FeCl}_3/\text{N}_2\text{O}_4/\text{EtOAc}$	5
(c) $\text{Fe}/\text{NOCl}/\text{N}_2\text{O}_4$	6
(d) Attainment of the composition $\text{Fe}(\text{NO}_3)_3 \cdot \text{N}_2\text{O}_4$.	7
2.2 <u>Analysis</u>	
(a) Total nitrogen by the Kjeldahl method	8
(b) N_2O_4 content by Ce(IV) titration of NO_2^-	10
(c) Iron by Atomic Absorption.	10
2.3 <u>Vibrational Spectrum of $\text{Fe}(\text{NO}_3)_3 \cdot \text{N}_2\text{O}_4$</u>	
(a) Infrared spectrum	10
(b) Raman spectrum	12
2.4 <u>The infrared spectrum of $\text{Fe}(\text{NO}_3)_3 \cdot x\text{N}_2\text{O}_4$</u>	12
2.5 <u>Formulation of the adducts between $\text{Fe}(\text{NO}_3)_3$ and N_2O_4</u>	15
<u>as $\text{Fe}(\text{NO}_3)_3 \cdot x\text{N}_2\text{O}_4$.</u>	
2.6 <u>X-ray powder diffraction data</u>	16

	Page
3. VAPOUR PRESSURE STUDIES ON THE $\text{NOFe}(\text{NO}_3)_3\text{-N}_2\text{O}_4$ SYSTEM	23
3.1 <u>Experimental</u>	
(a) Apparatus	23
(b) Standard procedures	26
(c) Calibration of the apparatus	27
(d) The density of N_2O_4 vapour at 10°C	28
(e) Sample preparation	29
(f) The dissociation vapour pressure of $\text{Fe}(\text{NO}_3)_3\cdot n\text{N}_2\text{O}_4$ at 10°C	30
3.2 <u>Results and discussion</u>	32
(a) The density of N_2O_4 vapour at 10°C	32
(b) The dissociation vapour pressure of $\text{Fe}(\text{NO}_3)_3\cdot n\text{N}_2\text{O}_4$ at 10°C	33
(i) $n = 1.5$	36
(ii) $n > 1.5$	36
(iii) $1 < n < 1.5$	39
(iv) $n \sim 1$	42
3.3 <u>Conclusions</u>	42
3.4 <u>Appendices</u>	43
4. PROPERTIES OF $\text{Fe}(\text{NO}_3)_3\cdot 1.5\text{N}_2\text{O}_4$	46
4.1 <u>Preparation</u>	46
4.2 <u>Infrared and Raman spectra</u>	47
4.3 <u>Magnetic moment</u>	51
4.4 <u>Mössbauer spectrum</u>	52
4.5 <u>Possible Structures</u>	55
4.6 <u>X-ray powder diffraction data</u>	56
4.7 <u>The reaction of $\text{Fe}(\text{NO}_3)_3\cdot 1.5\text{N}_2\text{O}_4$ with N_2O_4</u>	60
4.8 <u>The evacuation of $\text{Fe}(\text{NO}_3)_3\cdot 1.5\text{N}_2\text{O}_4$ at room temperature</u>	61
4.9 <u>Attempts to coordinate NO^+ by N_2O_4 in compounds other than $\text{NO}^+\text{Fe}(\text{NO}_3)_4^-$</u>	61
4.10 <u>The coordination of NO^+ by NOCl</u>	62

	Page
5. <u>SINGLE CRYSTAL X-RAY STUDY OF $\text{Fe}(\text{NO}_3)_3 \cdot 1.5\text{N}_2\text{O}_4$</u>	69
6. <u>SOLUTIONS OF $\text{Fe}(\text{NO}_3)_3 \cdot x\text{N}_2\text{O}_4$ IN 100% HNO_3</u>	72
6.1 <u>Introduction</u>	72
6.2 <u>Preparation of 100% HNO_3</u>	73
6.3 <u>The vibrational spectrum of 100% HNO_3</u>	73
6.4 <u>The vibrational spectrum of solutions of $\text{Fe}(\text{NO}_3)_3 \cdot x\text{N}_2\text{O}_4$ in 100% HNO_3</u>	78
6.5 <u>^{14}N n.m.r. of $\text{NO}^+\text{Fe}(\text{NO}_3)_4^-$ in 100% HNO_3</u>	83
7. <u>BEHAVIOUR OF $\text{Fe}(\text{NO}_3)_3 \cdot x\text{N}_2\text{O}_4$ IN $\text{HNO}_3/\text{N}_2\text{O}_4$ MIXTURES</u>	84
7.1 <u>$\text{HNO}_3/\text{N}_2\text{O}_4$ phase diagram</u>	84
7.2 <u>Effect of $\text{Fe}(\text{NO}_3)_3 \cdot x\text{N}_2\text{O}_4$ on the $\text{HNO}_3/\text{N}_2\text{O}_4$ phase system</u>	84
(a) General considerations	84
(b) Experimental study	86
7.3 <u>Spectroscopic studies of $\text{Fe}(\text{NO}_3)_3 \cdot x\text{N}_2\text{O}_4$ in $\text{HNO}_3/\text{N}_2\text{O}_4$ mixtures</u>	87
7.4 <u>Extraction of solutions of $\text{Fe}(\text{NO}_3)_3 \cdot x\text{N}_2\text{O}_4$ in HNO_3 by N_2O_4</u>	90
(a) Batch-wise extraction	91
(b) "Continuous" extraction	93
7.5 <u>Solids produced from extraction experiments</u>	96
(a) Infrared spectra	96
(b) X-ray powder patterns	98
(c) Analysis	98
(d) Conclusions	99
7.6 <u>The phase behaviour of the $\text{NOFe}(\text{NO}_3)_4/\text{N}_2\text{O}_4/\text{H}_2\text{O}$ system: a ^1H n.m.r. study</u>	100
(a) Experimental	100
(b) Results	101
(c) Conclusions	103

	Page
7.7 Rationalisation of the behaviour of the $\text{Fe}(\text{NO}_3)_3 \cdot x\text{N}_2\text{O}_4 / \text{HNO}_3 / \text{N}_2\text{O}_4$ system	104
8 THE FLOW APPARATUS AND FLOW EXPERIMENTS	106
8.1 Construction	106
8.2 Test Sections and flow experiments	108
(a) Gauze filters	108
(b) Needle valves	109
8.3 Modification of the flow apparatus	110
8.4 Further flow experiments	111
(a) Stainless steel needle valve test section	111
(b) Mild steel needle valve test section	115
8.5 Summary of results	125
9 CORROSION STUDIES BY SCANNING ELECTRON MICROSCOPY	127
9.1 Experimental	127
9.2 Results	129
(a) Mild steel	129
(b) Stainless steel	131
9.3 Conclusions	131
10 STABILITY IN CONTACT WITH N_2O_4 OF POTENTIAL ADDITIVES FOR FLOW DECAY PREVENTION.	134
APPENDIX Determination of the "water" content of liquid N_2O_4 by ^1H n.m.r.	137
REFERENCES	139

SUMMARY

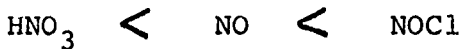
The compound $\text{Fe}(\text{NC}_3)_3 \cdot \text{N}_2\text{O}_4$ was previously identified as the principal constituent of deposits responsible for flow-decay of liquid propellant N_2O_4 in steel systems. In the light of this, an extensive re-investigation of N_2O_4 adducts of $\text{Fe}(\text{NO}_3)_3$ has been carried out, including the measurement of equilibrium vapour pressures at 10°C in the system $\text{Fe}(\text{NO}_3)_3 \cdot n\text{N}_2\text{O}_4$ for a range of values of n from 6.0 to 1.0. The compound of greatest significance in this system is thus shown to be of composition $\text{Fe}(\text{NO}_3)_3 \cdot 1.5\text{N}_2\text{O}_4$. A comprehensive study of the properties of this compound has therefore been made and the constituent species of the solid $\text{Fe}(\text{NO}_3)_3 \cdot 1.5\text{N}_2\text{O}_4$ have been identified as NO^+ (solvated by NO_2) and $\text{Fe}(\text{NO}_3)_4^-$. A single crystal X-ray study has confirmed the presence of this dodecahedral tetranitrato-ferrate(III) anion, but determination of the structure of the cationic species is still in progress.

The contamination of propellant N_2O_4 by the products (principally HNO_3) of its reaction with H_2O was expected to influence the physical and chemical nature of the flow-decay deposit. The behaviour of $\text{Fe}(\text{NO}_3)_3 \cdot x\text{N}_2\text{O}_4$ ($x = 1.0$ to 1.5) in 100% HNO_3 and in $\text{HNO}_3/\text{N}_2\text{O}_4$ and $\text{H}_2\text{O}/\text{N}_2\text{O}_4$ mixtures has therefore been studied and $\text{Fe}(\text{NO}_3)_3 \cdot x\text{N}_2\text{O}_4$ shown to remain solid and undecomposed up to a "water" content of 0.22 wt.% in liquid N_2O_4 .

A flow apparatus for liquid N_2O_4 has been built and flow experiments conducted primarily for the purpose of isolating and identifying flow decay material. Such experiments using liquid N_2O_4 containing ca 0.1% " H_2O " and a mild steel needle valve as collection system resulted in deposition of a solid which gave,

after removal of liquid N_2O_4 , an infra-red spectrum and X-ray powder diffraction pattern identical to those of $Fe(NO_3)_3 \cdot 1.5N_2O_4$. The flow apparatus has also been used to investigate the effect of hold tank thermal conditioning and hold tank - heat exchanger temperature differential on the rate of flow decay.

The corrosive effect on steels, of pure liquid N_2O_4 and samples of liquid N_2O_4 containing small known amounts of one of the common impurities $NOCl$, HNO_3 or NO has been observed by scanning electron microscopy. The corrosive effect is shown to follow the sequence



The stability in contact with liquid N_2O_4 of several potential organic additives for flow decay prevention has been assessed by regular monitoring of mixtures by 1H n.m.r. over a period of 8 months.

LIST OF TABLES

Table

2.1 Vibrational Spectrum of $\text{Fe}(\text{NO}_3)_3 \cdot \text{N}_2\text{O}_4$	11
2.2 X-Ray Powder Diffraction Data (CuK_α) for $\text{Fe}(\text{NO}_3)_3 \cdot \text{N}_2\text{O}_4$	18
2.3 X-Ray Powder Diffraction Data for Unevacuated Reaction Products	20
3.1 The Density of N_2O_4 as a function of pressure at 10°C	43
3.2 Vapour pressures of $\text{Fe}(\text{NO}_3)_3 \cdot n\text{N}_2\text{O}_4$, run 1	44
3.3 Vapour pressures of $\text{Fe}(\text{NO}_3)_3 \cdot n\text{N}_2\text{O}_4$, run 2	45
4.1 The infra-red spectrum of $\text{Fe}(\text{NO}_3)_3 \cdot 1.5\text{N}_2\text{O}_4$ and related compounds in nujol mulls (cm^{-1})	49
4.2 The Raman spectrum of solid $\text{Fe}(\text{NO}_3)_3 \cdot 1.5\text{N}_2\text{O}_4$ and related compounds	50
4.3 Magnetic moments of $\text{Fe}(\text{NO}_3)_3 \cdot 1.5\text{N}_2\text{O}_4$ and related compounds	51
4.4 d-values for $\text{Fe}(\text{NO}_3)_3 \cdot 1.5\text{N}_2\text{O}_4$ prepared from $\text{FeCl}_3/\text{EtOAc}/\text{N}_2\text{O}_4$	58
4.5 d-values for $\text{Fe}(\text{NO}_3)_3 \cdot 2\text{H}_2\text{O}$ and unidentified decomposition product of $\text{Fe}(\text{NO}_3)_3 \cdot 1.5\text{N}_2\text{O}_4$ in air	59
4.6 The vibrational spectrum of $\text{FeCl}_3 \cdot 2\text{NOCl}$	65
4.7 The vibrational spectrum of NOCl	66
6.1 Vibrational spectrum of 100% HNO_3	77
6.2 Vibrational spectrum of $\text{Fe}(\text{NO}_3)_3 \cdot x\text{N}_2\text{O}_4$ in 100% HNO_3 solution	81
7.1 Batch-wise extraction of $\text{Fe}(\text{NO}_3)_3 \cdot \text{N}_2\text{O}_4$ in HNO_3 by dry N_2O_4	92

X

7.2 Continuous extraction of $\text{Fe}(\text{NO}_3)_3 \cdot x\text{N}_2\text{O}_4$ in HNO ₃ by dry N ₂ O ₄	95
8.1 Conditions used for flow experiments with mild steel needle valve test section	120
8.2 d-spacings (Å) of flow-decay compound compared with those of $\text{Fe}(\text{NO}_3)_3 \cdot 1.5\text{N}_2\text{O}_4$, $\text{Fe}(\text{NO}_3)_3 \cdot 2\text{H}_2\text{O}$ and flow-decay compound isolated by Rocketdyne workers	125
10.1 Stability in contact with N ₂ O ₄ of potential additives for flow decay prevention	134

LIST OF FIGURES

Figure

2.1 I.R. Spectrum of $\text{Fe}(\text{NO}_3)_3 \cdot \text{N}_2\text{O}_4$	10
2.2 Change in I.R. spectrum on altering the composition of $\text{Fe}(\text{NO}_3)_3 \cdot x\text{N}_2\text{O}_4$	13
3.1 Apparatus for the Measurement of the Vapour Pressure of $\text{Fe}(\text{NO}_3)_3 \cdot n\text{N}_2\text{O}_4$	24
3.2 Sample Vessel A	25
3.3 The density of N_2O_4 vapour at 10°C	33
3.4 The Vapour Pressure of $\text{Fe}(\text{NO}_3)_3 \cdot n\text{N}_2\text{O}_4$ at 10°C	35
3.5 Equilibration of $\text{Fe}(\text{NO}_3)_3 \cdot n\text{N}_2\text{O}_4$ at $n = 2.2$ to $n = 1.5$	37
3.6 The effect of lowering the vapour pressure of N_2O_4 over $\text{Fe}(\text{NO}_3)_3 \cdot 1.5\text{N}_2\text{O}_4$	38
3.7 The rate of evolution of N_2O_4 from $\text{Fe}(\text{NO}_3)_3 \cdot n\text{N}_2\text{O}_4$ after certain periods of time	40
3.8 Evolution of N_2O_4 by $\text{Fe}(\text{NO}_3)_3 \cdot n\text{N}_2\text{O}_4$ at n close to 1	41
4.1 I.R. Spectra (nujol mull) of $\text{Fe}(\text{NO}_3)_3 \cdot 1.5\text{N}_2\text{O}_4$	48
4.2 The Mössbauer spectrum of $\text{Fe}(\text{NO}_3)_3 \cdot 1.5\text{N}_2\text{O}_4$	53
4.3 The Mössbauer spectrum of $\text{Fe}(\text{NO}_3)_3 \cdot 2\text{H}_2\text{O}$	54
4.4 The Vapour Pressure of $\text{FeCl}_3 \cdot n\text{NOCl}$ at 0°C	63
6.1 Apparatus for the preparation of 100% HNO_3	74
6.2 I.R. Spectrum of HNO_3	75
6.3 Raman Spectrum of HNO_3	76
6.4 I.R. Spectrum of a solution of $\text{Fe}(\text{NO}_3)_3 \cdot x\text{N}_2\text{O}_4$ in HNO_3	79

6.5 Raman Spectrum of $\text{Fe}(\text{NO}_3)_3 \cdot x\text{N}_2\text{O}_4$ in 100% HNO_3	80
7.1 $\text{HNO}_3/\text{N}_2\text{O}_4$ phase diagram	85
7.2 I.R. Spectrum of solution of N_2O_4 in HNO_3	88
7.3 Typical I.R. spectrum of $\text{Fe}(\text{NO}_3)_3 \cdot x\text{N}_2\text{O}_4$ in HNO_3 containing N_2O_4	89
7.4 Liquid-liquid extractor	94
7.5 Typical I.R. spectrum of solid extraction product of $\text{Fe}(\text{NO}_3)_3 \cdot x\text{N}_2\text{O}_4$ in HNO_3 by N_2O_4	97
7.6 Addition of H_2O to N_2O_3^+ $\text{Fe}(\text{NO}_3)_4^-$ in N_2O_4	102
8.1 Schematic diagram of the flow apparatus	107
8.2 Typical flow run with stainless steel needle valve	113
8.3 Valves operative in dismantling test section	114
8.4 Test section valve (mild steel)	116
8.5 I.R. Spectrum (nrjol mull) of material isolated from valve needle	118
8.6 Mild Steel Needle Valve - Flow Series 1	12..
8.7 Mild Steel Needle Valve - Flow Series 5	123
9.1 Vessel used in corrosion studies	129.

NOMENCLATURE

A_1 totally symmetric vibrational mode.
A.R. analytical reagent (grade of chemical).
antisym. antisymmetric.

Schoenflies point group symbols (molecular symmetry).

C_s one symmetry plane only.
 C_{2v} two-fold axis and two symmetry planes.
 D_{2d} four-fold rotation-reflection axis, three two-fold axes and two symmetry planes.

 d perpendicular spacing between crystal planes.
'H n.m.r. proton nuclear magnetic resonance.
 I intensity.
i.d. internal diameter.
I.R. infrared.

Intensities of infrared absorption bands

vw	very weak.	vs	very strong
w	weak	b	broad
m	medium	sh	shoulder
s	strong	sp	sharp

Kel-F polychlorotrifluoroethylene (PCTFE).
 K_p equilibrium constant in terms of partial pressures.
 ν vibrational mode.
 $N(III)$ nitrogen in +3 oxidation state (eg. in NO_2^-).
PTFE polytetrafluoroethylene (Teflon).
 $P2_1/c$ Hermann-Mauguin crystallographic space group symbol indicating a primitive lattice with a two-fold screw axis perpendicular to a c glide plane.
R Raman.
S.V.P. saturation vapour pressure.
str. stretching mode.

sym. symmetric.
t time.
 ΔT temperature difference between hold tank and
heat exchanger (flow apparatus).

Units

\AA angstrom (10^{-10} metre).
B.M. Bohr magneton (0.9273×10^{-20} erg gauss $^{-1}$).
 cm^{-1} reciprocal centimetre (wavenumber).
MHz megahertz (frequency).
 μ micron (10^{-6} metre).
mw milliwatt.
nm nanometre (10^{-9} metre)
p.s.i. pounds per square inch.

1. INTRODUCTION

When the work described in this Final Report was being planned and organised, some of the basic features of the flow decay problem were not understood. Our approach to the problem was largely determined by the fact that there was no general agreement as to the physical or chemical nature of the material which separated when liquid dinitrogen tetroxide which had been contained in iron vessels flowed through narrow apertures. Thus, some reports (e.g. (1)) suggested that the compound which separated was crystalline in form whereas others (e.g. (2)) attributed flow decay to the separation of a viscous liquid. The work carried out under this Contract was therefore directed towards this particular aspect, and falls broadly under two headings. Firstly, we considered it necessary to set up a full-scale flow rig in our own laboratories, in order to obtain and isolate the flow decay product. This part of the work has been completed as far as was necessary within the terms of reference of this Contract. A technique has been developed by means of which the "water" content of the bulk liquid dinitrogen tetroxide can be determined by proton nuclear magnetic resonance. The technique has been used to monitor the purity of the tetroxide used in the flow experiments, and the results show that when liquid dinitrogen tetroxide within specification purity is used in the flow apparatus, the flow decay product is a crystalline solid. Opportunity has also been taken to examine some of the parameters which influence the extent of flow decay (such as temperature, temperature gradient, orifice size etc.) This part of the work gives some indication of the physical conditions which favour flow decay. However, these particular observations

were incidental to our main theme, and we would not claim that they represent a definitive investigation. Nevertheless, it is pleasing to note that the general conclusions (especially concerning the importance of a temperature gradient during liquid flow) support those of another recent investigations designed specifically to identify the relevant parameters³. Our flow decay results are described towards the end of the Report (Section 8) because it is more convenient to describe the chemical nature of the product isolated from needle valves after the compounds themselves have been discussed.

The second aspect of our work involves the nature of the flow decay material, and related compounds. Earlier reports^{1,2} suggested that this material was probably an adduct of iron nitrate, $\text{Fe}(\text{NO}_3)_3$, with dinitrogen tetroxide, and formulated this as $\text{Fe}(\text{NO}_3)_3 \cdot \text{N}_2\text{O}_4$, or $\text{NO}^+ \text{Fe}(\text{NO}_3)_4^-$, in accordance with our own original description of this compound⁴. We have therefore extended, and refined, present knowledge on this compound, and Section 2 discusses preparative methods, vibrational spectra and X-ray powder diffraction data. During this work we were impressed by the tenacity with which N_2O_4 in excess of that required by the $\text{Fe}(\text{NO}_3)_3 \cdot \text{N}_2\text{O}_4$ formulation was held in the solid, and therefore undertook the vapour pressure study described in Section 3. This gave clear evidence that it is the compound $\text{Fe}(\text{NO}_3)_3 \cdot 1.5\text{N}_2\text{O}_4$ which is important in this system, and which exists in the presence of excess liquid dinitrogen tetroxide. Further study of this compound was stimulated by the observation that this was indeed also the material collected from the needle valves of the flow rig, and thus responsible for flow decay. In Section 4 we describe an extensive study of the properties of this compound with particular emphasis on the spectroscopic properties by means of which the 1.1.5 compound can be distinguished

from the 1:1 compound. The product is represented as $N_2O_3^+ Fe(NO_3)_4^-$. The cation has special interest since it may be a more complicated entity than is represented by the simple formulation $N_2O_3^+$, and methods designed to prevent flow decay may well involve attack at, or modification of, this cation. Section 4 includes some speculation on the structure of this cation, based on spectroscopic, and magnetic evidence. In an attempt to establish the cation structure, a full single crystal x-ray study of the 1:1.5 compound has been undertaken (Section 5) but this is not yet complete.

When water is added to dinitrogen tetroxide, nitric acid is produced and in the presence of soluble salts a second liquid phase is salted out containing the salt and a high concentration of nitric acid. This offers a feasible basis on which to interpret the separation of viscous gums during flow decay and we have been able to observe the transition in the flow decay material from solid to gum during addition of water to the tetroxide medium. Sections 6 and 7 describe an extensive survey of the chemistry of the iron compounds in solution in pure nitric acid, and in tetroxide-nitric acid mixtures, together with the various phase equilibria involved.

Corrosion studies were not included in our original terms of reference, but we have taken the opportunity (presented by the availability of a scanning electron microscope in the University) to examine the effect which various impurities in liquid dinitrogen tetroxide have on iron and steel surfaces. Section 9 makes reference to the effect of dissolved nitrosyl chloride, nitric acid and nitric oxide; the results have some relevance when considering the impurities responsible for solution of iron, and

the chemical state in which iron is present in solution in
dinitrogen tetroxide.

2. PRELIMINARY INVESTIGATIONS ON THE NATURE OF THE ADDUCTS
BETWEEN $\text{Fe}(\text{NO}_3)_3$ AND N_2O_4

During the course of the work described in this report, the known methods for the preparation of compounds of composition $\text{Fe}(\text{NO}_3)_3 \cdot x\text{N}_2\text{O}_4$ ($x \geq 1$) have been reinvestigated and, where possible, refined. Additionally, certain new synthetic procedures have been explored.

2.1 Methods of preparation and purification

a) The reaction of $\text{Fe}(\text{CO})_5$ and N_2O_4 in CCl_4

A solution of $\text{Fe}(\text{CO})_5$ in CCl_4 was slowly added to excess N_2O_4 in CCl_4 , with stirring, at 0°C . The experimental arrangement ensured that mixing of the reactants took place under the surface of the N_2O_4 solution in order to minimise the formation of the product $\text{FeO}(\text{NO}_3)_5$ by vapour phase reaction. A vigorous reaction occurred and a mixture of two products was formed, a yellow smoke (presumed to be $\text{FeO}(\text{NO}_3)_5$) and a gummy solid. This mixed product was isolated on a filter-stick, evacuated briefly to remove solvent and excess reactants and was then left to stand for 24 hours in contact with fresh dry N_2O_4 , which effects complete conversion of $\text{FeO}(\text{NO}_3)_5$ to an N_2O_4 adduct of $\text{Fe}(\text{NO}_3)_3$.⁵ The product was filtered and dried by evacuation.

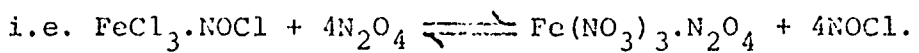
b) The reaction of FeCl_3 and N_2O_4 in EtOAc

This was the first discovered synthetic route to the compound $\text{Fe}(\text{NO}_3)_3 \cdot \text{N}_2\text{O}_4$ ⁶ and, at the commencement of the present work, was considered to be the method most likely to be chosen. (As substantial quantities of the compound $\text{Fe}(\text{NO}_3)_3 \cdot \text{N}_2\text{O}_4$ were to be used, this preparation was performed on a relatively large scale).

A.R. FeCl_3 (50 g) was dissolved in dry EtOAc (200 ml) and the solution was added to dry N_2O_4 (200 ml). The mixture was set aside overnight. Excess N_2O_4 and most of the EtOAc was then removed by evacuation (10^{-2} mm) yielding a dark red viscous syrup. Addition of a large excess of dry N_2O_4 resulted in immediate precipitation of yellow/brown crystals. These were isolated using a filter-stick and washed with dry N_2O_4 . Addition of dry N_2O_4 to the filtrate yielded a further crop of crystals. In some preparations using this method, the product was found to contain a small amount of Fe_2O_3 (identified by I.R. spectroscopy). This contaminant was removed by dissolution of the product in EtOAc followed by filtration, reprecipitation and washing with N_2O_4 . It was recognised that the oxide impurity might be present in the FeCl_3 starting material or could alternatively be formed by decomposition of the product. Thus, all solutions used in the preparation, reprecipitation or attempted recrystallisation of $\text{Fe}(\text{NO}_3)_3 \cdot x\text{N}_2\text{O}_4$ compounds were filtered through fine glass sinters before use.

c) The reaction of $\text{FeCl}_3 \cdot \text{NOCl}$ and N_2O_4

Metallic iron does not react to any significant extent at room temperature with liquid N_2O_4 or mixtures with EtOAc but the addition of small quantities of FeCl_2 or FeCl_3 to an EtOAc solution promotes a steady reaction with the metal.⁴ This behaviour results from the production of NOCl by solvolysis of the added chloride. NOCl reacts vigorously with metallic iron^{7,8} to give $\text{FeCl}_3 \cdot \text{NOCl}$ which in excess N_2O_4 is expected to undergo complete solvolysis to give the corresponding compound in the N_2O_4 system:



The advantage of this reaction is that it should provide a direct route to the desired N_2O_4 adduct without the addition (and the need for subsequent removal) of an organic donor solvent.

$NOCl$ was condensed onto spectroscopically pure iron at -78^0C and allowed to warm slowly to room temperature. A steady reaction occurred and a yellow-brown powder was deposited. This was evacuated ($10^{-2}mm$) overnight to remove excess $NOCl$, and a large excess of N_2O_4 was then added. A gentle reaction occurred over about three days. Excess N_2O_4 was then removed by evacuation ($10^{-2}mm$) and the resulting powder tested for chloride. If necessary, the powder was treated with further amounts of N_2O_4 until the chloride test was negative.

d) Attainment of the composition $Fe(NO_3)_3 \cdot N_2O_4$

The initial product arising from each of the above preparative methods contains an amount of N_2O_4 in excess of that required by the formulation $Fe(NO_3)_3 \cdot N_2O_4$ ($NO^+Fe(NO_3)_4^-$) and usually exhibits bands due to molecular N_2O_4 in the infra-red spectrum (see Section 2.4). The actual N_2O_4 content of individual products was monitored by use of the analytical techniques described in Section 2.2.

The precise composition $Fe(NO_3)_3 \cdot N_2O_4$ may be achieved where necessary by evacuation ($10^{-2}mm$ at about 20^0C), of the initial products of the above reactions for several days during which time the " N_2O_4 content" of the compound may be monitored by intermittent nitrite analysis (Section 2.2) and infra-red spectroscopy (Section 2.3). The reluctance with which this iron compound loses the N_2O_4 which is in excess of the above formulation is one of its most striking features and one which is not

encountered to any comparable extent in N_2O_4 adducts of other metal nitrates.

An alternative possible method of preparation of $Fe(NO_3)_3 \cdot N_2O_4$ was prompted by the observation that dissolution of $Fe(NO_3)_3 \cdot xN_2O_4$ in $MeNO_2$ (in which it is highly soluble) released NO_2 . It was hoped that vacuum distillation of the resulting solution might bring about the separation of $Fe(NO_3)_3 \cdot N_2O_4$. After several days evacuation ($10^{-2} mm\ Hg$, $25^\circ C$) the residue was a homogeneous-looking brown solid. The infra-red spectrum, and X ray powder pattern (Table 2.2) were very similar to those of $Fe(NO_3)_3 \cdot N_2O_4$ (Fig. 2.1), and although analysis also indicated this composition, a small but significant carbon content (0.5-1.0%) was found. This method for the preparation of $Fe(NO_3)_3 \cdot N_2O_4$ was therefore reluctantly abandoned.

2.2 Analysis

The following procedures were adopted in the analysis of the products obtained by the methods of Section 2.1.

a) Total nitrogen by the Kjeldahl method.

Total nitrogen content was determined by a modified Kjeldahl method using Devarda's Alloy. Adducts were first hydrolysed in alkali to ensure retention of all nitrogen in the form of NO_3^- and NO_2^- . Hydrolysates were prepared by a "closed-bottle" technique in which a known weight of sample was placed in a thin-walled glass bulb which was broken in a sealed vessel, in the presence of a known volume of 2M sodium hydroxide. Aliquots of this solution were then treated with Devarda's Alloy and further sodium hydroxide in a Kjeldahl apparatus and the liberated NH_3 was steam distilled into a known volume of standard boric acid which was titrated against standard HCl using a mixture of bromocresol green and methyl red as indicator.

b) N_2O_4 content by Ce(IV) titration of NO_2^-

Further aliquots of the above hydrolysate were used. Each aliquot was added to a known excess of acidified standard cerium(IV) sulphate solution which was back-titrated against standard iron(II) ammonium sulphate solution. N_2O_4 (or NO^{+}) yields an equimolar amount of NO_2^- on alkaline hydrolysis.

c) Iron by atomic absorption.

Iron determinations were carried out by means of a Southern Analytical A3000 Atomic Absorption Spectrometer. Solutions of adducts were prepared in dilute nitric acid and diluted appropriately. A calibration curve was obtained using solutions of known iron concentration. These were prepared by dissolution of spectroscopically pure iron in dilute nitric acid to give a nominally 100 ppm stock solution which was then diluted with dilute nitric acid to obtain standards in the concentration range required for optimum sensitivity.

2.3 Vibrational Spectrum of $Fe(NO_3)_3 \cdot N_2O_4$

a) Infra-red spectrum

The infra-red spectrum was recorded on a Perkin-Elmer 457 spectrometer using AgCl windows. Nujol mulls were prepared in a dry box.

A typical spectrum of the compound $Fe(NO_3)_3 \cdot N_2O_4$ is shown in Fig. 2.1 and the bands are listed and assigned in Table 2.1. This spectrum provides evidence for formulation as $NO^{+}[Fe(NO_3)_4]^-$ since it is virtually identical in the covalent nitrate region to that of the compound $(Ph_4As)^+[Fe(NO_3)_4]^-$ which was shown to contain a discrete anion of dodecahedral (D_{2d}) symmetry by means of a single crystal x-ray investigation.⁹

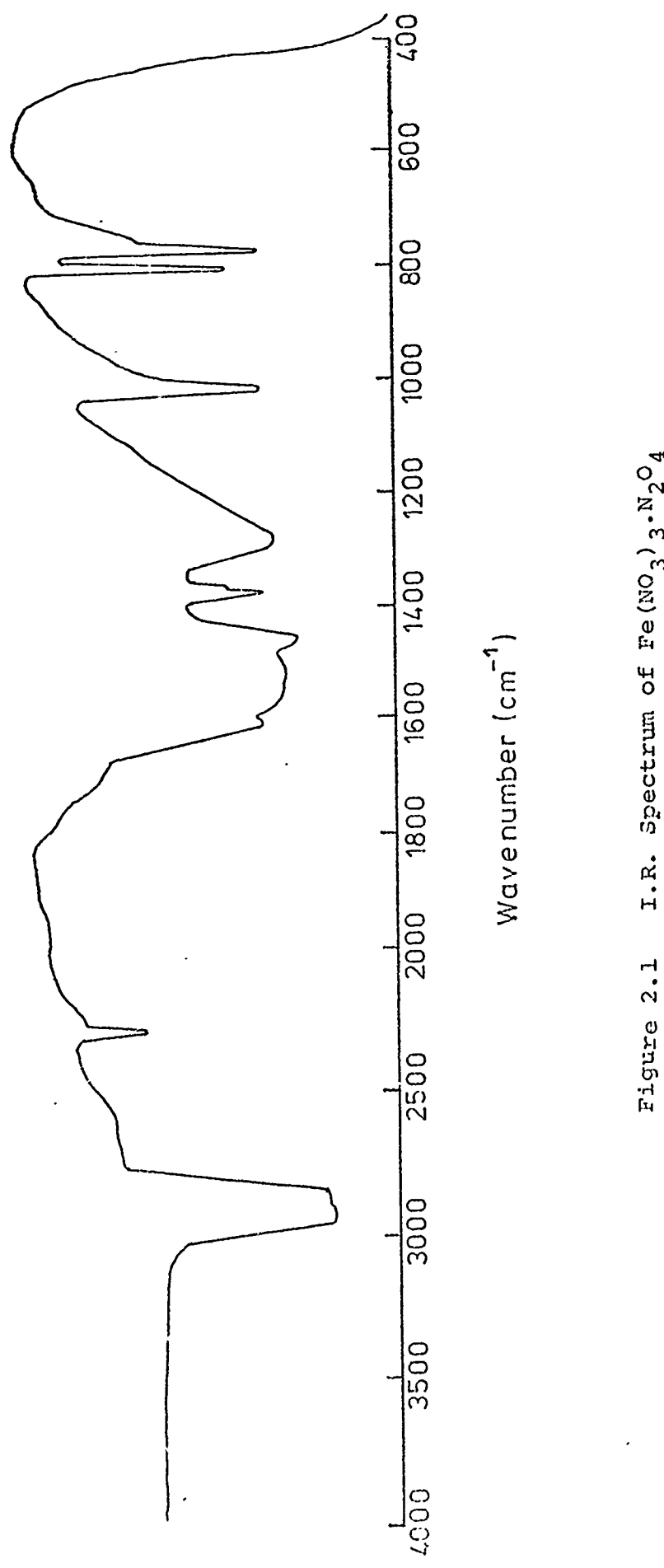


Figure 2.1 I.R. Spectrum of $\text{Re}(\text{NO}_3)_3 \cdot \text{N}_2\text{O}_4$

TABLE 2.1

Vibrational Spectrum of $\text{Fe}(\text{NO}_3)_3 \cdot \text{N}_2\text{O}_4$

Infra-red (cm^{-1}) Nujol mull	Raman (cm^{-1})	Assignment (C_{2v} bidentate nitrate model)
2298 m, sp	2302 s	NO^+ stretch
2230 vw, sh		NO^+ stretch
1598 s	1608 s)
1548 vs, b	1570 s) ν_1 N-O stretch
1295 s, b	1263 mw	ν_4 NO_2 antisymm. stretch
1018 s, sp	1030 m	ν_2 NO_2 symm. stretch
798 s, sp	784 m	ν_6 out of plane bend
764 vs, sp	769 m	ν_3 NO_2 antisymm. bend
	364 m	metal-oxygen stretch

Four symmetrically bidentate nitrate groups are disposed around iron(III) in this anion. No evidence for the presence of NO_3^- ion or nitrato-species other than $\text{Fe}(\text{NO}_3)_4^-$ is obtained from the infra-red spectrum of $\text{Fe}(\text{NO}_3)_3 \cdot \text{N}_2\text{O}_4$. The bands attributable to the anion $\text{Fe}(\text{NO}_3)_4^-$ in $\text{Fe}(\text{NO}_3)_3 \cdot \text{N}_2\text{O}_4$ are thus assigned in Table 2.1 in terms of bidentate bonding of nitrate groups (i.e. C_{2v} symmetry of the FeO_2NO unit). The presence of two bands assigned to NO^+ is discussed below (Section 2.4).

b) Raman spectrum

The Raman spectrum of $\text{Fe}(\text{NO}_3)_3 \cdot \text{N}_2\text{O}_4$ was recorded using a Cary 81 spectrometer and a Spectra-Physics 125 He-Ne laser as an excitation source (output approx. 60mW at 632.8 nm). The sample was contained in a sealed glass cell. The observed bands are listed and assigned in Table 2.1. Further support for the bidentate nitrate assignments given in this Table is obtained from the sequence of relative intensities of the three highest-frequency Raman shifts attributable to nitrate fundamentals at ca 1600, 1250 and 1000 cm^{-1} , i.e. the sequence:- strong, weak, strong. This agrees with the general observation that for symmetrically bidentate species the band at ca 1250 cm^{-1} (the N-O anti-symmetric stretch) is weak and without exception the least intense of the three bands¹⁰. In the case of unidentate nitrato-complexes, however, this band is generally fairly strong and is by no means the least intense of the three bands.

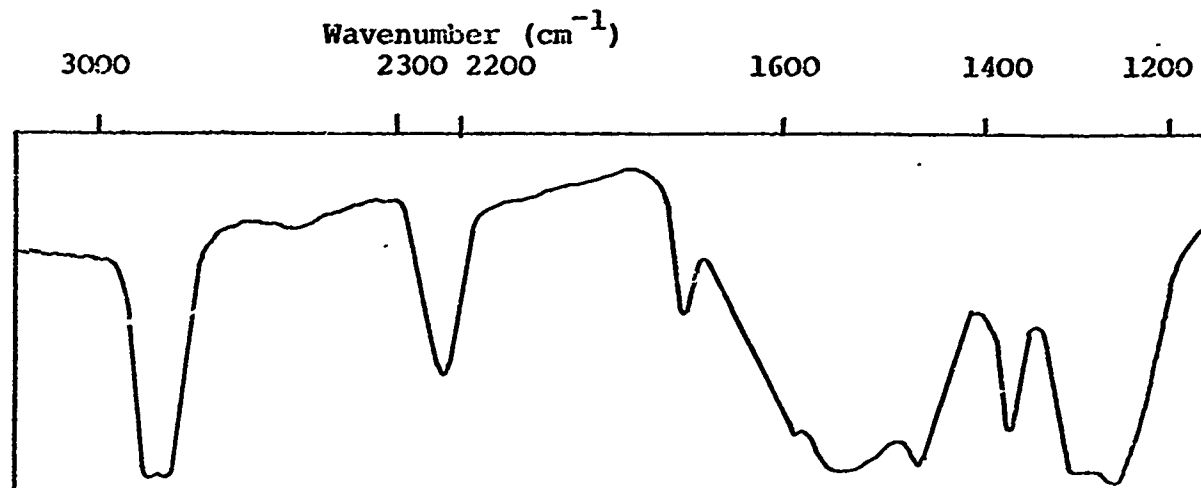
The above vibrational spectroscopic results are in good agreement with previous work on the compound $\text{Fe}(\text{NO}_3)_3 \cdot \text{N}_2\text{O}_4$.^{4,11}

2.4 The infra-red spectrum of $\text{Fe}(\text{NO}_3)_3 \cdot x\text{N}_2\text{O}_4$

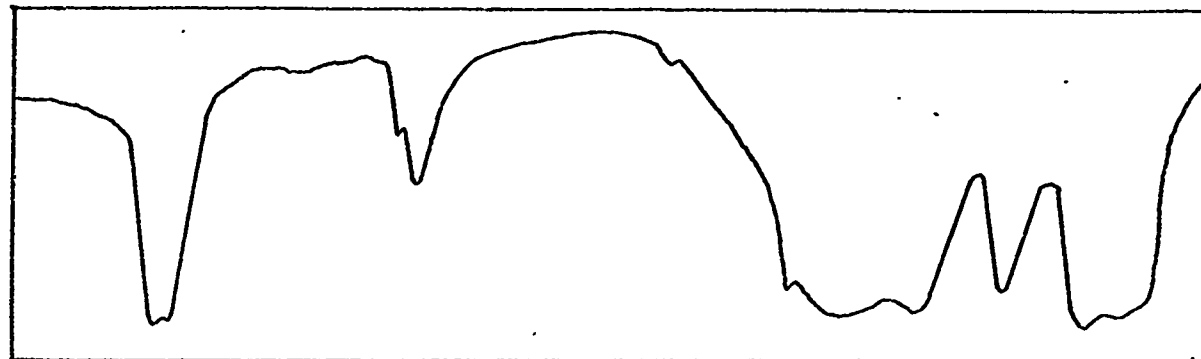
The infra-red spectrum of the initial (unvacuumed)

- 13 -
Figure 2.2

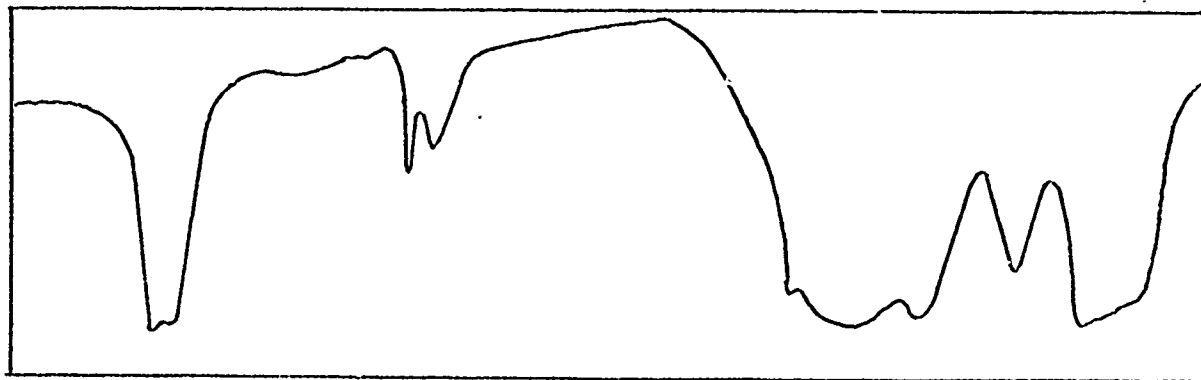
Change in I.R. spectrum on altering the composition of $\text{Fe}(\text{NO}_3)_3 \cdot x\text{N}_2\text{O}_4$



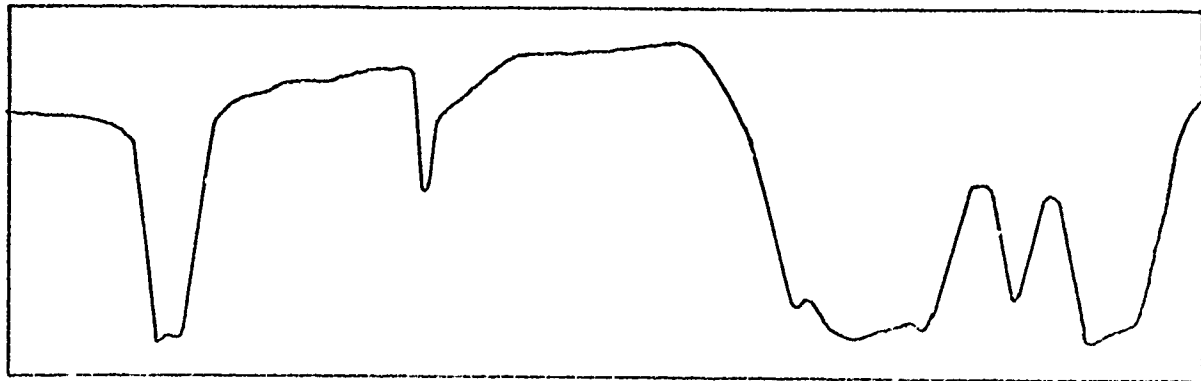
(a) Sample of $\text{Fe}(\text{NO}_3)_3 \cdot x\text{N}_2\text{O}_4$ as prepared from NOFeCl_4 .



(b) Sample as above after 3 days evacuation (10^{-2} mm).



(c) Same sample after 6 days evacuation (10^{-2} mm).



(d) Same sample after 2 weeks evacuation (10^{-2} mm).

products of the preparative reactions described in Section 2.1 showed a very intense band at 2230cm^{-1} (Fig. 2.2(a)), together with bands due to molecular N_2O_4 .* On evacuation of a product from the $\text{KUF}\text{eCl}_4/\text{N}_2\text{O}_4$ reaction (10^{-2}mm) for 3 days the molecular N_2O_4 bands and the band at 2230cm^{-1} decreased in intensity and a further band appeared at 2298cm^{-1} (Fig. 2.2(b)). After evacuation for a further 3 days the two bands in the NO^+ region were of comparable intensity (Fig. 2.2(c)) and after 2 weeks the 2298cm^{-1} band was the more intense with the 2230cm^{-1} band as a shoulder (Fig. 2.2(d)). It may be noted that the bands attributable to the $\text{Fe}(\text{NO}_3)_4^-$ anion are uninfluenced by the mode of preparation of the compound or by the presence of N_2O_4 in excess of the formulation $\text{Fe}(\text{NO}_3)_3 \cdot \text{N}_2\text{O}_4$. This provides a clear indication that the "excess" N_2O_4 is not associated with the $\text{Fe}(\text{NO}_3)_4^-$ moiety. Previous work in these laboratories supports the contention that $\text{Fe}(\text{NO}_3)_4^-$ has the same structure whatever the cationic species associated with it.¹¹

On dissolving the evacuated compound in ethyl acetate and reprecipitating with N_2O_4 , the spectrum reverted to that of Fig. 2.2(a). These observations lead to the conclusion that excess N_2O_4 is associated in some way with the NO^+ cation, perhaps in an analogous manner to that known for diethylnitrosamine^{13, 14} in which two molecules of this solvent coordinate to NO^+ , producing a consequent shift in the infra-red stretching frequency of the latter. This led to the prediction that the compound $[(\text{N}_2\text{O}_4)_2\text{NO}]^+\text{Fe}(\text{NO}_3)_4^-$ ($\text{Fe}(\text{NO}_3)_3 \cdot 3\text{N}_2\text{O}_4$) might be fairly stable.¹⁵

Alternatively, NO^+ perhaps associates with NO_2 to form the species $(\text{NO}_2)\text{NO}^+$ which Goulden and Millen^{16, 17} suggested was present in solutions of N_2O_4 in 100% KNO_3 on the basis of a * at about 1740, 1260 and 740cm^{-1} .¹²

15

Raman spectroscopic study. Thus, it was acknowledged that $[(NO_2)NO]^+Fe(NO_3)_4^-$ ($Fe(NO_3)_3 \cdot 1.5N_2O_4$) might also be an identifiable species in the $Fe(NO_3)_3 \cdot xN_2O_4$ system. Whatever the precise nature of the association causing the change in NO^+ band position, the net result is the same i.e. a lowering of the $N=O^+$ bond order and thus a lowering of the energy of vibration is brought about by electron donation to NO^+ . The stoichiometry of the species giving rise to the lowered NO^+ band at ca 2230 cm^{-1} is investigated in Section 3, and a study of its properties forms Section 4. The band observed at ca 2300 cm^{-1} (Table 2.1, Fig. 2.1, Fig. 2.2) is assigned to the "free" NO^+ cation.

It is also relevant to note at this point that association of $NOCl$ and NO^+ is considered to occur in certain metal halide-nitrosyl chloride adducts.¹⁸ In section 4.10 the vibrational spectrum of a compound containing the species $(NOCl)NO^+$ is investigated, and possible structures for this cation are considered.

2.5 Formulation of the adducts between $Fe(NO_3)_3$ and N_2O_4 as $Fe(NO_3)_3 \cdot xN_2O_4$

The vibrational spectra of material of analytical composition $Fe(NO_3)_3 \cdot N_2O_4$ support the ionic formulation $NO^+Fe(NO_3)_4^-$. However, the initial product from each of the preparative routes described in Section 2.1 had a higher N_2O_4 content than that for $Fe(NO_3)_3 \cdot N_2O_4$, and these products were for convenience written as $Fe(NO_3)_3 \cdot xN_2O_4$. However, the infrared spectra of these materials (Section 2.4) indicate that they contain $Fe(NO_3)_4^-$, NO^+ and/or NO^+ associated with N_2O_4 (depending on the N_2O_4 content) and (usually, but not always) molecular N_2O_4 itself.

It is shown later (Section 4.2) that the molecular N_2O_4 seen in such infra-red spectra can be attributed to decomposition in contact with mulling agents.

Although the maximum value observed for x in the formulation $Fe(NO_3)_3 \cdot xN_2O_4$ is ca 2.5 (observed for the product from the reaction of $Fe_3(CO)_{12}$ and N_2O_4 at $0^\circ C$), more typical values for x arising for products from the preparative methods described above are in the range ca 1.0 to ca 1.5.

The molecular species present in these products are NO^+ , NO^+ (coordinated) and $Fe(NO_3)_4^-$ and the stoichiometry and nature of the coordinated NO^+ species are discussed in Section 4 below. However, for brevity, the designation $Fe(NO_3)_3 \cdot xN_2O_4$ will throughout this report refer to materials of this nature, where the value of x was not precisely determined but lay within the region 1.0 to 2.5. The formula $Fe(NO_3)_3 \cdot N_2O_4$ will be used only for materials analytically close to the 1:1 stoichiometry. In the next Section (3) it is desirable to distinguish further situations where the number of " N_2O_4 molecules" in the " N_2O_4 adduct" of iron(III) nitrate is known with a fair degree of precision, but is variable. This number is represented as n and the resulting systems are designated $Fe(NO_3)_3 \cdot nN_2O_4$.

2.6 X-ray powder diffraction data

X-ray powder photographs were obtained as a matter of course for all samples produced in preparative and in "extraction" experiments (Section 7.5), wherever this was possible i.e. when the material was neither too wet nor gel-like. The reasons for taking powder photographs of products from the preparative experiments were two-fold. Firstly, to establish characteristic X-ray powder photographs for the adducts $Fe(NO_3)_3 \cdot xN_2O_4$ and

secondly to observe any correlation between the change in the X-ray powder pattern and the change in the value of x.

The powder patterns were obtained using a Phillips X-ray powder diffractometer with an 11cm camera and either CuK_α or FeK_α radiation. Typical d-spacings and intensities are recorded in Tables 2.2 and 2.3.

The powder patterns observed may be classified into two distinct groups. The patterns listed in Table 2.2 all result from preparations in which the final product was evacuated for some time prior to examination (except for c).

The analysis of samples a,b and c corresponded to $\text{Fe}(\text{NO}_3)_3 \cdot \text{N}_2\text{O}_4$ these samples and exhibited characteristic bands in their infra-red spectra (Section 2.3a). In the nitrosonium (NO^+) region of these spectra, the dominant band occurred at 2298cm^{-1} (m,sp) with a very weak shoulder at ca 2230cm^{-1} . It is of interest to note that previous workers at Rocketdyne¹ produced a sample (d) which also gave the characteristic powder photograph of the 1:1 adduct.

The patterns listed in Table 2.3 are clearly of a different type and are characteristic of samples which have not been evacuated after preparation. Again, each of these compounds has a typical infra-red spectrum which differs significantly in the nitrosonium region from that observed for the samples in Table 2.2. A strong broad band occurs at ca 2230cm^{-1} and the sharp 2298cm^{-1} band observed in the 1:1 adducts is absent. Sample (a) was analysed and shown to be of composition $\text{Fe}(\text{NO}_3)_3 \cdot 1.5\text{N}_2\text{O}_4$. This compound is further discussed in Sections 3 and 4.

TABLE 2.2. X-Ray Powder Diffraction Data (CuK α) for $\text{Fe}(\text{NO}_3)_3 \cdot \text{N}_2\text{O}_4$						
(a) $\text{Fe}(\text{NO}_3)_3 \cdot \text{N}_2\text{O}_4$	(b) $\text{Fe}(\text{NO}_3)_3 \cdot \text{N}_2\text{O}_4$ re-crystallised from MgNO_2	(c) $\text{Fe}(\text{NC}_3)_3 \cdot \text{N}_2\text{O}_4$ re-crystallised from $\text{HNO}_3/\text{N}_2\text{O}_4$	(d) $\text{Fe}(\text{NO}_3)_3 \cdot \text{N}_2\text{O}_4$ re-crystallised from $\text{EtOAc}/\text{N}_2\text{O}_4$			
d-spacing (Å)	Intensity	d-spacing (Å)	d-spacing (Å)	Intensity	d-spacing (Å)	Intensity
6.3	100	6.4	100	6.3	100	6.3
6.0	5	5.6	30	5.7	70	5.8
5.7	80	5.6	80	5.7	70	5.8
5.2	50	5.1	10	5.1	60	5.3
4.9	20	4.9	70	4.8	5	
4.7	20	4.6	5	4.6	30	
4.4	20	4.4	5	4.42	2	
4.23	30	4.1	20	4.21	5	4.20
3.98	2	3.93	2			
3.66	70	3.66	70	3.61	50	3.70
3.43	60	3.41	50	3.41	50	3.48
3.20	30	3.19	40	3.21	30	3.20
3.11	40	3.06	50	3.08	40	3.10
3.06	50	3.06	70	2.98	50	3.00
2.98	60	2.96	2			
2.91	2	2.90	2	2.43	30	2.44
2.44	30	2.43	20			m

TABLE 2.2 (Cont.)

(a) $\text{Fe}(\text{NO}_3)_3 \cdot \text{N}_2\text{O}_4$		(b) $\text{Fe}(\text{NO}_3)_3 \cdot \text{N}_2\text{O}_4$ recrystallised from MeNO_2		(c) $\text{Fe}(\text{NO}_3)_3 \cdot \text{N}_2\text{O}_4$ recrystallised from $\text{HNO}_3/\text{N}_2\text{O}_4$		(d) $\text{Fe}(\text{NO}_3)_3 \cdot \text{N}_2\text{O}_4$ recrystallised from $\text{EtOAc}/\text{N}_2\text{O}_4$	
d-spacing (\AA)	Intensity	d-spacing (\AA)	Intensity	d-spacing (\AA)	Intensity	d-spacing (\AA)	Intensity
2.35	20	2.31	5				
2.25	60	2.27	5	30	2.28	m	
2.12	5				2.17	w	
2.08	5						
2.04	5						
1.98	5				1.98	w	
1.93	5						

TABLE 2.3 X-Ray Powder Diffraction Data for Unevacuated Reaction Products

(a) Initial product from $\text{FeCl}_3/\text{N}_2\text{O}_4/\text{EtOAc}$ preparation (FeK_{α})	(b) Initial product from $\text{FeCl}_3\text{-NOCl}/\text{N}_2\text{O}_4$ preparation (CuK_{α})	(c) $\text{Fe}(\text{NO}_3)_3\text{-N}_2\text{O}_4$ from $\text{FeCl}_3/\text{N}_2\text{O}_4/\text{EtOAc}$ preparation, recrystallised from $\text{HNO}_3/\text{N}_2\text{O}_4$ (CuK_{α})	(d) $\text{Fe}(\text{NO}_3)_3\text{-N}_2\text{O}_4$ from $\text{FeCl}_3/\text{N}_2\text{O}_4/\text{EtOAc}$ preparation, recrystallised from N_2O_4 (CuK_{α})
9.25	?	9.08	7.5
9.29	20		
8.23	10		
7.56	60		
7.20	70	7.31	60
6.81	30	7.0	6.7 ^{v.s.}
6.31	80	6.2	6.30 ^{v.s.}
5.65	30	5.6	5.64 ^w
5.45	5		
5.20	15	5.05	5.19 ^m
4.61	100	4.56	4.61 ^{v.v.s.}
4.42	30	4.36	4.35 ^w
4.27	30		
4.10	50	4.03	4.07 ^m
3.77	70	3.74	3.75 ^s
3.60	60	3.55	3.56 ^s
3.44	60	3.38	3.41 ^s
3.36	5		
3.28	40	3.22	3.24 ^s
		50	70 ^s

TABLE 2.3 (Cont.)

(a) Initial product from FeCl ₃ /N ₂ O ₄ /EtOAc preparation (FeK _α)		(b) Initial product from FeCl ₃ ·NOCl/N ₂ O ₄ preparation (CuK _α)		(c) Fe(NO ₃) ₃ ·N ₂ O ₄ from FeCl ₃ /N ₂ O ₄ /EtOAc pre- paration, recrystallised from N ₂ O ₄ (CuK _α)		(d) Fe(NO ₃) ₃ ·N ₂ O ₄ from recrystallised from N ₂ O ₄ (CuK _α)	
d-spacing (Å)	Intensity	d-spacing (Å)	Intensity	d-spacing (Å)	Intensity	d-spacing (Å)	Intensity
3.00	20	3.01	2	3.02	5		
2.81	50	2.80	20	2.81	20	2.80	m
2.68	10	2.66	2				
2.60	20	2.57	20	2.59	50	2.60	w
2.45	50	2.42	30	2.43	5	2.44	m

In summary, it is now possible to identify powder photographs characteristic of the distinct compounds $\text{Fe}(\text{NO}_3)_3 \cdot \text{N}_2\text{O}_4$ and $\text{Fe}(\text{NO}_3)_3 \cdot 1.5\text{N}_2\text{O}_4$. It is perhaps surprising that a powder photograph indicating the presence of both these phases has only been observed for one sample (Section 7.5b) during the present studies. However, the sensitivity of X-ray powder photography is only sufficient to allow detection of 5 - 10% of a second phase and this sensitivity is further reduced by CuK_α irradiation of samples containing iron.

3. VAPOUR PRESSURE STUDIES ON THE NOFe(No₃)₃.nN₂O₄ SYSTEM

3.1 Experimental.

(a) Apparatus

In an attempt to obtain evidence for stable compositions in the Fe(No₃)₃.nN₂O₄ system other than the well-known n = 1, by vapour pressure measurements, the following design considerations had to be taken into account:

- i) N₂O₄ has a narrow liquid range at atmospheric pressure, -11 to +21°C.
- ii) At the lower temperatures, the vapour pressure is low, making difficult the measurement of possibly small changes in the vapour pressure over a solid containing N₂O₄.
- iii) At lower temperatures, any adducts formed in the Fe(No₃)₃.nN₂O₄ system will be more stable than at higher temperatures.
- iv) The attainment of the equilibrium vapour pressure will be slower at lower temperatures, as the limiting factor in this attainment is likely to be the transport of N₂O₄ through the solid lattice.
- v) N₂O₄ vigorously attacks mercury and greases except for fluorochlorocarbon greases (e.g. 'Kel-F').
- vi) The moisture-sensitive nature of the Fe(No₃)₃.xN₂O₄ requires special precautions for transfer into the apparatus used for vapour pressure measurement.

Accordingly, the apparatus shown schematically in Fig. 3.1 was constructed. The Fe(No₃)₃.nN₂O₄ system to be studied was contained in vessel A (Fig. 3.2) which fitted tightly into the sample compartment B, allowing A to be broken by rotation of the extended stopper in the B34 neck of B after evacuation of the apparatus. Pressures were measured using a spiral gauge, C, and the calibrated bulb D was used to change the composition of the system as later described. The

Fig. 3.1 Apparatus for the Measurement of the
Vapour Pressure of $\text{Fe}(\text{NO}_3)_3 \cdot n\text{N}_2\text{O}_4$.

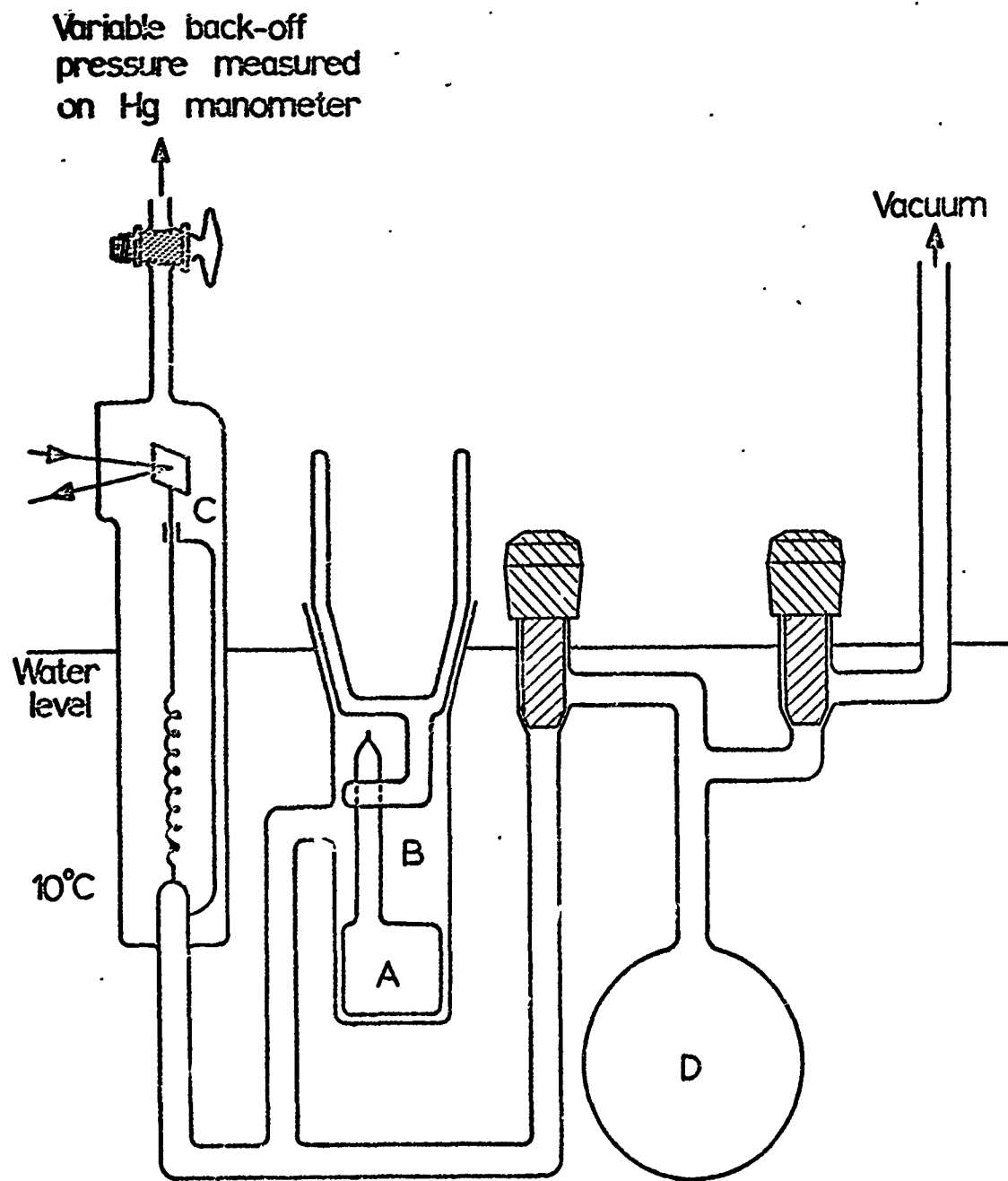
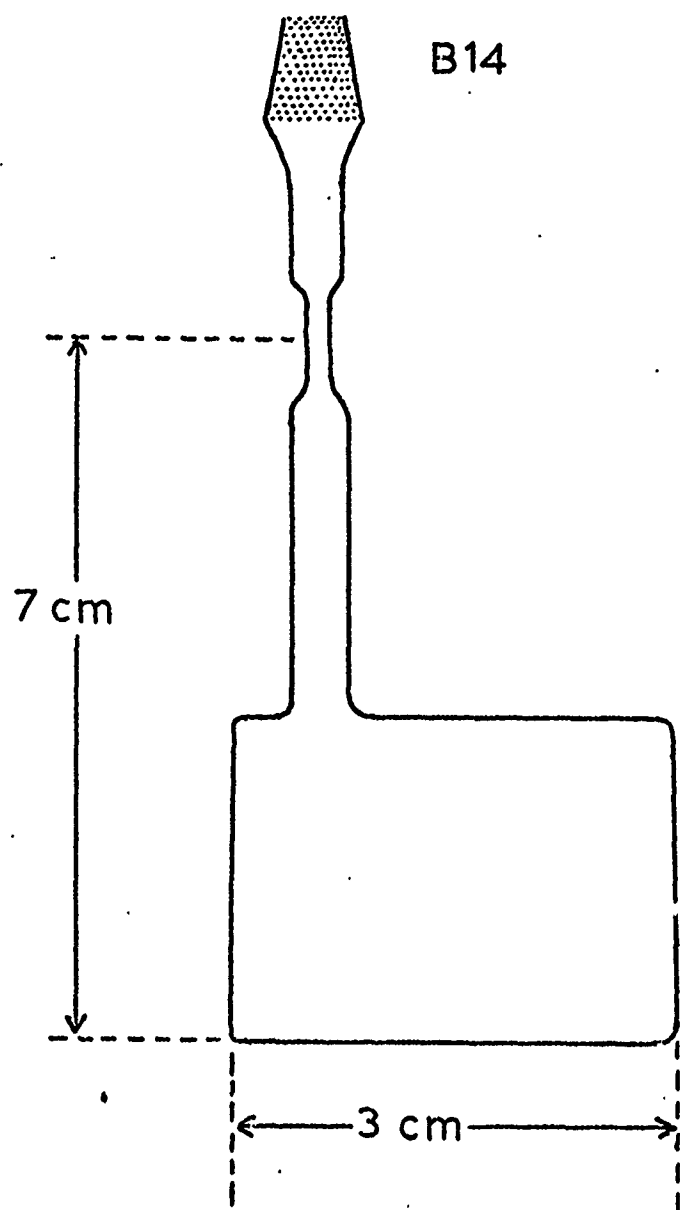


FIGURE 3.2
SAMPLE VESSEL A

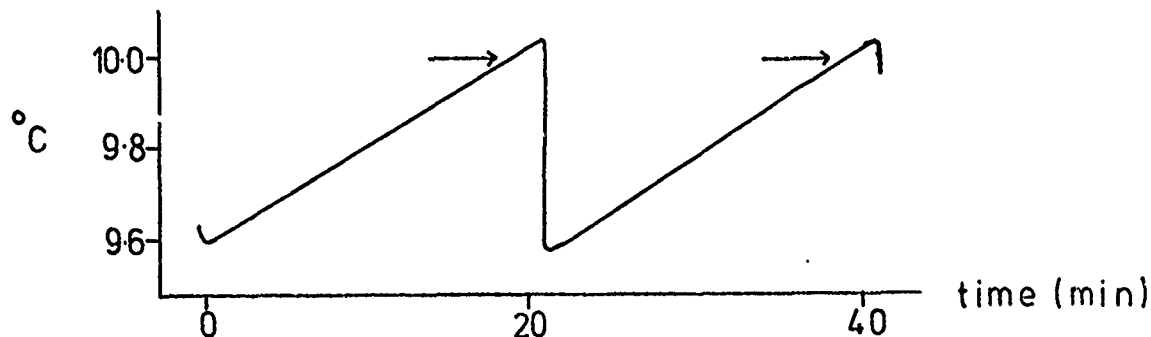


whole apparatus was immersed in a water bath, which contained a copper coil through which cooled, 1,1,1-trichloroethane was circulated. The cooling of the refrigerant was controlled by the temperature in the water bath, which was stirred at a constant rate. This enabled the water bath to maintain a given temperature to $\pm 0.2^{\circ}\text{C}$.

Taps T_1 and T_2 , and the stopper in B were greased with a small amount of degassed (3 weeks, 25°C , 10^{-2} mm Hg) 'Kel-F' grease. Initially a temperature of 0°C was selected (S.V.P. of N_2O_4 ca 26 cm Hg^{19}) as a reasonable compromise between the conflicting design considerations, but preliminary experiments showed that the 'Rotaflow' P.T.F.E. taps incorporated in the apparatus, leaked slightly at this temperature. They were, however, completely satisfactory at 10°C , and this temperature was used for the vapour pressure studies.

(b) Standard procedures

The thermostat arrangement used, allowed an appreciable change in the temperature of the water bath used for cooling the sample (\pm ca 0.2°C). The thermal cycling of this bath followed the pattern:



In order to obtain reproducible conditions in those measurements where the pressure change with temperature was appreciable compared with the pressure change with time, measurements were taken when the thermometer reading was 10.0°C during the slow heating portion

of the thermal cycle, arrowed on the above diagram. This method has the advantage that all thermal hysteresis effects can be eliminated, and that significant results can be obtained even though the 10.0°C measured on the thermometer may not correspond precisely with that of the sample. Throughout this section references to a temperature of 10.0°C carry this meaning.

In those measurements where the pressure change with time was large compared with the pressure change with temperature, namely in the study of the initial rate of evolution of N_2O_4 from a solid containing N_2O_4 when the pressure above the solid was suddenly decreased from its equilibrium value, it was convenient to make these measurements during one of the heating portions from ca 9.6 to ca 10.1°C .

The experimental arrangement was such that the full scale deflection of the spiral gauge corresponded to approximately 9 cm Hg and hence a change in pressure in B of this magnitude could be followed without change in the 'backoff' pressure in C.

(c) Calibration of the apparatus

The volume of bulb D was found, before construction of the apparatus as in Fig. 3.1, by filling with water at a known temperature and weighing the water contained in it. The volume was 300 ml.

The spiral gauge used had a sensitivity of approximately 90° per atmosphere, and an optical lever approximately one metre long provided a scale reading change of 3.57 cm per cm Hg. The calibration was linear up to at least 8 cm Hg

pressure difference, and independent of the absolute pressure in the outer jacket C.

The volume of the sample compartment B and the associated tubing (ie. up to T_1) was found by filling B with nitrogen at a known pressure. Bulb D was evacuated, T_2 closed and T_1 opened and the new pressure measured. This was repeated several times with different initial pressures of gas. A Boyle's law calculation neglecting non-ideality corrections provided a sufficiently accurate value for the volume of B (120 ml).

(d) The Density of N_2O_4 vapour at $10^{\circ}C$

The gaseous dissociation $N_2O_4 \rightleftharpoons 2NO_2$ has been the object of considerable study (19, 20, 21 and references therein). These studies were directed towards determination of thermodynamic functions for this reaction, and were not generally concerned with systems close to the saturation vapour pressure, although very accurate values for the vapour pressure over a range of temperature have been recorded¹⁹. In the present work the initial pressure readings were to be at the S.V.P. and the composition of the system being studied was to be change by successive removal of known amounts of N_2O_4 . In view of the necessity for accurate knowledge of the amount of N_2O_4 removed, it was considered desirable to measure the density of N_2O_4 vapour as a function of pressure, rather than rely on interpolation of the literature values of K_p , assuming this to be independent of pressure, and assuming the behaviour to be ideal at all pressures. This was performed by filling bulbs B and D with N_2O_4 (which had previously been dried by distillation from P_2O_5 and then multiply degassed) to a selected pressure, measured with the spiral gauge and a

suitable back-off pressure in C. When the temperature in the cooling bath reached 10.0°C the pressure was measured, T₁ was closed and the N₂O₄ in D was condensed into a previously weighed ampoule, flamed sealed and reweighed. This was repeated for several different pressures of N₂O₄. At pressures appreciably below the S.V.P. (ca 44 cm Hg at 10°C¹⁹), the pressure was a monotonic function of temperature, and hence the value recorded at 10.0°C was taken as representative of the equilibrium behaviour of the system. Close to the S.V.P., however, the pressure changes during the thermal cycling were sudden and the values recorded at 10.0°C on successive cycles were not as reproducible as those at lower pressures. This behaviour was ascribed to superheating and supercooling of the sample. The error in the pressure readings close to the S.V.P. was small (ca 0.6 in 43 cm Hg) but it was decided that when the composition of the system Fe(NO₃)₃.nN₂O₄ was to be changed at vapour pressures close to the S.V.P., the N₂O₄ should be distilled into a weighed ampoule, sealed and reweighed. At lower pressures the calibration obtained above provided a convenient and accurate measure of the change in composition.

(e) Sample Preparation

The sample vessel A shown in Figs. 3.1 and 3.2 containing Fe(NO₃)₃.nN₂O₄ of accurately known n was prepared as follows. Fe(NO₃)₃.N₂O₄ was loaded into A (which had been previously weighed) in a dry-box, by means of a funnel to avoid the deposition of solid on the constriction, and then capped,

removed from the dry-box and weighed. It was then attached to a vacuum line and several times degassed. An approximately known pre-selected weight of degassed N_2O_4 was distilled onto the sample, the vessel was flame sealed at the constriction and the weight of N_2O_4 distilled into the sample was found accurately by difference.

The vessel was then set aside for several weeks at $25^{\circ}C$ to allow equilibration.

The weight of $Fe(NO_3)_3 \cdot N_2O_4$ to be used was specified by the desired spacing of the points on the vapour pressure vs. composition plot; the minimum possible change in n corresponds to 300 ml of N_2O_4 vapour at the pressure at which the N_2O_4 is removed from the system. A change in n of 0.5 when the system develops a pressure close to the S.V.P. of N_2O_4 requires about 5 g of $Fe(NO_3)_3 \cdot N_2O_4$ to be used. The weight of N_2O_4 to be distilled into the sample vessel may be found from the weight of $Fe(NO_3)_3 \cdot N_2O_4$ and the desired initial n .

(f) The dissociation vapour pressure of $Fe(NO_3)_3 \cdot nN_2O_4$ at $10^{\circ}C$

The sample vessel A containing $Fe(NO_3)_3 \cdot nN_2O_4$ prepared as described above was placed in the sample compartment B (Fig. 3.1), after making a scratch with a glass-knife at the bottom of the narrow neck. The stopper to B was replaced, and the whole apparatus evacuated for 30 minutes. Then Tap T_1 was closed, B was surrounded by a Dewar flask containing liquid nitrogen and the stopper to B was rotated to break the neck of A. The Dewar containing liquid nitrogen was then removed from B. The water bath containing the whole apparatus was filled and allowed to attain its

regular thermal cycling at close to 10°C.

The pressure developed at the initial composition was measured by means of the spiral gauge and a suitable 'back-off' pressure in the outer jacket C. When constant readings on several successive thermal cycles were obtained, the system was deemed to have reached equilibrium, and the pressure at 10.0°C was recorded.

The composition of the system was altered by expansion of the N_2O_4 vapour in B into bulb D by opening T_1 , followed by estimation of the amount of N_2O_4 in bulb D as described above. At a convenient time T_1 was closed and the new system, with a changed n was then allowed to equilibrate.

On opening T_1 to alter the composition of the system, the pressure of N_2O_4 dropped to approximately one quarter of its previous value. The rate at which the solid evolved N_2O_4 to re-attain its equilibrium vapour pressure was followed

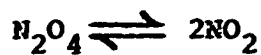
- (a) to determine the initial rate of evolution, and hence compare the ease with which N_2O_4 was lost from $Fe(NO_3)_3 \cdot nN_2O_4$ at various values of n.
- (b) To monitor the increase in pressure over the whole period to the equilibrium value, and hence to determine how soon a sufficient approximation to the equilibrium value was reached.

The composition of the solid, n(solid), could be calculated by making a small correction to n (system) (found from the initial composition and the amount of N_2O_4 removed), to allow for the N_2O_4 in the vapour phase above the solid. All the quoted figures of n in the tables and graphs refer to n(solid).

3.2 Results and Discussion

(a) The density of N_2O_4 vapour at $10^{\circ}C$

The measured density of N_2O_4 vapour is shown on Fig. 3.3 and tabulated in Section 3.3. The curve was calculated as follows. For the gas phase dissociation



K_p is defined by

$$K_p = \frac{p_{NO_2}^2}{p_{N_2O_4}}$$

where p_{NO_2} and $p_{N_2O_4}$ represent the partial pressures. If a fraction α of the N_2O_4 dissociates at a given temperature, and if it is assumed that the mixture behaves ideally, then

$$p_{NO_2} = \frac{2\alpha}{1+\alpha} \cdot P$$

and
$$p_{N_2O_4} = \frac{1-\alpha}{1+\alpha} \cdot P$$

where $P (= p_{NO_2} + p_{N_2O_4})$ represents the total pressure developed by the system.

$$\text{Then } K_p = \frac{4\alpha^2 P}{(1-\alpha)^2}$$

So if K_p is known at a certain temperature α may be found as a function of P . However, if the system behaves ideally then the density d will be given by

$$d = \frac{1}{1+\alpha} d_{N_2O_4}^{\circ}$$

where $d_{N_2O_4}^{\circ}$ is the density N_2O_4 vapour would have at the temperature and pressure considered, if it did not dissociate

Fig. 3.3 The density of N_2O_4 vapour at 10°C

Points : experimental
Curve : calculated

Density
(mg/300 ml)

600

500

400

300

200

100

Pressure (cm Hg)

0

16

24

32

40

SVP

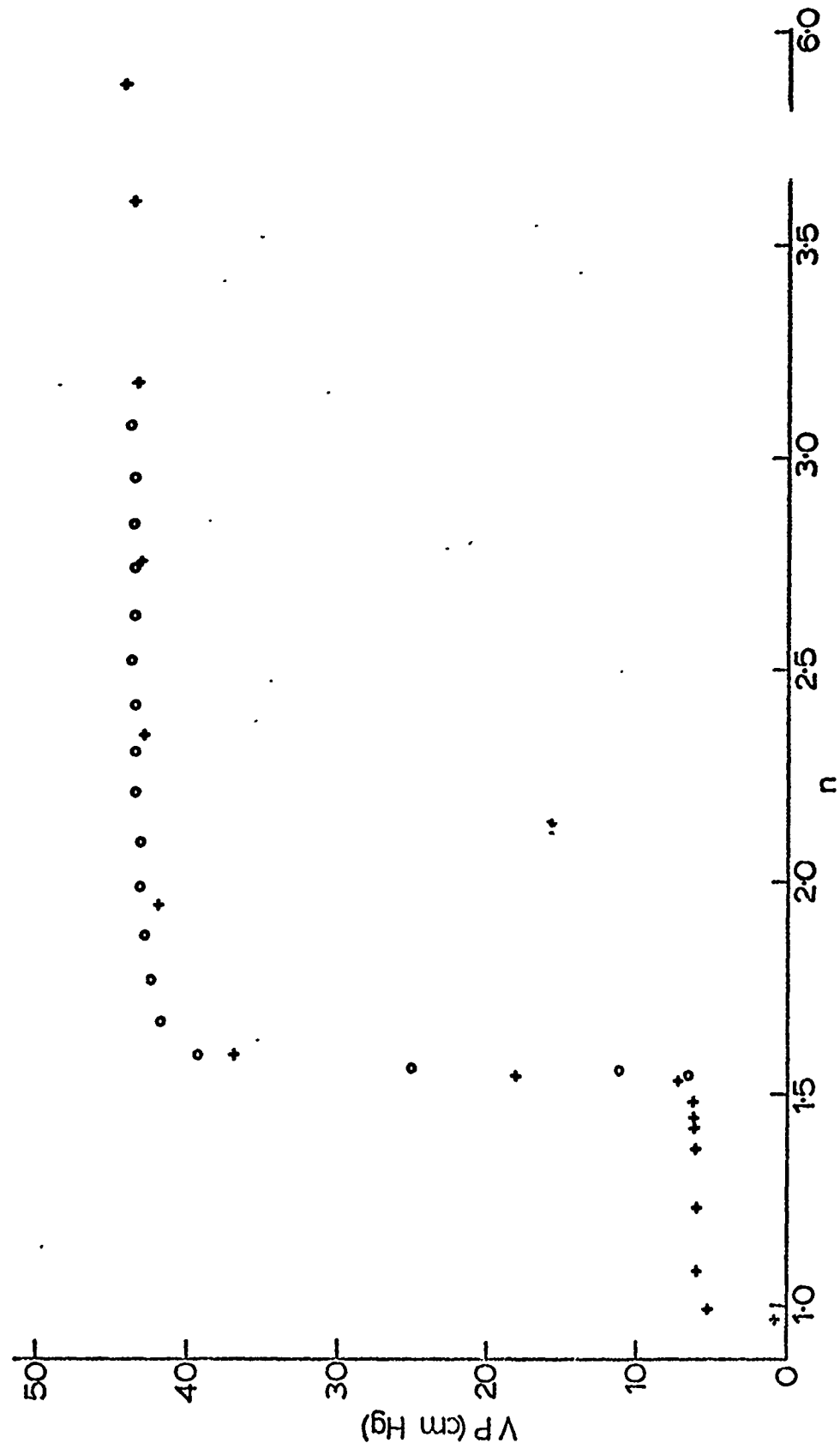
and behaved ideally. This is easily calculable.

A value for K_p of 0.041 atm. at 10.16°C was interpolated from the data of Giauque and Kemp¹⁹. The curve in Fig. 3.3 is calculated from this value of K_p and the assumption of ideal behaviour. The agreement between the experimental and rather crudely approximated calculated values is close for all except the highest pressure reading (which was subject to some inaccuracy in the experimental value due to superheating and supercooling). This is very satisfactory and the calculated density at low pressures, where the deviations from ideality would be smaller, and for which accurate density measurements would be difficult to obtain, was used with confidence. The agreement of the experimental figures with the values calculated using a model assuming ideal behaviour do not imply that the model used was correct. This agreement may be fortuitous, and due to the counterbalancing of the effects of two erroneous assumptions. However, the literature does indicate that the variation of K_p with P is negligible below 0.35 atm. at -40 to 0°C ²¹, though at 25°C and above, K_p does vary slightly with P , and this deviation has been attributed to non-ideal behaviour²⁰.

(b) The dissociation vapour pressure of $\text{Fe}(\text{NO}_3)_3 \cdot n\text{N}_2\text{O}_4$

The 'equilibrium' vapour pressures derived from the results of two separate experiments are shown in Fig. 3.4 and tabulated in Section 3.4. In Fig. 3.4 the crosses correspond to run 1 and the circles to run 2. Marked decreases in the vapour pressure of $\text{Fe}(\text{NO}_3)_3 \cdot n\text{N}_2\text{O}_4$ occur close to $n = 1.5$ and $n = 1.0$. The decrease at $n = 1.0$ is reasonable, as $\text{Fe}(\text{NO}_3)_3 \cdot \text{N}_2\text{O}_4$ (ie. $\text{NO}^+\text{Fe}(\text{NO}_3)_4^-$) might be expected to have a very low vapour pressure of N_2O_4 . Again, the closeness of the value for n (solid) to 1.0 when the vapour pressure

Fig. 3.4 The Vapour Pressure of $\text{Fe}(\text{NO}_3)_3 \cdot \text{N}_2\text{O}_4$ at 10°C



falls sharply may be taken as an indication that the accumulated handling errors are not large.

An indication that pressures close to equilibrium are being attained is presented in Fig . 3.5
The results will be considered in turn for the four regions:
 $n = 1.5$, $n > 1.5$, $1 < n < 1.5$ and $n \sim 1$.

(i) $n = 1.5$

In each experiment a sharp fall in the vapour pressure of $\text{Fe}(\text{NO}_3)_3 \cdot n\text{N}_2\text{O}_4$ occurred close to $n = 1.5$. In one case (Fig . 3.6) a solid with $n = 1.543$ under 18 cm Hg of N_2O_4 had approximately three quarters of this vapour phase N_2O_4 rapidly removed. (The calculated $t=0$ figure is on the basis of an isothermal expansion at 10°C of the contents of bulb B into B plus D). The solid remained stable and showed only very slight evolution of N_2O_4 in 20 hrs. That the same solid is in equilibrium with 18 cm Hg of N_2O_4 and 7 cm Hg of N_2O_4 is a clear indication of the existence of a vertical step in the P vs n diagram ie. there is a single condensed phase, a solid with $n = 1.5$, which is in equilibrium with vapour.

The work described in Section 2 pointed to the affinity of $\text{NO}^+\text{Fe}(\text{NO}_3)_4^-$ for N_2O_4 , and it was noted that the infra-red spectrum of $\text{Fe}(\text{NO}_3)_3 \cdot x\text{N}_2\text{O}_4$ was consistent with its containing N_2O_3^+ . $(\text{N}_2\text{O}_3^+\text{Fe}(\text{NO}_3)_4^- \equiv \text{Fe}(\text{NO}_3)_3 \cdot 1.5\text{N}_2\text{O}_4)$. The preparation and investigation of some properties of the species $\text{Fe}(\text{NO}_3)_3 \cdot 1.5\text{N}_2\text{O}_4$ is described in Section 4.

(ii) $n > 1.5$

There is some evidence from the 'equilibrium' data

Fig. 3.5
Equilibration of $\text{Fe}(\text{NO}_3)_3 \cdot n \text{N}_2\text{O}_4$ at
 $n = 2.2$ to $n = 1.5$

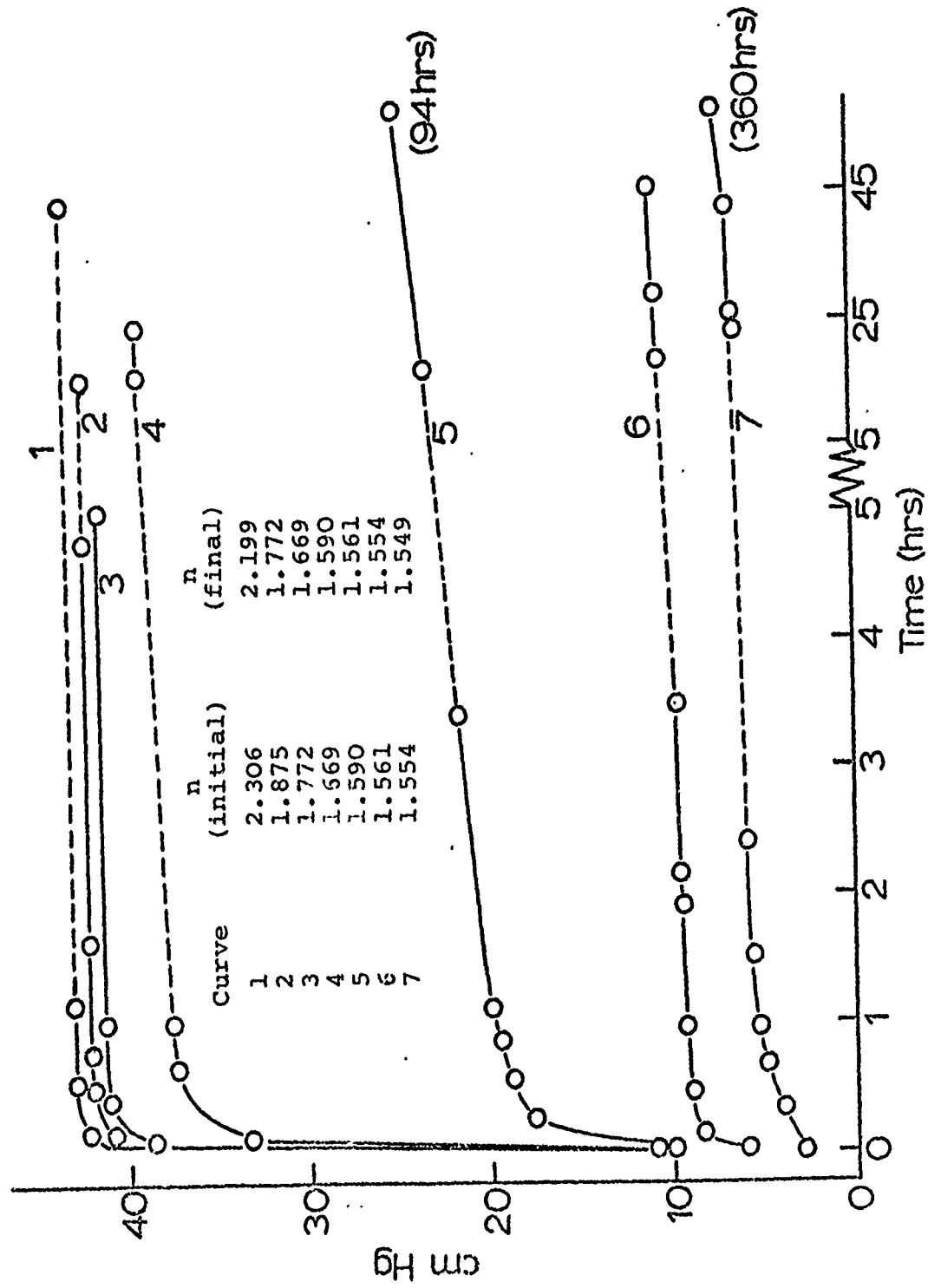
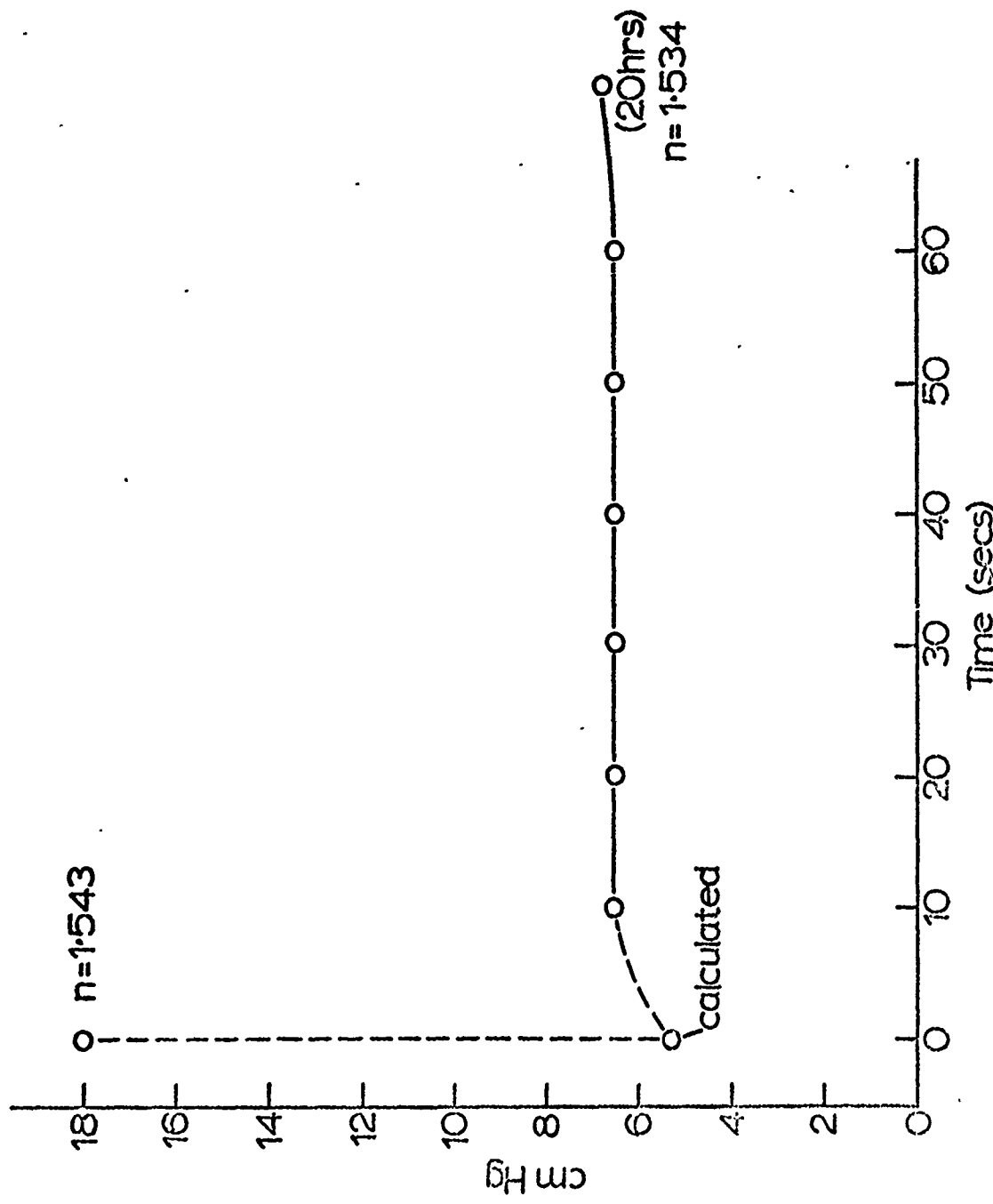


Fig. 3.6
The effect of lowering the vapour pressure of
 N_2O_4 over $\text{Fe}(\text{NO}_3)_3 \cdot 1.5 \text{N}_2\text{O}_4$



(Fig. 3.4) that $\text{Fe}(\text{NO}_3)_3 \cdot 1.5\text{N}_2\text{O}_4$ retains further N_2O_4 , though precise interpretation of this data is difficult. Consideration of the rate of evolution of N_2O_4 from $\text{Fe}(\text{NO}_3)_3 \cdot n\text{N}_2\text{O}_4$ when the pressure of N_2O_4 is suddenly lowered (Fig. 3.7) provides more convincing evidence for this association, in that the rate of evolution of N_2O_4 from $\text{Fe}(\text{NO}_3)_3 \cdot n\text{N}_2\text{O}_4$ with $n = 1.5$ to 1.7 is significantly less than the rate of evolution with $n > 1.7$. However, as the rate of evolution is plotted against the initial n , and not the surface n , interpretation of these data is also difficult. It is tempting to speculate that $\text{Fe}(\text{NO}_3)_3 \cdot 1.75\text{N}_2\text{O}_4$ might be a significant species in this system, although its high dissociation vapour pressure makes it unlikely that the 'extra' $0.25\text{N}_2\text{O}_4$ is strongly bonded.

It is of interest to note that for n above ca 2 the vapour pressure is very close to the S.V.P. of N_2O_4 . However, up to at least $n = 3.1$, the attainment of the equilibrium vapour pressure is not so rapid as to imply the presence of free liquid N_2O_4 .

(iii) $1 < n < 1.5$

The vapour pressure over this region is substantially constant (Figs. 3.4 and 3.8). This behaviour would be required by the phase rule if two phases, with $n = 1$ and $n = 1.5$, were present in differing proportions over this range. Although it is not permissible to infer that there are two phases in this region, it may be deduced that whatever is the constitution of $\text{Fe}(\text{NO}_3)_3 \cdot n\text{N}_2\text{O}_4$ with $1 < n < 1.5$, the chemical potential of the NO_2 in the solid remains substantially constant over this range. The most likely explanation of this behaviour would seem

Fig. 3.7. The rate of evolution of N_2O_4 from $\text{Fe}(\text{NO}_3)_3 \cdot n\text{N}_2\text{O}_4$ -

after certain periods of time

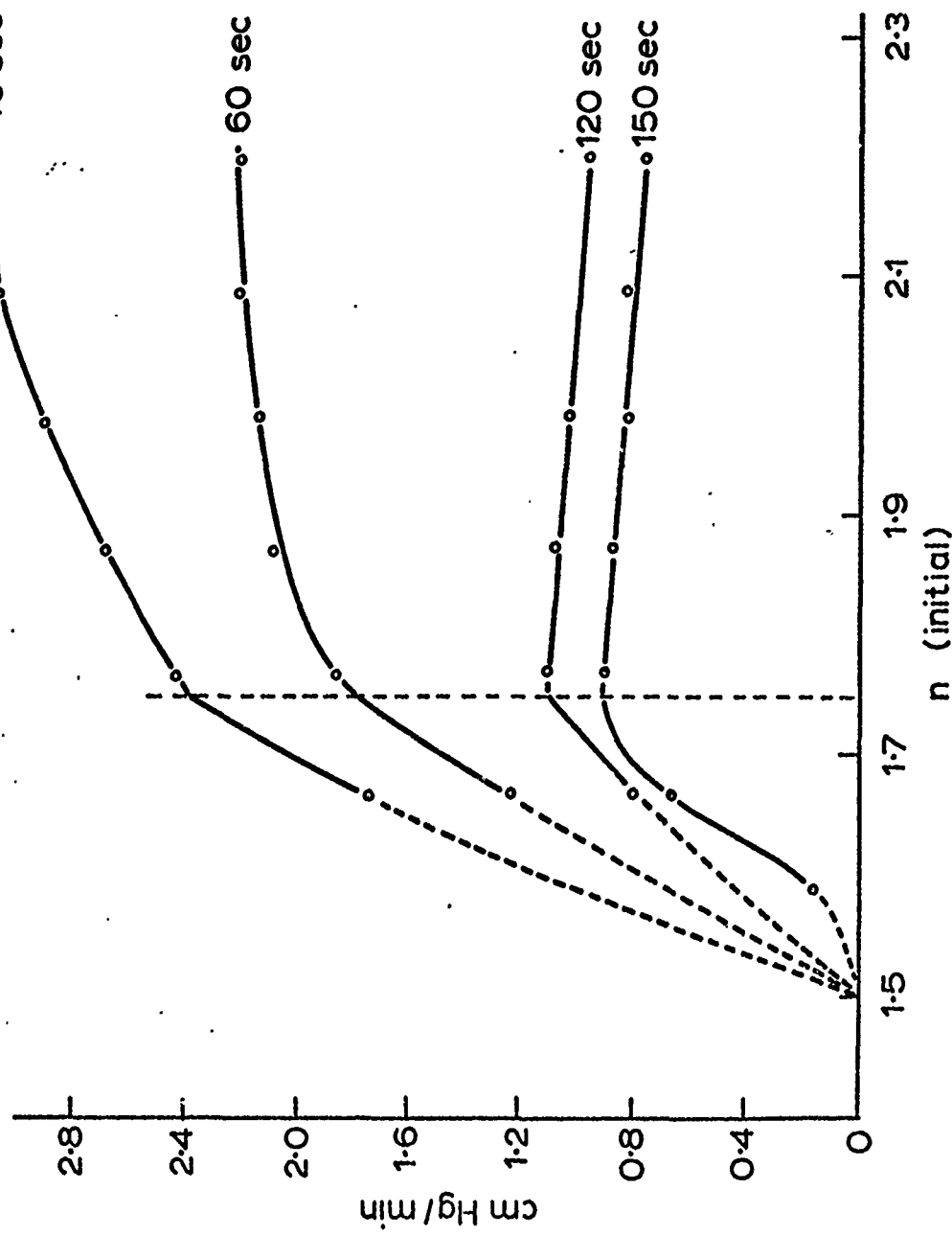
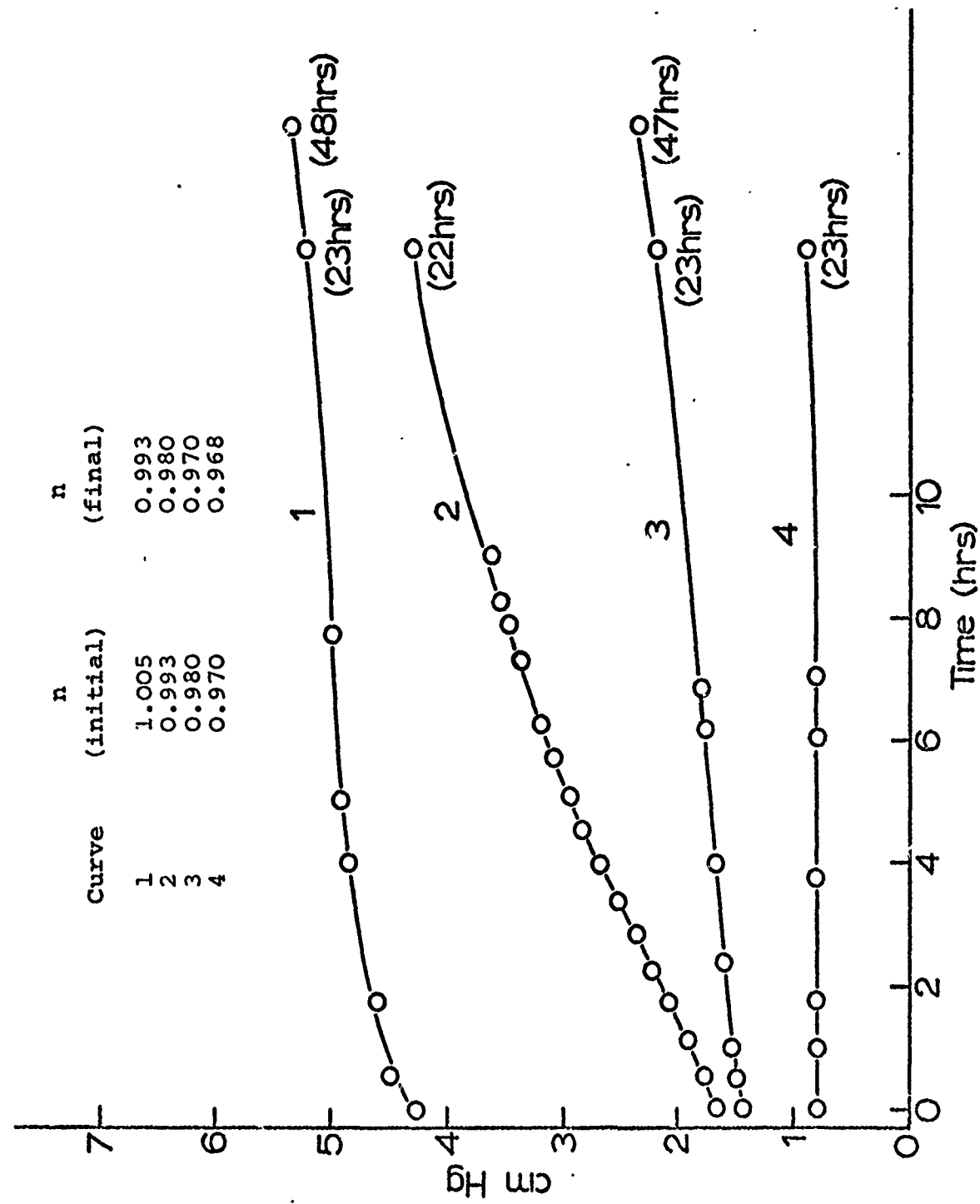


Fig. 3.8 Evolution of N_2O_4 by $Fe(NO_3)_3$ in N_2O_4 at
 n close to 1



- 42 -

to be that materials with $1 < n < 1.5$ are mixtures of two different phases, with $n = 1$ and $n = 1.5$.

(iv) $n \approx 1$

The significance of the sharp drop in vapour pressure at $n = 1$ has been noted above. Fig. 3.8 gives an indication that, although equilibrium is not being reached, a marked change in the properties of the system is taking place with a very small change in n . Hence it is reasonable to conclude that at $n = 1$ there is also, ideally, a vertical drop in the P vs n diagram.

3.3 Conclusions

Evidence has been found for the existence of the compound $\text{Fe}(\text{NO}_3)_3 \cdot 1.5\text{N}_2\text{O}_4$ at 10°C . The preparative, analytical, spectroscopic and X-ray powder diffraction results for materials $\text{Fe}(\text{NO}_3)_3 \cdot x\text{N}_2\text{O}_4$ described in Section 2 are thus rendered more easily intelligible in the light of the existence of this new compound. There is no evidence for the formation of compounds $\text{Fe}(\text{NO}_3)_3 \cdot n\text{N}_2\text{O}_4$ with n greater than about 2. The slight affinity of $\text{Fe}(\text{NO}_3)_3 \cdot 1.5\text{N}_2\text{O}_4$ for N_2O_4 will decrease at higher temperatures. It thus appears likely that the limiting composition of $\text{Fe}(\text{NO}_3)_3 \cdot n\text{N}_2\text{O}_4$ in contact with liquid N_2O_4 (ie. *in situ* flow-decay material) at normal ambient temperatures can, for all practical purposes, be taken as $\text{Fe}(\text{NO}_3)_3 \cdot 1.5\text{N}_2\text{O}_4$.

3.4 Appendices

TABLE 3.1

The density of N₂O₄ as a function of pressure at 10°C

Pressure (cm. Hg)	Measured Density (mg/300 ml)	Calculated Density (mg/300 ml)
14.15	179.4	180.1
20.32	265.8	266.6
25.35	336.5	338.0
29.55	398.2	398.4
30.40	412.3	410.6
33.45	458.6	454.5
35.70	490.5	487.2
40.27	557.5	553.4
42.95	605.3	592.9

TABLE 3.2

Vapour pressures of $\text{Fe}(\text{NO}_3)_3 \cdot n\text{N}_2\text{O}_4$, run 1.

n	'Equilibrium' pressure (cm. Hg)	Time allowed to equilibrate (hr.)
5.751	44.15	8
5.316	43.75	16
4.884	43.70	.4
4.464	43.70	70
4.032	43.40	13
3.608	43.50	24
3.183	43.35	24
2.750	43.05	24
2.344	42.85	26
1.951	41.90	16
1.600	36.90	170
1.543	18.00	19
1.534	6.95	20
1.490	6.15	24
1.452	6.05	24
1.429	6.00	89
1.374	5.91	43
1.238	5.82	218
1.083	5.71	96
0.993	5.22	48
0.968	0.88	25

TABLE 3.3

Vapour pressures of $\text{Fe}(\text{NO}_3)_3 \cdot n\text{N}_2\text{O}_4$, run 2

n	'Equilibrium' pressure (cm. Hg)	Time allowed to equilibrate (hr.)
3.070	43.70	1½
2.959	43.65	2
2.850	43.60	1
2.741	43.55	1½
2.631	43.45	1
2.525	43.65	13
2.414	43.45	1½
2.306	43.35	1
2.199	43.50	43.
2.092	43.20	5½
1.985	43.15	19
1.875	42.85	4
1.772	42.50	16
1.669	41.75	5½
1.590	39.35	24
1.561	25.00	93
1.554	11.05	48
1.549	7.35	360

4. PROPERTIES OF $\text{Fe}(\text{NO}_3)_3 \cdot 1.5\text{N}_2\text{O}_4$

The vapour pressure studies on the $\text{Fe}(\text{NO}_3)_3 \cdot n\text{N}_2\text{O}_4$ system indicated that the compound $\text{Fe}(\text{NO}_3)_3 \cdot 1.5\text{N}_2\text{O}_4$ was stable at 10°C if maintained under a pressure of at least 6 cm Hg of N_2O_4 . The work described in this section was an attempt to prepare, characterise and investigate some properties of this material at room temperature.

4.1 Preparation

A sample of $\text{Fe}(\text{NO}_3)_3 \cdot x\text{N}_2\text{O}_4$ prepared as described in Section 2 from $\text{FeCl}_3/\text{EtOAc}/\text{N}_2\text{O}_4$ was dissolved in the minimum volume of ethyl acetate at room temperature. The resulting viscous solution was filtered in a closed system through a 30 micron ('Porosity 3') glass sinter and evacuated for 18 hours (10^{-2} mmHg, 20°C). Excess liquid N_2O_4 was poured onto the resulting syrup. The mixture was shaken, and then maintained at -20°C for several hours when a brown, crystalline and apparently homogeneous solid was formed. This was filtered in a closed system, the solid (ca. 2g) washed well with liquid N_2O_4 and then tipped into a Schlenk tube while excluding air by means of a countercurrent of nitrogen. The Schlenk tube (of volume ca. 100 ml) was removed to a vacuum line, cooled to -196°C and degassed, and then a small amount of N_2O_4 was condensed onto the solid. (In terms of the overall composition of the system this amount was insignificant; it served only to increase the vapour pressure of N_2O_4 over the solid). The solid was allowed to warm to room temperature, and the intensity of the brown colour of the vapour above the solid was noted visually. The vapour was allowed to expand into an approximately equal

evacuated volume, whereupon the intensity of the brown colour of the vapour decreased considerably. The vessel containing the solid was then sealed, and the vapour pressure of N_2O_4 as monitored by the intensity of the brown colour did not increase noticeably during 24 hours. Analysis of the solid at this stage showed that $Fe(NO_3)_3 \cdot 1.5N_2O_4$ was produced ($N(III) = 5.48\%$, $Fe(NO_3)_3 \cdot 1.5N_2O_4$ requires 5.52%).

The solid was dark brown, and slowly developed a slight atmosphere of N_2O_4 . It was totally soluble in water. It may be noted that a product analysing as $Fe(NO_3)_3 \cdot 1.5N_2O_4$ was noted previously⁴ but was not further characterised.

4.2 Infra-red and Raman spectra

The infra-red spectrum in nujol and halocarbon mulls was measured on a Perkin-Elmer 457 spectrometer. The spectrum in nujol is shown in Fig. 4.1. The Raman spectrum of the solid was measured using a Spectra-Physics 125 He-Ne laser, 632.8nm line, and a Cary 81 spectrophotometer. The infra-red and Raman spectra are compared in Tables 4.1 and 4.2 with some compounds containing the tetranitratoferrate(III) anion. It is immediately recognised that $Fe(NO_3)_3 \cdot 1.5N_2O_4$ contains $Fe(NO_3)_4^-$, and does not contain any 'free' NO_4^+ in contrast to $Fe(NO_3)_3 \cdot N_2O_4$. There is no evidence for molecular N_2O_4 in the solid from the Raman spectrum, and the rate of development of the N_2O_4 bands in the infra-red spectrum of a nujol mull (Fig. 4.1) also makes it appear likely that $Fe(NO_3)_3 \cdot 1.5N_2O_4$ contains no molecular N_2O_4 . All the N_2O_4 seen in the spectrum is attributable to sample decomposition in contact with nujol. Decomposition occurred in a similar manner when halocarbon oil was used as a mulling agent, but was slower. Nitrate ion was

Fig. 4.1

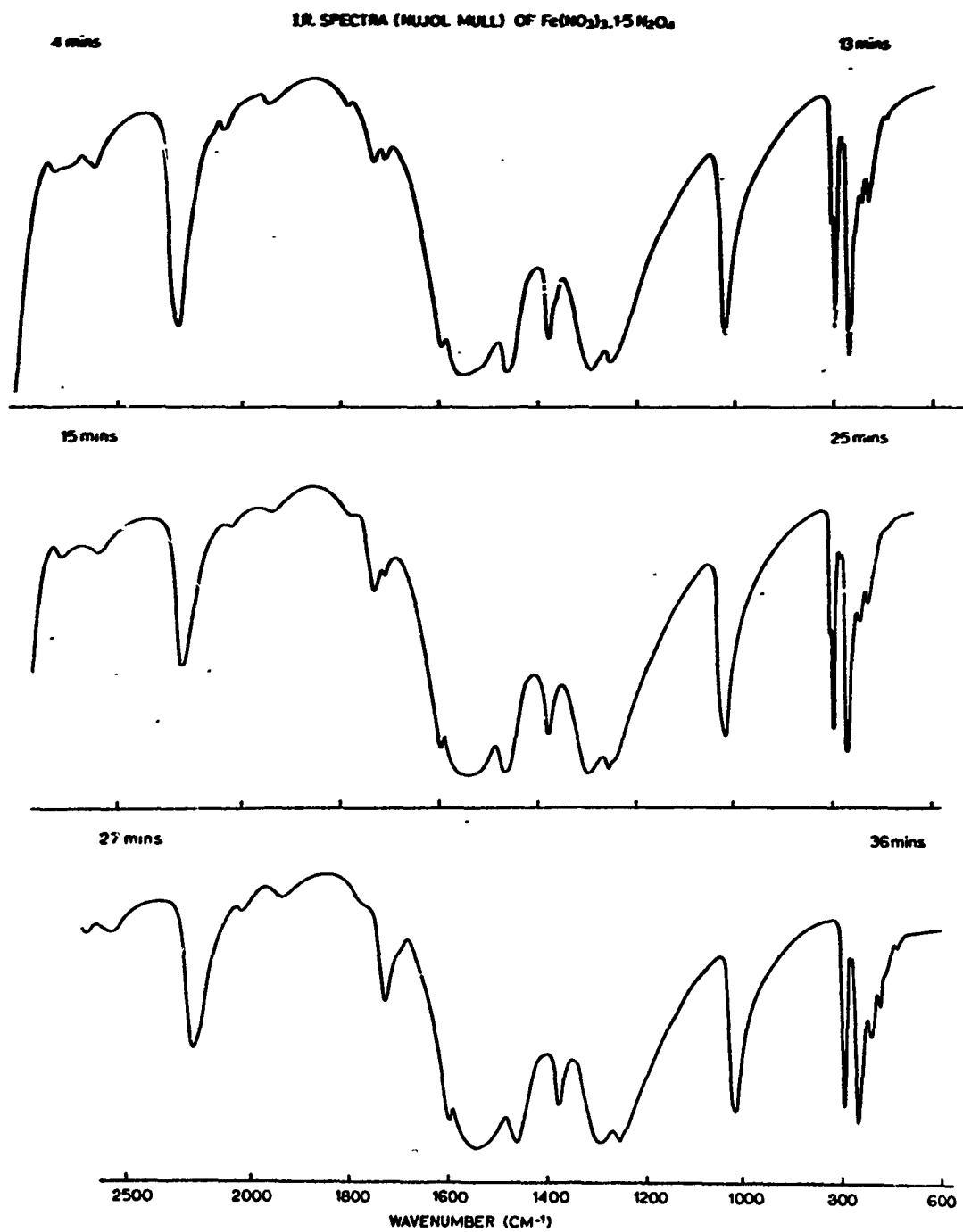


TABLE 4.1

The infra-red spectrum of $\text{Fe}(\text{NO}_3)_3 \cdot 1.5\text{N}_2\text{O}_4$ and related compounds
in nujol mulls (cm^{-1})

$\text{Fe}(\text{NO}_3)_3 \cdot 1.5\text{N}_2\text{O}_4$	$\text{Ph}_4\text{As}^+\text{Fe}(\text{NO}_3)_4^-$	$\text{NO}^+\text{Fe}(\text{NO}_3)_4^-$	Assignment (C_{2v} bidentate nitrate model)
2730 w b			$\nu_1 + \nu_2$
2570 w b		2298 m sp	$2\nu_4$
2235 vs b (A)		2230 vw b	NO^+ Coordinated NO^+
2040 vw b			$2\nu_2$
1940 w b			
1785 w b (A)			Coordinated NO^+
1735 b (B)			N_2O_4
1710 w b (A)			Coordinated NO^+
1600 s sp	1598 mw	1598 s sp)	ν_1 (N=O str.)
1560 vs vb	1542 s	1548 vs b)	
1300 vs b	1287 s)	1295 s b)	
	1280 sh))	ν_4 (NO_2 antisym. str.)
1255 vs b	1255)	
1250 sp (B)			N_2O_4
1020 vs sp	1014 s	1018 s sp	ν_2 (NO_2 sym. str.)
803 m vsp	801 m	789 s sp)	
800 s vsp)	ν_6 (NO_3 out of plane)
784 w vsp)	
770 s sp	766 s	764 vs sp	ν_3 (NO_2 sym. bend)
746 sp (B)			N_2O_4
717 vw			ν_5 (NO_2 antisym. bend)
695 vw			
(A) Decreases with time		(B) Increases with time	
References: N_2O_4 12		$\text{Ph}_4\text{As}^+\text{Fe}(\text{NO}_3)_4^-$ 11	

TABLE 4.2

The Raman spectrum of solid $\text{Fe}(\text{NO}_3)_3 \cdot 1.5\text{N}_2\text{O}_4$

$\text{Fe}(\text{NO}_3)_3 \cdot 1.5\text{N}_2\text{O}_4$	$\text{Ph}_4\text{As}^+ \text{Fe}(\text{NO}_3)_4^-$	$\text{NO}^+ \text{Fe}(\text{NO}_3)_4^-$	$\text{NO}^+ \text{Fe}(\text{NO}_3)_4^-$	Assignment
(a)	(b)	(a)	(a)	$(\text{C}_{2v} \text{ bidentate nitrate model})$
		*	2302 s sp	NO^+
2250 s b				
1600 m	1610 w	1615 ms	1610 ms	Co-ordinated NO^+
1580 ms	1588 s	1585 ms	1570 s	ν_1 ($\text{N}=\text{O}$ str.)
1550 w.	1550 w.	1550 mw	1550 mw	
1255 w			1263 mw	ν_4 (NO_2 antisym. str.)
1030 s sp	1031 s	1030 ms	1030 m	ν_2 (NO_2 sym str.)
785 m sp	782 m	788 mw	784 mw	ν_6 (NO_3 out of plane)
769 m sp	769 mw	770 mw	769 m	ν_3 (NO_2 sym. bend)
362 w	355 w	360 w	364 m	Metal-oxygen stretch

(a) this work

(b) ref 11

* Not investigated.

absent, and there was no evidence for the presence of other nitrato-iron species than $\text{Fe}(\text{NO}_3)_4^-$. Hence the cationic species contained in $\text{Fe}(\text{NO}_3)_3 \cdot 1.5\text{N}_2\text{O}_4$ is of empirical formula N_2O_3^+ , and contains at least one N-O bond of bond order close to 3. The bands attributable to this cation are those marked (A) in Table 4.1. Possible structures of this species will be discussed in Section 4.5.

4.3 Magnetic moment

The effective magnetic moment measured by the Gouy technique was 5.8 B.M. at 15°C, and measured by the Faraday method was 5.6 B.M. at 16°C. These values are compared with similar figures for other compounds containing tetra-nitratoferrate(III) in Table 4.3.

Table 4.3

	Mag. Moment B.M.	Temp. °C	Ref.
$\text{Fe}(\text{NO}_3)_3 \cdot 1.5\text{N}_2\text{O}_4$	5.8	15	
	5.6	16	
$\text{Ph}_4\text{As}^+ \text{Fe}(\text{NO}_3)_4^-$	5.85	18	11
$\text{Et}_3\text{NH}^+ \text{Fe}(\text{NO}_3)_4^-$	5.96	20	22
$\text{Et}_4\text{N}^+ \text{Fe}(\text{NO}_3)_4^-$	6.03	20	22
$\text{NO}^+ \text{Fe}(\text{NO}_3)_4^-$	5.83	16.5	4
$\text{NO}_2^+ \text{Fe}(\text{NO}_3)_4^-$	5.82	19	4

"Spin only" value for 5 unpaired electrons, 5.92 B.M.

The room temperature moment of $\text{Fe}(\text{NO}_3)_3 \cdot 1.5\text{N}_2\text{O}_4$ is consistent with its containing $\text{Fe}(\text{NO}_3)_4^-$ and a diamagnetic cation, (eg. $\text{N}_4\text{O}_6^{2+}$, rather than N_2O_3^+ which is expected to contain 1 unpaired electron.) However, this conclusion cannot necessarily be drawn from the measured moment for the

following reasons:

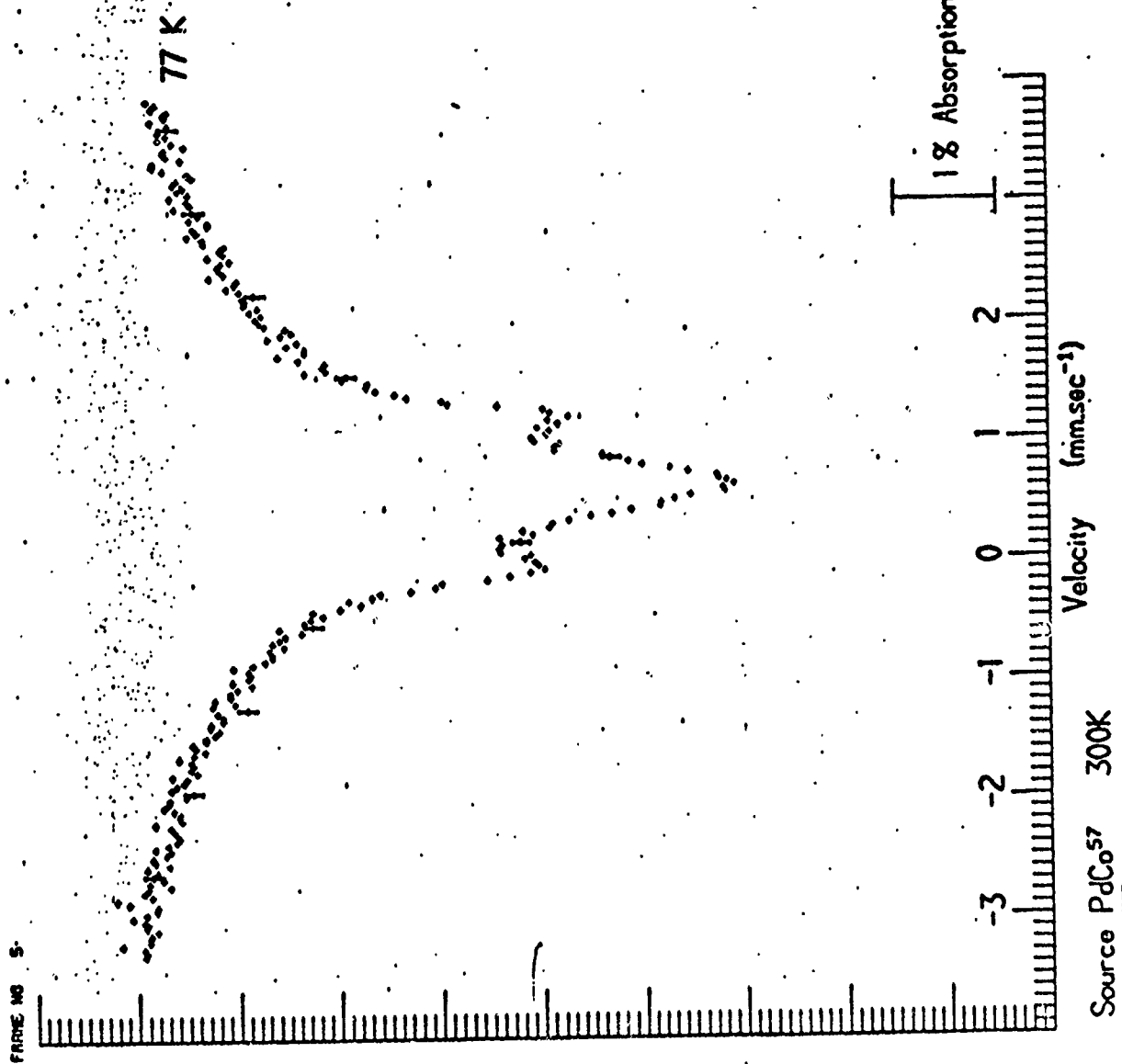
- A) A lattice containing a paramagnetic anion, viz. $\text{Fe}(\text{NO}_3)_4^-$ as well as N_2O_3^+ might have a lowered magnetic moment by antiferromagnetic coupling.
- B) Sufficient interaction between N_2O_3^+ units in the lattice to cause spin pairing could arise without the existence of significant bonding between them.

Some resolution of these alternatives might be provided by a measurement of the magnetic moment at various temperatures. However, this was not undertaken, as the crystal structure determination on this compound which is reported in Section 5 should provide direct information on the nature of the cation without the uncertainties involved in interpretation of magnetic data.

4.4 Mössbauer spectrum

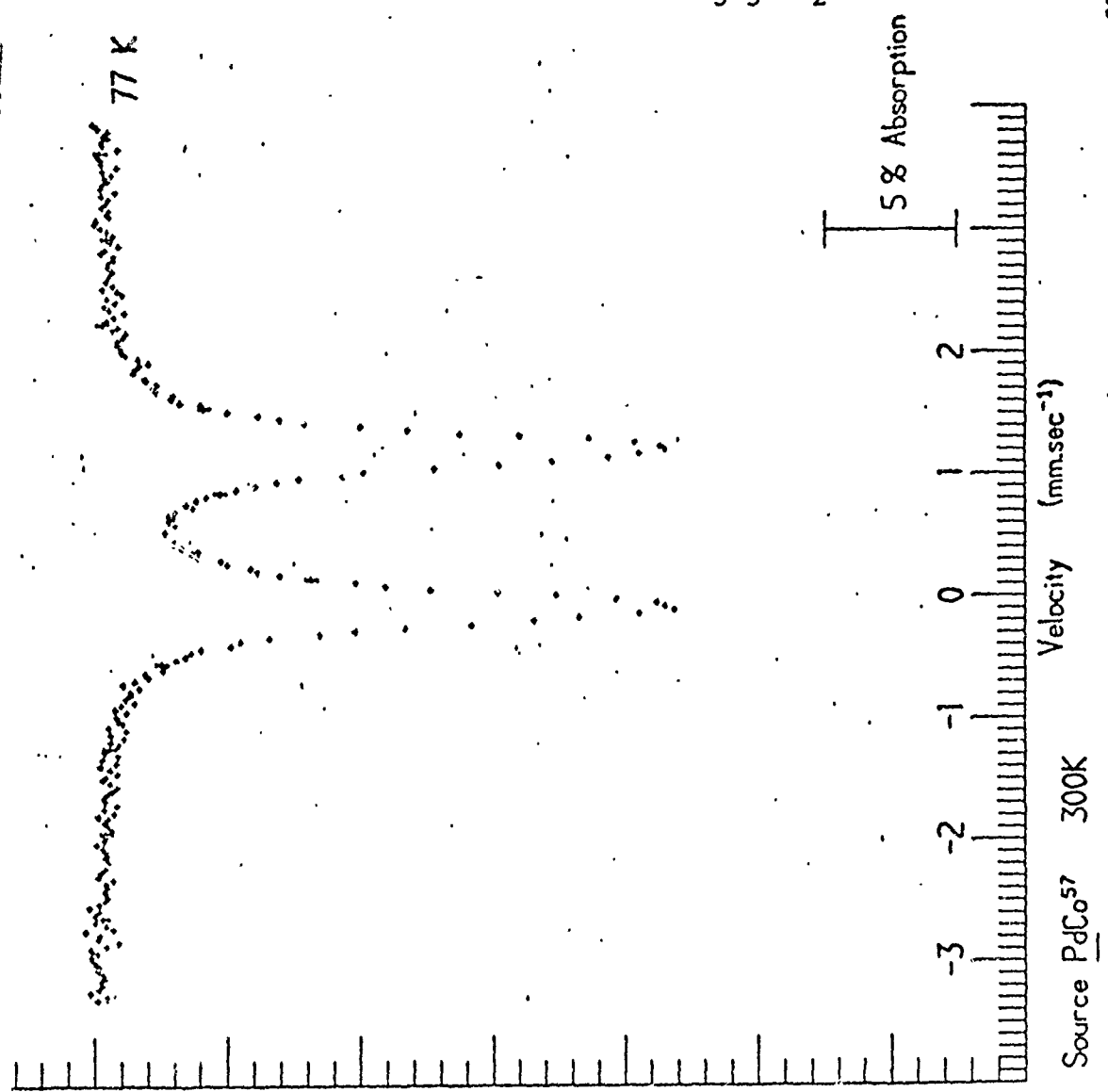
The Mössbauer spectrum is shown in Fig. 4.2. The peaks at $-0.15 \text{ mm sec}^{-1}$ and $+1.15 \text{ mm sec}^{-1}$ with respect to $\text{Pd}/^{57}\text{Co}$ are assigned to $\text{Fe}(\text{NO}_3)_3 \cdot 2\text{H}_2\text{O}$ (see Fig. 4.3), which is formed when $\text{Fe}(\text{NO}_3)_3 \cdot 1.5\text{N}_2\text{O}_4$ decomposes in the presence of water vapour (see Section 4.6). The remainder of the spectrum is a singlet at an isomer shift of $+0.55 \text{ mm sec}^{-1}$. This is assigned to tetranitratoferrate(III) and the lack of quadrupole splitting indicates that the anion has close to cubic symmetry. The width at half height of this line is ca 1.0 mm sec^{-1} and is hence appreciably broadened from the Heisenberg line width (ca 0.15 mm sec^{-1}), which may

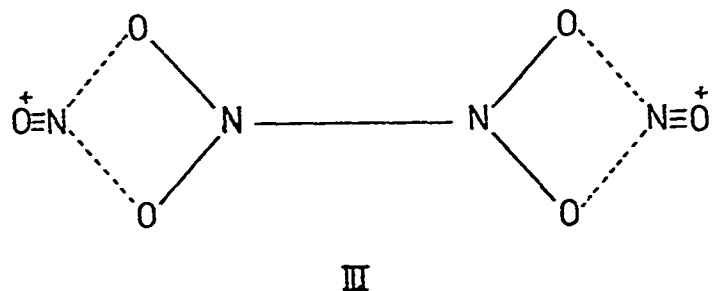
Fig. 4.2 The Mössbauer spectrum of $\text{Fe}(\text{NO}_3)_3 \cdot 1.5\text{N}_2\text{O}_4$



25/05/72/01

Fig. 4.3. The Mössbauer spectrum of $\text{Fe}(\text{NO}_3)_3 \cdot 2\text{H}_2\text{O}$





III

Non-planar species similar to I, II and III, although possible, are considered less likely because the opportunity for π -overlap would be lost.

Whatever the cationic species, the assignment of the bands at 1785 cm^{-1} and 1710 cm^{-1} is difficult. Their low intensities argue against assignment to fundamental modes of any of the structures, I, II or III.

The coordination of NO^+ by NO_2 has been postulated previously to explain the Raman spectrum of $\text{N}_2\text{O}_4/\text{HNO}_3$ mixtures and the presence of the species N_2O_3^+ was proposed.¹⁶ A later investigation of the magnetic susceptibility of the mixtures showed them to be diamagnetic, so that the presence of an N_2O_3^+ monomer seems unlikely.²³

4.6 X-ray powder diffraction data

The X-ray powder diffraction pattern was measured using a Phillips X-ray powder diffractometer camera of radius 11 cm and $\text{FeK}\alpha$ radiation. Interplanar spacings and visually estimated intensities are listed in Table 4.4. Some preliminary attempts were made to index this very complex pattern, using a computer programme capable of indexing orthorhombic or higher symmetry systems. No satisfactory indexing was obtained.

The usual technique of obtaining X-ray powder diffraction patterns of moisture sensitive compounds involves filling degassed (200°C , 10^{-2} mm Hg, 16 hr.) capillary tubes with the solid in a dry-box, sealing with silicone grease before removal from the dry-box, followed by flame sealing of the tube. A number of powder photographs of $\text{Fe}(\text{NO}_3)_3 \cdot 1.5\text{N}_2\text{O}_4$ has been obtained and in several cases, a set of lines additional to those arising from $\text{Fe}(\text{NO}_3)_3 \cdot 1.5\text{N}_2\text{O}_4$ is seen. The intensity of these additional lines progressively increased as consecutive powder photographs were run on the same tube of sample. This extra set of lines was caused by gradual decomposition due to improper sealing of the X-ray tubes.

The material giving rise to the extra set of lines was identified as $\text{Fe}(\text{NO}_3)_3 \cdot 2\text{H}_2\text{O}$ by comparison with X-ray powder data for an authentic sample of this compound prepared by the published method²⁴. Interplanar spacings and intensities for $\text{Fe}(\text{NO}_3)_3 \cdot 2\text{H}_2\text{O}$ are recorded on Table 4.5. Extra lines were also occasionally observed due to the presence of an unidentified compound thought perhaps to be a hydrate of iron(III) nitrate lower than $\text{Fe}(\text{NO}_3)_3 \cdot 2\text{H}_2\text{O}$. Interplanar spacings and intensities for this material are also listed in Table 4.5.

The difficulty of sealing the Lindemann glass (lithium beryllium borate) X-ray capillary tubes when containing iron compounds has been previously noted in these laboratories, and the problem was solved by multiple running of several sample tubes filled in the usual way and then flame sealed.

TABLE 4.4

d-values for $\text{Fe}(\text{NO}_3)_3 \cdot 1.5\text{N}_2\text{O}_4$ prepared from $\text{FeCl}_3/\text{EtOAc}/\text{N}_2\text{O}_4$

<u>d (Å)</u>	<u>Intensity</u>
9.9	2
9.3	20
8.2	10
7.6	60
7.20	70
6.81	30
6.31	80
5.65	30
5.45	5
5.20	15
4.86	2
4.61	100
4.42	30
4.27	30
4.10	50
3.77	70
3.60	60
3.44	60
3.36	5
3.28	40
3.18	25
3.08	20
3.00	20
2.81	50
2.68	10
2.60	20
2.45	50
2.40	15
2.34	15
2.31	15
2.21	50
2.14	15
2.07	10
1.99	15
1.91	5
1.87	10
1.84	10
1.81	10
1.76	15

TABLE 4.5

d-values for $\text{Fe}(\text{NO}_3)_3 \cdot 2\text{H}_2\text{O}$ and unidentified decomposition product
of $\text{Fe}(\text{NO}_3)_3 \cdot 1.5\text{N}_2\text{O}_4$ in air.

<u>$\text{Fe}(\text{NO}_3)_3 \cdot 2\text{H}_2\text{O}$</u>		<u>Unidentified product</u>	
d-spacing (Å)	Intensity	d-spacing (Å)	Intensity
6.57	80	7.32	70
6.10	80	7.01	80
4.95	5	6.16	80
4.08	40	5.58	15
3.75	2	5.05	10
3.68	20	4.56	100
3.59	20	4.36	5
3.44	5	4.03	15
3.35	100	3.75	40
3.20	15	3.56	40
3.15	15	3.38	50
2.99	10	3.22	50
2.81	15	3.01	2
2.73	5	2.80	15
2.67	5	2.66	2
2.51	10	2.57	15
2.48	10	2.42	30
2.43	2	2.29	10
2.35	30	2.18	20
2.30	2		
2.22	5		
2.06	20		
1.98	20		
1.90	10		

An alternative and more convenient method was developed, in which the X-ray capillary tube was removed from the dry-box, sealed with silicone grease, and then sealed at a length suitable to fit into the X-ray camera with melted 'Apiezon L' grease, which has a melting point slightly above room temperature.

It is of interest to note that before the compound $\text{Fe}(\text{NO}_3)_3 \cdot 1.5\text{N}_2\text{O}_4$ had been isolated and identified, its characteristic X-ray diffraction pattern was also observed in the products of reactions involving:

- A) The recrystallisation of $\text{Fe}(\text{NO}_3)_3 \cdot x\text{N}_2\text{O}_4$ from $\text{MeNO}_2/\text{N}_2\text{O}_4$ mixtures (cf. recrystallisation from MeNO_2 (Section 2.1) which gives the pattern of $\text{Fe}(\text{NO}_3)_3 \cdot \text{N}_2\text{O}_4$).
- B) The recrystallisation of $\text{Fe}(\text{NO}_3)_3 \cdot \text{N}_2\text{O}_4$ from $\text{HNO}_3/\text{N}_2\text{O}_4$, on occasion (see Section 7.5).
- C) The initial product of the reaction of NOFeCl_4 and N_2O_4 (see Section 2.1 and Fig. 2.2).

4.7 The reaction of $\text{Fe}(\text{NO}_3)_3 \cdot 1.5\text{N}_2\text{O}_4$ with N_2O_4

The studies on the vapour pressure of $\text{Fe}(\text{NO}_3)_3 \cdot n\text{N}_2\text{O}_4$, described in Section 3, indicated that there was some association of $\text{Fe}(\text{NO}_3)_3 \cdot 1.5\text{N}_2\text{O}_4$ with further N_2O_4 . An attempt was made to study this association by means of X-ray powder photography. $\text{Fe}(\text{NO}_3)_3 \cdot 1.5\text{N}_2\text{O}_4$ was loaded into a capillary tube in a dry-box and liquid N_2O_4 was pipetted onto the solid.

The tube and contents were then frozen in liquid nitrogen, sealed with silicone grease, removed from the dry box while still immersed in liquid nitrogen, and flame sealed.

No discernible change in the powder pattern occurred over 4 months, and hence the further N_2O_4 associated with $Fe(NO_3)_3 \cdot 1.5N_2O_4$, indicated by the vapour pressure studies, appears to be present as weakly bound lattice N_2O_4 or NO_2 molecules. This is consistent with its high dissociation vapour pressure.

4.8 The evacuation of $Fe(NO_3)_3 \cdot 1.5N_2O_4$ at room temperature

The effect of evacuation on $Fe(NO_3)_3 \cdot xN_2O_4$ has been followed by infrared spectroscopy (Section 2.4, Fig. 2.2). The initial product employed in these studies may now be identified as the compound $Fe(NO_3)_3 \cdot 1.5N_2O_4$. The bands attributable to molecular N_2O_4 seen in Fig. 2.2 are now attributed to sample decomposition in contact with nujol (see Section 4.2 and Fig. 4.1).

4.9 Attempts to coordinate NO^+ by N_2O_4 in compounds other than $NO^+Fe(NO_3)_4^-$

The vibrational spectrum of $Fe(NO_3)_3 \cdot 1.5N_2O_4$ showed only three bands assignable to its cationic component. It was hoped that other NO^+ compounds would form 'adducts' with NO_2 and that in these cases the anion vibrations might not obscure the vibrational spectrum of cationic species such as $N_2O_3^{2+}$ or $N_4O_6^{2+}$.

No evidence could be obtained for the reaction of $NO^+BF_4^-$ (by IR and X-ray diffraction) or $NO^+HSO_4^-$ (by IR) with liquid

N_2O_4 even after 16 hr. contact at room temperature. $NO^+SbCl_6^-$ was reacted with liquid N_2O_4 for 20 minutes at room temperature. The product was incompletely soluble in water, and its infrared spectrum indicated the presence of nitrato-groups in the product. No bands definitely attributable to a coordinated cationic species were seen.

4.10 The coordination of NO^+ by $NOCl$.

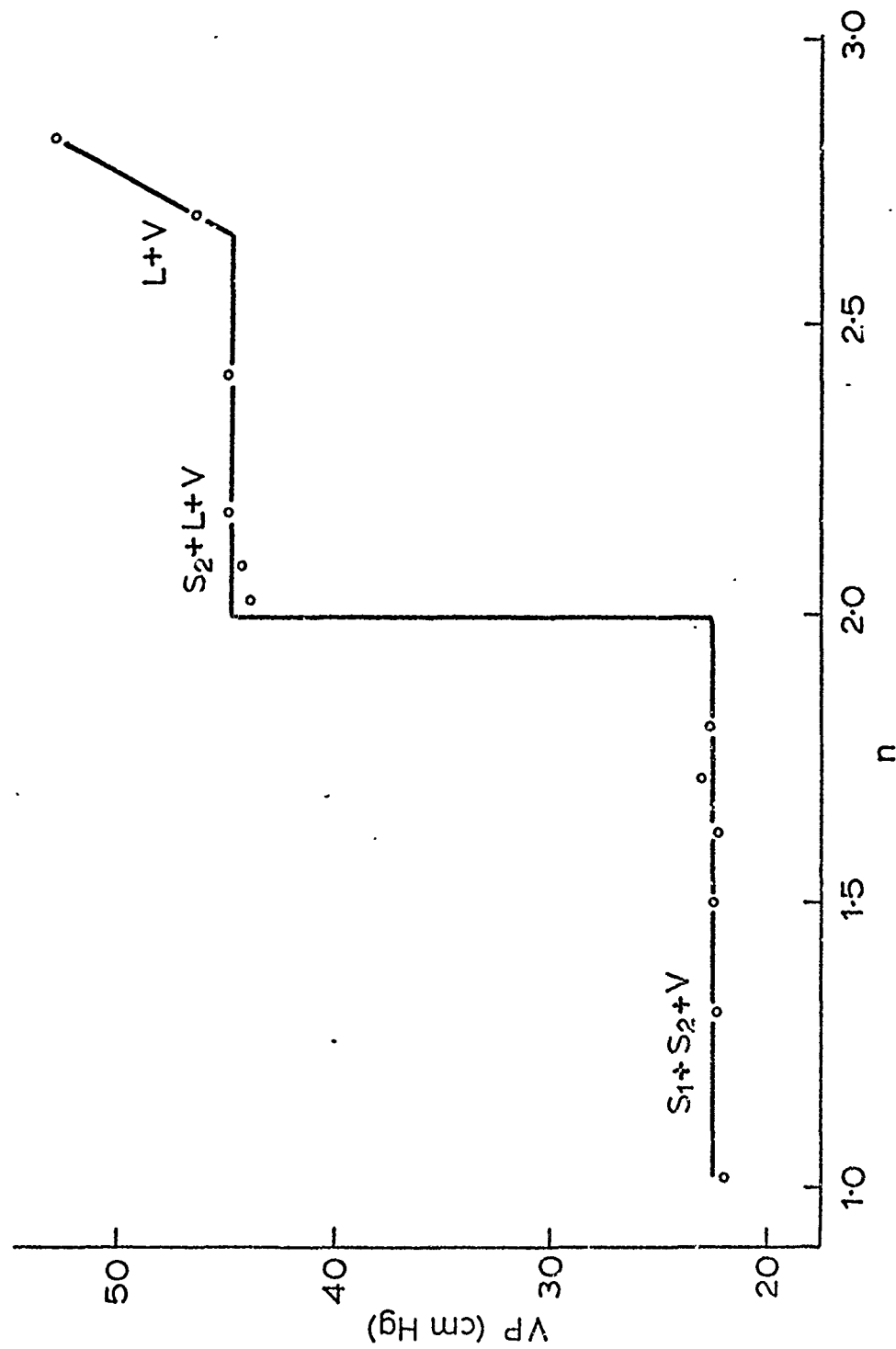
The conductance of NO^+ salts in $NOCl$ has been considered to involve the species $NO^+.NOCl$ ^{18,25}. There is no agreement at present however on its structure. It has been represented as linear²⁵ or $O=N-Cl-N=O$ ('W' shape). The compound $FeCl_3 \cdot 2NOCl$ has been shown to exist¹⁸. It was considered on (insufficient) magnetic evidence not to be a nitrosyl-iron complex, and it was suggested²⁶ that it should be represented as $(NO^+.NOCl)FeCl_4^-$.

The vapour pressure of the $NOFeCl_4^-$ - $NOCl$ system at $0^\circ C$ is shown in Fig. 4.4. The phases present in the $FeCl_3 \cdot nNOCl$ system are indicated in this Figure ($S_1 = FeCl_3 \cdot NOCl$, $S_2 = FeCl_3 \cdot 2NOCl$, L = liquid, V = vapour).

Pure iron sheet (5g.) was dissolved in $NOCl$ (ca 100 ml.) which was maintained at $-15^\circ C$ for 16 hr., by which time reaction appeared to have ceased. It was then maintained at $-33^\circ C$ and most of the $NOCl$ was evaporated under vacuum. It was then heated to $0^\circ C$ and gently evacuated until there was just no liquid phase visible. The composition should at this point be $FeCl_3 \cdot 2NOCl$ (see Fig. 4.4). The product was removed to a dry box, and was noted to be liquid at room temperature. A sample was pipetted into a Raman cell, capable

Fig. 4.4.

The Vapour Pressure of $\text{FeCl}_3 \cdot n \text{NOCl}$ at 0°C

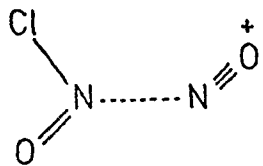


of withstanding several atmospheres pressure, which was then removed from the dry box and flame sealed. Several samples were placed between AgCl plates, and an infra-red spectrum obtained.

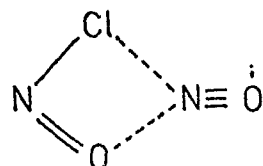
Vibrational spectroscopic data for the product are shown in Table 4.6. The band at 2170 cm^{-1} (IR), 2186 cm^{-1} (R) is attributed to NOFeCl_4^- , formed by sample decomposition, due to the high vapour pressure of NOCl developed by the product. NO^+ in $\text{NO}^+\text{FeCl}_4^-$ produces a band at 2200 cm^{-1} ⁴². The rest of the spectrum indicates that $\text{FeCl}_3 \cdot 2\text{NOCl}$ contains FeCl_4^- and NO^+NOCl . The $\text{N}\equiv\text{O}^+$ frequency is lowered to 1950 cm^{-1} (cf. 2235 cm^{-1} in NO^+NO_2 , in $\text{Fe}(\text{NO}_3)_3 \cdot 1.5\text{N}_2\text{O}_4$), indicative of strong bonding between the NO^+ and NOCl . The bands assigned to the "NOCl" component of the species NO^+NOCl are compared in Table 4.7 with those of NOCl . NOCl liquid is known to be associated¹⁸; NOCl solution in N_2O_4 and NOCl gas will be progressively less associated. This trend is shown in the vibrational frequencies in Table 4.7.

The polarisation and frequencies of the bands render unlikely any centrosymmetric structure and the 'W' shaped structure for the ion NO^+NOCl .

The evidence available at present indicates the most likely structure to be I or II:



I



II

TABLE 4.6

The vibrational spectrum of $\text{FeCl}_3 \cdot 2\text{NOCl}$.

IR (cm^{-1})	R (cm^{-1})	Assignment
2170 s b	2186 s b(p)	'free' NO^+
1950 vs vb	ca. 2000 vw sh	$\text{NO}^+\cdot\text{NOCl}$, NO^+
1595 s b	a	$\text{NO}^+\cdot\text{NOCl}$, NO str.
500 m b	490 w b(p)	$\text{NO}^+\cdot\text{NOCl}$, NCl str.
c	332 m sp(p)	FeCl_4^- (ν_1 , A_1)*
c	260 s b(p)	$\text{NO}^+\cdot\text{NOCl}$, NOCl bend
c	101 w	FeCl_4^- (ν_2)*

* FeCl_4^- in NaFeCl_4 :	ν_1 330 cm^{-1}	s(p) Ref 27
	ν_2 106	m
	ν_3 385	w diffuse
	ν_4 133	w

a too weak to be observed

c not investigated

(p) polarised

TABLE 4.7

The vibrational spectrum of NOCl

	NOCl gas	NOCl. 28	NOCl. 25% in N ₂ O ₄	NOCl. liquid	NO ₂ NOCl in NOCl ₃ , 2NOCl
IR			R	R	R
NO str.	1800		a	a	a
NC1 str.	595	559w		548w	495 w b (p) 500 m b
ONCl bend	332	307s		292s	260 s b (p) c
					1595 s b

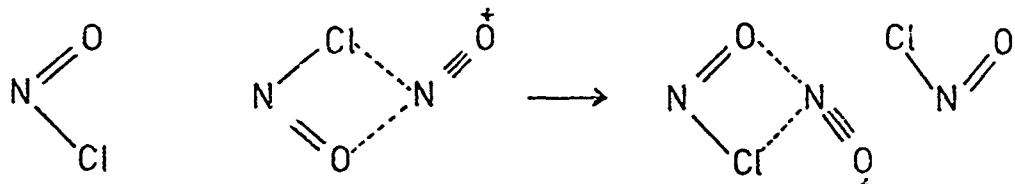
p too weak to be observed

c not investigated

(p) polarised

with a slight preference for II for the following reasons:-

A) The transport number observed for NO^+ in solutions of $\text{NO}^+\text{FeCl}_4^-$ in NOCl is estimated as about 0.9.¹⁸ The mode of association depicted in I cannot easily account for this high value, which seems to imply a special type of chain mechanism for conductance by NO^+ akin to the "proton switch" mechanism in certain protonic solvents eg. H_2SO_4 . Such a mechanism is more readily visualised in terms of associative mode II eg.



B) The non-observance of the $\text{N}\equiv\text{O}^+$ stretch in the Raman spectrum is striking in view of the high bond order. This effect is also noted in NOCl , and it may be that the low intensity is caused in each case by the proximity of the chlorine atom. (In N_2O_3 , whose structure is as I, but replacing Cl by O, the $\text{N}\equiv\text{O}$ stretch is strong²⁹).

An attempt was also made to obtain the compound $\text{SbCl}_5 \cdot 2\text{NOCl}$, by gradual evaporation of a solution of NOSbCl_6 in NOCl at -15°C . When the product was just completely solid, it was transferred to a dry box. An infra-red spectrum of the product in a nujol null gave no evidence of coordination of $\text{NO}^+\text{SbCl}_6^-$ with NOCl , but on repeated running of the same null, a broad

band at about 1920 cm^{-1} increased in intensity. This may be due to the formation of NOCl from $\text{NO}^+\text{SbCl}_6^-$ either by contact with nujol or by the heat of the infra-red beam, with subsequent coordination of NOCl to NO^+ .

SECTION 5

Single Crystal X-Ray study of $\text{Fe}(\text{NO}_3)_3 \cdot 1.5\text{N}_2\text{O}_4$

A sample of $\text{Fe}(\text{NO}_3)_3 \cdot x\text{N}_2\text{O}_4$ prepared from $\text{FeCl}_3/\text{EtOAc}/\text{N}_2\text{O}_4$ as in Section 2 was dissolved in ethyl acetate and the solution was filtered. On addition of a large excess of liquid N_2O_4 to this solution, yellow, plate-like crystals were deposited. These were filtered off and discarded. Excess N_2O_4 was added to the filtrate which was left to stand overnight at -20°C . The product was a batch (ca 0.2g) of discrete, cube-shaped crystals. Several of these were mounted into X-ray tubes along with a little liquid N_2O_4 , inside a dry-box. The tubes were then frozen in liquid nitrogen and removed from the dry box. They were then sealed in a flame, great care being taken not to allow any contact with moist air. Weissenberg photographs indicated the space group to be $\text{P}2_1/c$. 1731 reflections were collected to a Bragg angle of 20° on a 4-Circle Diffractometer. The calculated unit cell dimensions are:- $a = 10.419$, $b = 19.930$, $c = 14.435\text{\AA}$, $\beta = 128^\circ 53'$ in substantial agreement with those calculated for a different crystal used in a preliminary study, (Ref. 15 p.18) ie. $a = 10.218$, $b = 19.873$, $c = 14.337\text{\AA}$, $\beta = 123^\circ 18'$

A Patterson map yielded the coordinates of the iron atoms, and a Structure Factor calculation to derive signs to be used with the observed Structure Factors in calculating the Fourier Synthesis, was carried out. This first Fourier Synthesis was interpreted in terms of 25

atoms (2 iron atoms, 17 oxygen atoms and 6 nitrogen atoms).

These 25 atoms and their coordinates were then put into a Structure Factor calculation and this information was used to compute a Difference Fourier map. Examination of this map yielded a further 9 atoms.

The disposition of these 34 atoms has been interpreted as follows:- There are 2 iron atoms per asymmetric unit, and four nitrate groups associated with one of these iron atoms each exhibit bidentate coordination and are arranged in the same relative orientation as found for the compound $\text{Ph}_4\text{As}^+\text{Fe}(\text{NO}_3)_4^{-30}$. $\text{Fe}(\text{NO}_3)_3 \cdot 1.5\text{N}_2\text{O}_4$ thus becomes the second compound for which dodecahedral coordination of Fe(III) by eight oxygen atoms has been established. There is some doubt, however, at the moment as to the exact arrangement of the nitrate groups about the second iron atom. Three of the nitrate groups appear to be in the expected positions but the situation of the fourth is still uncertain. It is thought probable that the uncertainty in the location of this last nitrate group is affecting the interpretation of the remaining peaks in terms of a reasonable configuration for the cation.

It may be necessary to collect additional data using another crystal to assist this refinement of the last nitrate group. It had been hoped to complete the structure in time to include a full statement in the Final Report. This will not now be the case, but the work will be continued. We believe that the structure of the cation, and its position

in the crystal may well be very relevant to the separation of flow-decay material.

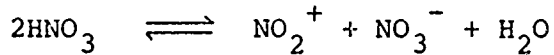
6. SOLUTIONS OF $\text{Fe}(\text{NO}_3)_3 \cdot x\text{N}_2\text{O}_4$ IN 100% HNO_3

6.1 Introduction

Since nitric acid is one of the contaminants of propellant N_2O_4 which may be involved in the production of the flow-decay material, it was of interest to examine the nature of $\text{Fe}(\text{NO}_3)_3 \cdot x\text{N}_2\text{O}_4$ in 100% nitric acid. This adduct forms apparently stable brown solutions in 100% HNO_3 and the infra-red and Raman spectra of such solutions were recorded in order to ascertain the species present.

Before discussion of these spectra, however, it is relevant to consider briefly the role of 100% HNO_3 as a reagent and solvent, its preparation in a pure state and its infrared and Raman spectra.

'100%' HNO_3 is a mixture of the free acid, acid anhydride and water in accordance with the equilibrium



for which several lines of physical evidence are available.³¹

The reagent has been used with little success in the preparation of anhydrous nitrates and its reactions with the anhydrous chlorides CrCl_2 , CrCl_3 , MnCl_2 , FeCl_2 , FeCl_3 ,²⁴ CoCl_2 , NiCl_2 , and CuCl_2 produce only hydrated nitrates.

In spite of this, 100% HNO_3 has been used with success in these laboratories in the recrystallization of anhydrous nitrate complexes, e.g. $\text{NO}_2^+ \text{Au}(\text{NO}_3)_4^-$ and $\text{K}^+ \text{Au}(\text{NO}_3)_4^-$.³²

6.2 Preparation of 100% HNO₃

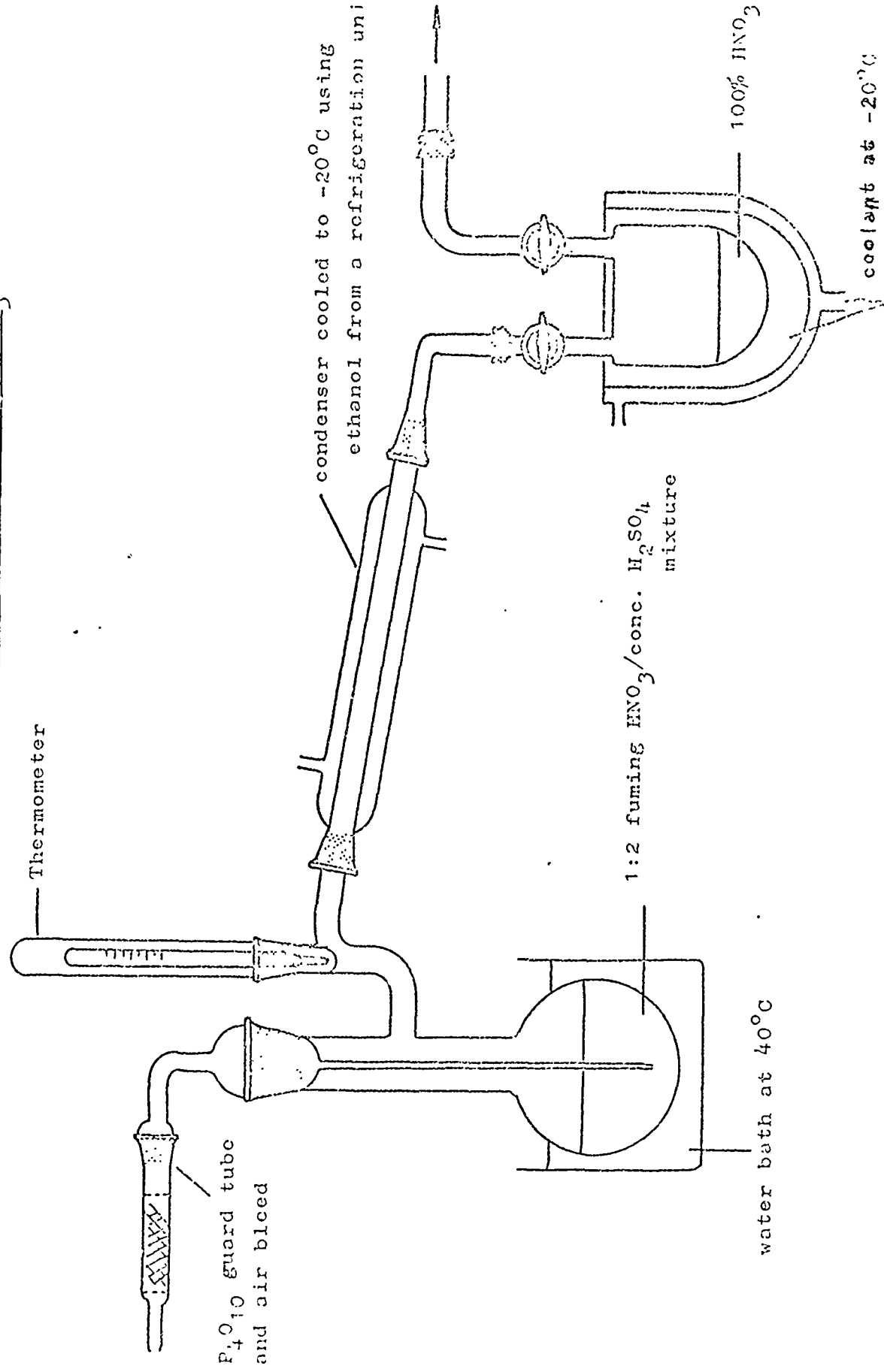
100% nitric acid is prepared using the apparatus illustrated in Fig. 6.1. A mixture of fuming HNO₃ and concentrated H₂SO₄ (1:2, v:v) is heated to 40°C (10⁻² mm) at which temperature 100% HNO₃ distils into the receiver. Yields are improved if both the condenser and receiver are cooled to ca -20°C. Acidimetric assay of the product was typically (100.5[±]0.5)%. Products which did not fall within these limits, or which showed the presence of a trace of sulphate (BaCl₂ test) were re-distilled.

6.3 The Vibrational Spectrum of 100% HNO₃

The infra-red spectrum of 100% HNO₃ was recorded on a Perkin-Elmer 457 spectrometer using a specially designed Kel-F solution cell fitted with silver chloride windows separated by a Teflon spacer (ca 10 μ). The Raman spectrum was recorded on a Cary 81 spectrophotometer using a Spectra-Physics 125 He-Ne laser as an excitation source (output approx. 60mW at 632.8 nm). Samples for Raman spectroscopy were contained in glass capillary cells (ca 1 mm i.d.) and were filled and sealed in a dry-box. Depolarisation ratios were determined in the usual manner. The values were obtained by calibration of the sample cell with CCl₄. The polarisation ratios for the bands of this compound are accurately known.

The bands attributable to 100% nitric acid are listed in Table 6.1 and are illustrated in Figs. 6.2 (infra-red) and 6.3 (Raman). The infra-red spectrum is as expected for

Figure 6.1 Apparatus for the preparation of 100% HNO_3



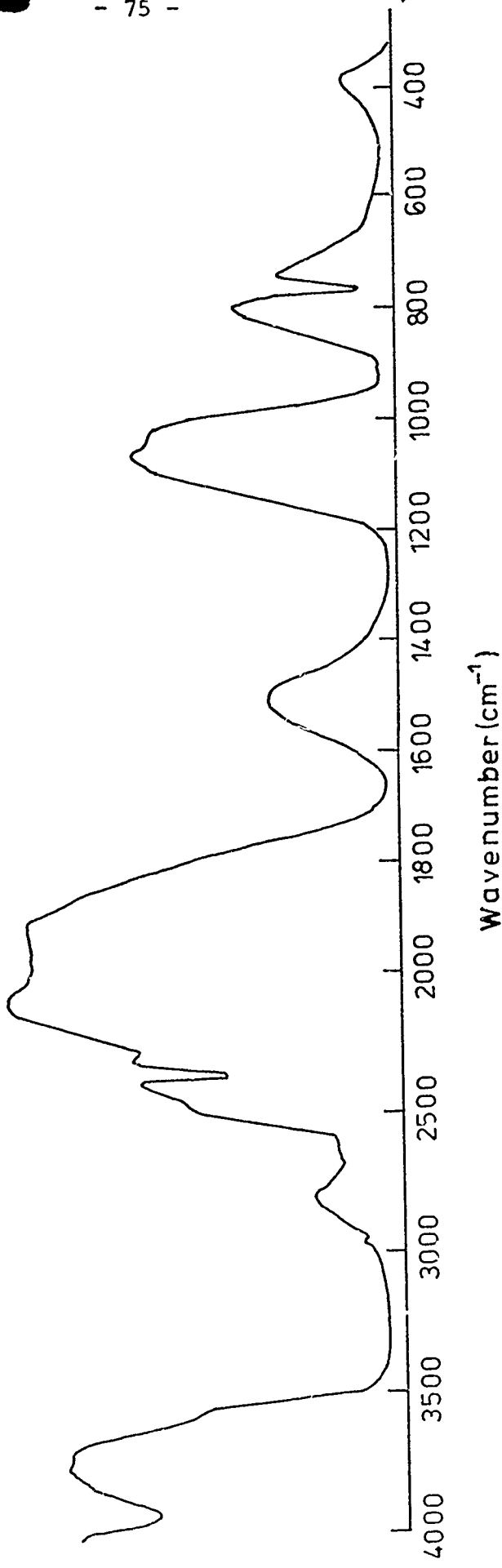


Fig. 6.2 I.R. Spectrum of HNO₃

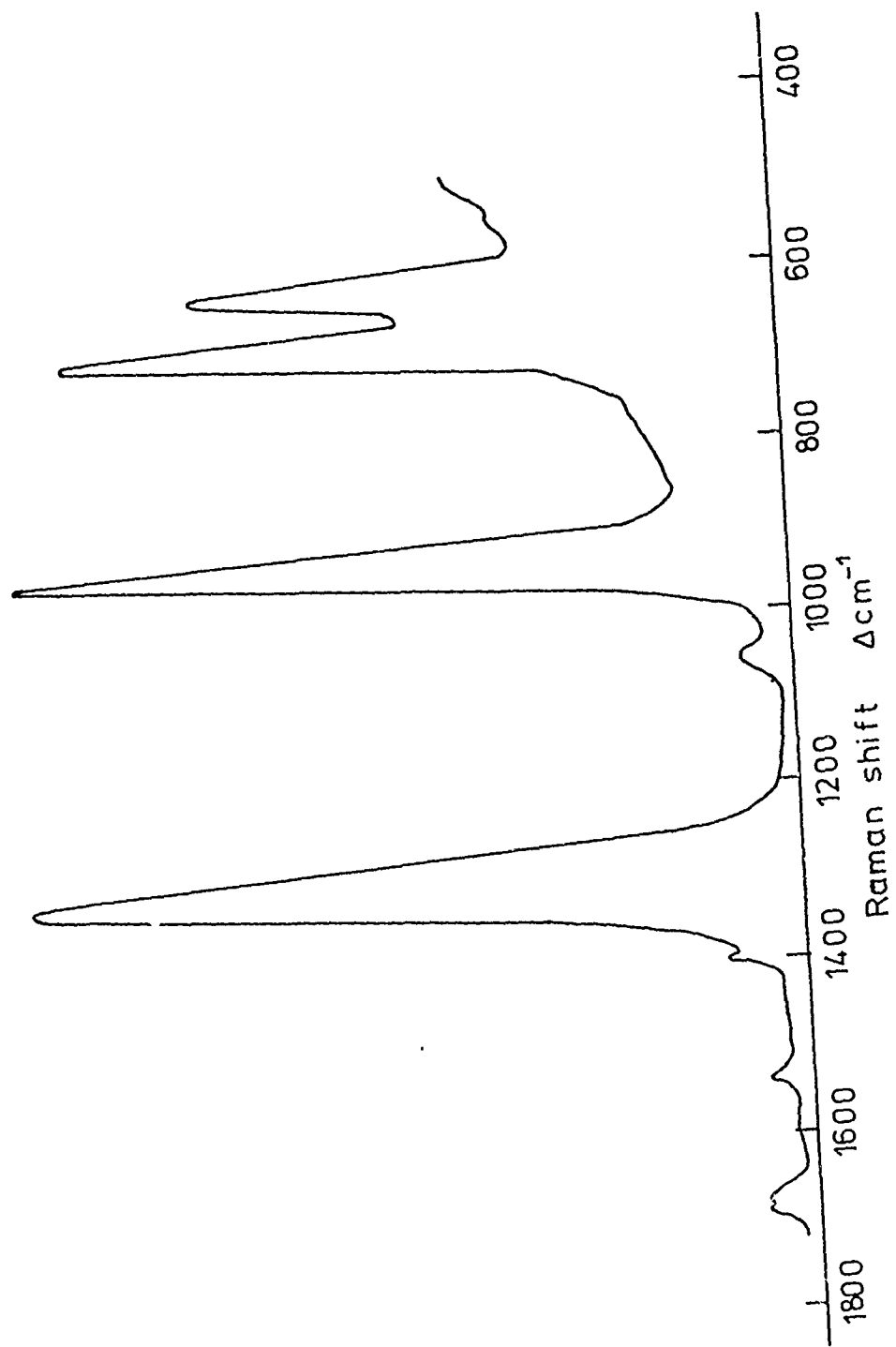


Fig. 6.3 Raman Spectrum of HNO₃

- 11 -
TABLE 6.1Vibrational spectrum of 100% HNO₃

Infra-red (cm ⁻¹)	Raman (cm ⁻¹)	Assignment *
3900 m		
3250 vs, vb		HNO ₃ ν ₁ (O-H str.)
2600 sh		HNO ₃ 2ν ₄
2365 m, sp		{
2355 sh		{ NO ₂ ⁺ ν ₃ (antisym. str.)
1670 vs, br	1683 w (dp)	HNO ₃ ν ₂ (NO ₂ antisym. str.)
	1539 w	HNO ₃ 2ν ₈
	1400 w	{ NO ₂ ⁺ ν ₁ (sym. str.)
		{ HNO ₃ ν ₃ (O-H in plane bend)
1300 vs, vb	1308 vs (p)	HNO ₃ ν ₄ (NO ₂ sym. str.)
	1058 w	NO ₃ ⁻ ν ₁ (sym. str.)
920 vs, b	929 vs, (p)	HNO ₃ ν ₅ (NO ₂ bend)
765 s		HNO ₃ ν ₈ (NO ₂ out of plane)
700-400 vs, vb	681 s (p)	HNO ₃ ν ₆ (N-OH str.)
	614 m (dp)	HNO ₃ ν ₇ (O-N-OH bend)

(p) polarised; (dp) depolarised.

* HNO₃ assignments after G. E. McGraw, D. L. Bernitt, and
 I. C. Hisatsune J. Chem. Phys. 42 237 (1965).

a unidentate covalent nitrate and is accordingly assigned in the C_s point group. A point of particular interest is the appearance of bands at 2365 and 2355 cm^{-1} which can be assigned to the antisymmetric stretching vibration of the nitronium ion (NO_2^+). These have been observed by earlier workers³³ and provide evidence for the 'self-ionisation' of the acid. The associated NO_3^- band would be expected at ca 830 cm^{-1} but is invariably weak and is not observed in this case.

The Raman spectrum of 100% nitric acid is again as expected for a unidentate covalent nitrate. It is similar to the spectrum reported by earlier workers³⁴ and also provides evidence for the 'self-ionisation' of the 100% acid. Weak bands observed at 1400 and 1058 cm^{-1} are characteristic of NO_2^+ (ν_1 symmetric stretch) and NO_3^- (ν_1 symmetric N-O stretch) respectively and can be varied in intensity by adding species which repress the self-ionisation of HNO_3 . For example, addition of very small quantities of water to the 100% acid diminishes the intensity of both the 1400 and 1058 cm^{-1} bands. Further addition of water allows the normal ionisation of the dilute acid to proceed. When NO_2^+ is added to the pure acid, the 1058 cm^{-1} band disappears and similarly the 1400 cm^{-1} band disappears if nitrate ion is added.

6.4 The Vibrational spectrum of solutions of $\text{Fe}(\text{NO}_3)_3 \cdot x\text{N}_2\text{O}_4$ in 100% HNO_3

The bands attributable to $\text{Fe}(\text{NO}_3)_3 \cdot x\text{N}_2\text{O}_4$ in 100% HNO_3 are listed in Table 6.2 and are illustrated in Figs. 6.4

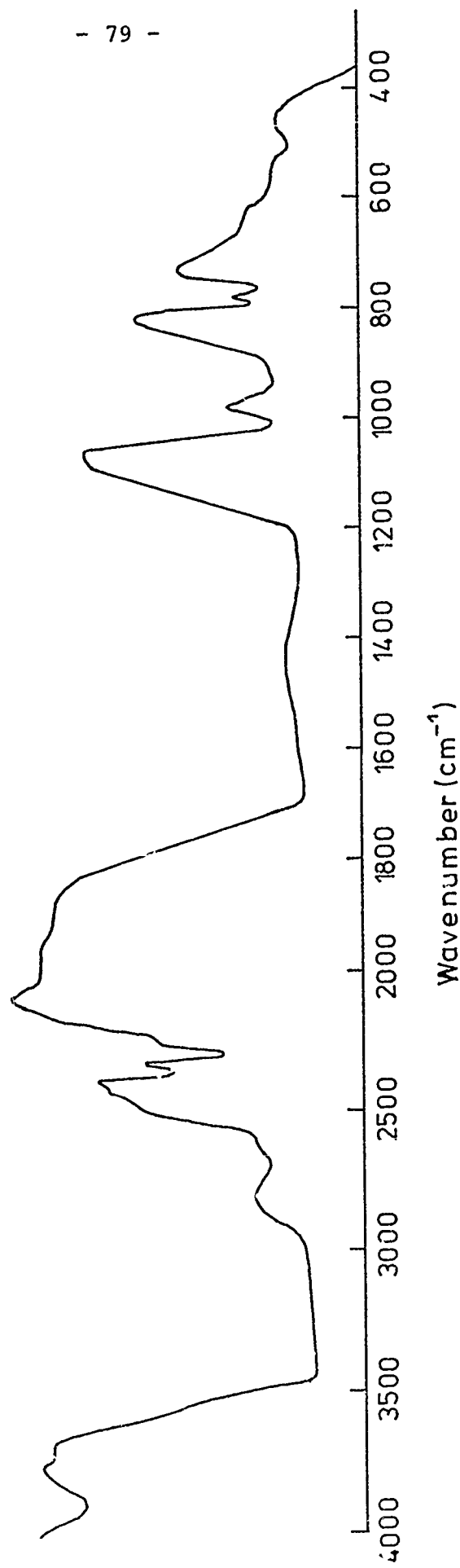


Fig. 6.4 I.R. Spectrum of a solution of $\text{Fe}(\text{NO}_3)_3 \cdot x\text{N}_2\text{O}_4$ in HNO_3

Fig. 5.2
Raman Spectrum of
 $\text{Fe}(\text{NO}_3)_3 \approx \text{N}_2\text{O}_4$ in 100% HNO_3

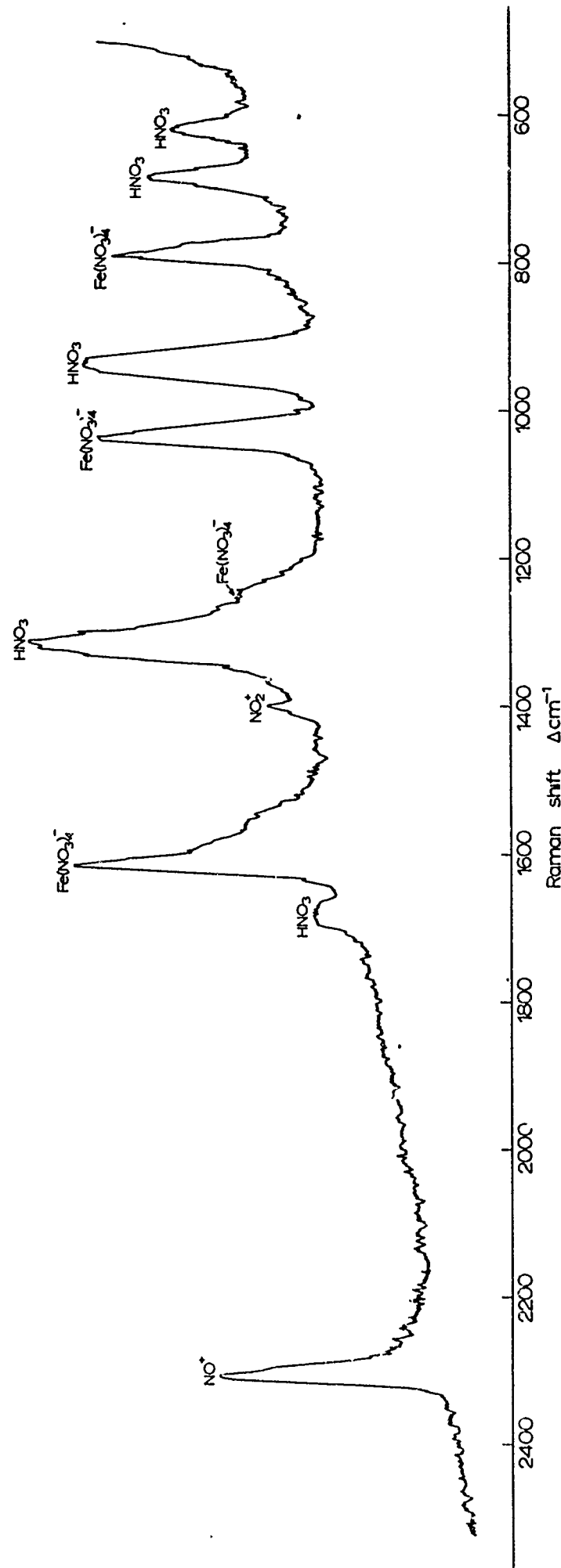


TABLE 6.2

Vibrational spectrum of $\text{Fe}(\text{NO}_3)_3 \cdot \text{xN}_2\text{O}_4$ in 100% HNO_3 solution

Infra-red (cm^{-1})	Raman (cm^{-1})	Assignment
		(C_{2v} bidentate nitrate model)
2295 s	2298 m	NO^+ stretch
2240 sh		NO^+ stretch
	1605 ms (p)	ν_1 $\text{N}=\text{O}$ stretch
	1250 w (dp)	ν_4 NO_2 asymm. stretch
1010 s, b	1028 ms (p)	ν_2 NO_2 symm. stretch
795 s, sp	785 m	ν_6 out of plane bend

(p) polarised; (dp) depolarised.

(infra-red) and 6.5 (Raman). The bands in each spectrum are consistent with the presence of a covalent nitrato-species of iron which may be identified with some confidence. The bands in the covalent nitrate region are virtually identical with those found for the solid $\text{Fe}(\text{NO}_3)_3 \cdot \text{N}_2\text{O}_4$ (see Table 2.1 and Fig. 2.1). This contains the dodecahedral anion $\text{Fe}(\text{NO}_3)_4^-$, in which four bidentate nitrate groups are symmetrically disposed around iron (III).

Strong evidence for the formation of $\text{Fe}(\text{NO}_3)_4^-$ ions from $\text{Fe}(\text{NO}_3)_3 \cdot \text{N}_2\text{O}_4$ dissolved in 100% HNO_3 has therefore been obtained and the stretching frequency of the expected NO^+ counter ion is observed at 2295 cm^{-1} ('free') and 2240 cm^{-1} ('coordinated'). No bands definitely attributable to molecular N_2O_4 were seen. Hence the coordinated nitrosonium ion discussed in Section 4.5 appears not to decompose in nitric acid. No change in the Raman spectrum of $\text{Fe}(\text{NO}_3)_3 \cdot \text{N}_2\text{O}_4$ in 100% HNO_3 was observed over a period of 24 hours, confirming the high stability of the above ionic species in this medium.

The further spectroscopic method for identifying the mode of coordination of nitrate groups in solution species, requires measurement of the depolarisation ratios of the three bands assigned to N-O stretching fundamentals (at ca 1600 , 1200 , 1000 cm^{-1}) in the Raman spectrum. The polarisation sequences predicted for unidentate and bidentate nitrate groups are as follows:

Band (cm^{-1})	<u>ca</u> 1600	<u>ca</u> 1200	<u>ca</u> 1000
Unidentate (C_{2v})	dp	p	p
Bidentate (C_{2v})	p	dp	p

p = polarised, dp = depolarised.

The polarisation sequence observed for $\text{Fe}(\text{NO}_3)_3 \cdot x\text{N}_2\text{O}_4$ in 100% HNO_3 is p, dp, p which indicates that the anion $\text{Fe}(\text{NO}_3)_4^-$ in HNO_3 solution still contains nitrate groups bonded in a bidentate fashion.

When $\text{Fe}(\text{NO}_3)_3 \cdot x\text{N}_2\text{O}_4$ is dissolved in 100% HNO_3 , the band observed at ca 1050 cm^{-1} in the pure acid disappears, whereas the band at 1400 cm^{-1} shows a slight increase in intensity. This behaviour might be expected, as the 'free' NO^+ in $\text{Fe}(\text{NO}_3)_3 \cdot x\text{N}_2\text{O}_4$ on dissolution can react with NO_3^- (from the 'self ionisation' of HNO_3), forming N_2O_4 , which can then coordinate to more 'free' NO^+ . This behaviour has been observed with solutions of $\text{NO}^+\text{HSO}_4^-$ and $\text{NO}^+\text{ClO}_4^-$ in HNO_3 .¹⁶ This decrease in the concentration of NO_3^- will lower the intensity of the 1050 cm^{-1} band, and allow further dissociation of HNO_3 , hence increasing the intensity of the 1400 cm^{-1} (NO_2^+) band.

6.5 ^{14}N n.m.r. of $\text{NO}^+\text{Fe}(\text{NO}_3)_4^-$ in 100% HNO_3

The ^{14}N n.m.r. spectra of 100% HNO_3 and several concentrations of $\text{NO}^+\text{Fe}(\text{NO}_3)_4^-$ in HNO_3 were recorded. Quite low concentrations of $\text{NO}^+\text{Fe}(\text{NO}_3)_4^-$ caused broadening and an up-field shift of the HNO_3 resonance and higher concentrations of $\text{NO}^+\text{Fe}(\text{NO}_3)_4^-$ broadened the signal to such an extent that it became unobservable. Thus no structural information on the nature of these solutions could be gained by this technique.

7. BEHAVIOUR OF $\text{Fe}(\text{NO}_3)_3 \text{xN}_2\text{O}_4$ IN $\text{HNO}_3/\text{N}_2\text{O}_4$ MIXTURES

7.1 $\text{HNO}_3/\text{N}_2\text{O}_4$ phase diagram

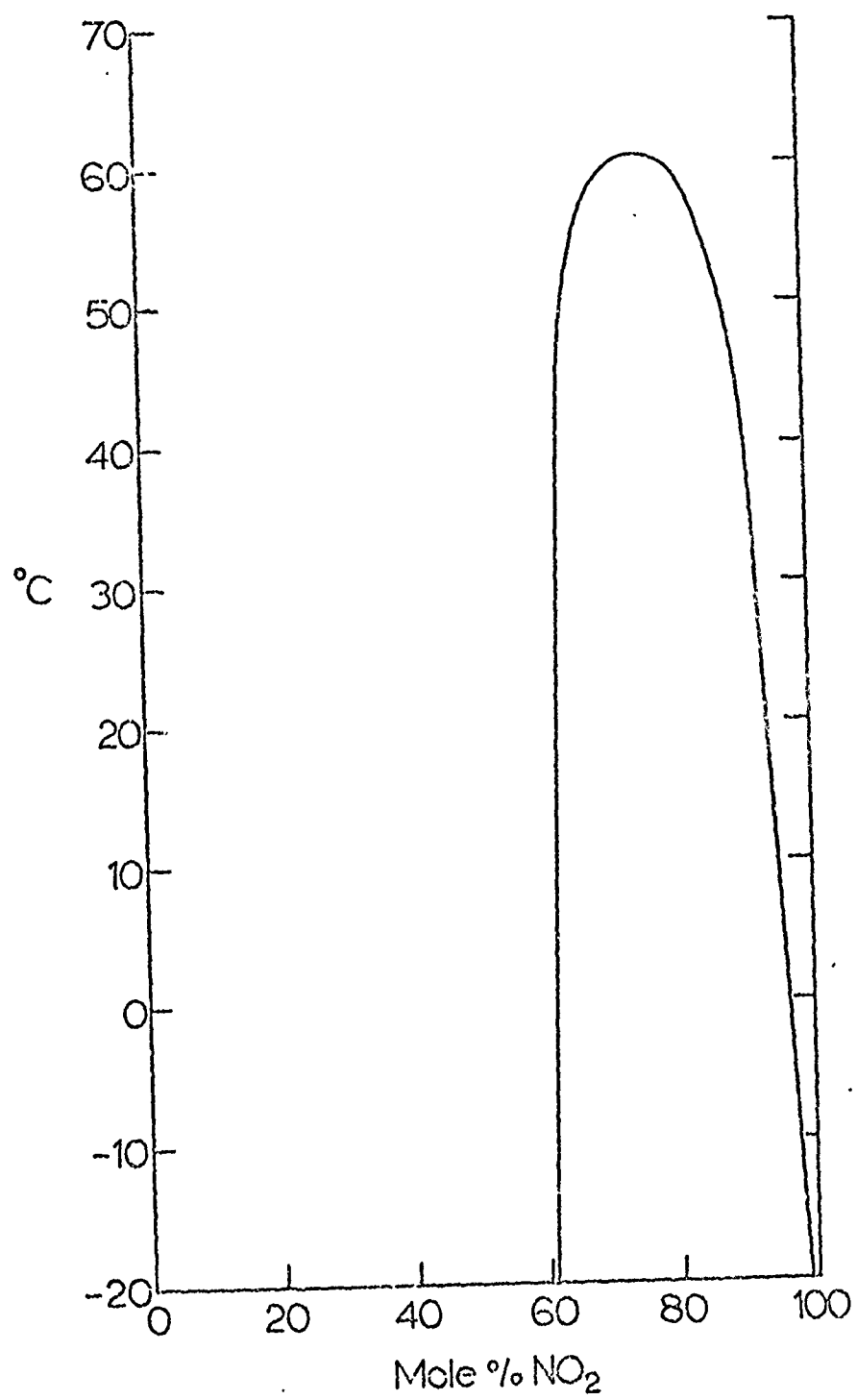
The $\text{HNO}_3/\text{N}_2\text{O}_4$ phase diagram^{35,36} is illustrated in Fig. 7.1. The points of relevance to the study of flow decay problems are: I. A relatively small amount of nitric acid of about 7 wt% at 25°C is sufficient to give rise to a second phase. This amount of nitric acid may be expressed as about 1.2 wt % water. II. The second phase which is formed on gradual addition of nitric acid to N_2O_4 contains almost all of the nitric acid and consists of about 46 wt % of nitric acid at 25°C. III. The slope of the mutual miscibility curve is large. A concentrated homogeneous solution of HNO_3 in N_2O_4 at 30°C, if cooled to 20°C, would give about 5% of a second phase, containing about 46 wt % of HNO_3 .

Experiments described below (Section 7.2(b)) indicate that the nitric acid-rich phase has a greater density than the N_2O_4 rich phase.

7.2 Effect of $\text{Fe}(\text{NO}_3)_3 \text{xN}_2\text{O}_4$ on the $\text{HNO}_3/\text{N}_2\text{O}_4$ phase system

a) General considerations

$\text{Fe}(\text{NO}_3)_3 \text{xN}_2\text{O}_4$ is very soluble in nitric acid although virtually insoluble in N_2O_4 ¹. There is also spectroscopic evidence (Section 6) that $\text{Fe}(\text{NO}_3)_3 \text{xN}_2\text{O}_4$ is ionised in nitric acid as $\text{Fe}(\text{NO}_3)_4^-$ and NO_4^+ . These considerations, and the simplicity of the $\text{HNO}_3/\text{N}_2\text{O}_4$ phase diagram, make it seem likely that behaviour analogous to the water-ether-inorganic salt system might occur: a high affinity of the salt for water, and hence of water for the salt, lowers the solubility of the ether in the



$\text{HNO}_3/\text{N}_2\text{O}_4$ phase diagram.

Fig. 7.1

water. The ether is therefore "salted out" from the aqueous phase. Likewise, the addition of a highly nitric acid-soluble material (e.g. $\text{Fe}(\text{NO}_3)_3 \cdot \text{xN}_2\text{O}_4$) to an $\text{HNO}_3/\text{N}_2\text{O}_4$ mixture was expected to bring about the separation of a second phase containing a large amount of nitric acid. Several experiments described below, have shown that a solution of $\text{ca } 2\text{g } \text{Fe}(\text{NO}_3)_3 \cdot \text{xN}_2\text{O}_4$ in $\text{ca } 10\text{ g } 100\% \text{ HNO}_3$ will dissolve only about 50% of its volume of N_2O_4 before a second less dense phase separates. (Compare HNO_3 , which will dissolve about 100% of its volume of N_2O_4). Higher concentrations of $\text{Fe}(\text{NO}_3)_3 \cdot \text{xN}_2\text{O}_4$ limit the solubility of N_2O_4 in the HNO_3 phase even further.

b) Experimental Study

Fuming nitric acid was dropped into stirred N_2O_4 at 15°C , and the fate of each drop observed with a low-power microscope. About 5 ml of nitric acid could be added to 80 ml N_2O_4 before the separation of a second phase occurred. When separation did occur, the second phase was denser than the bulk N_2O_4 . The globules which formed showed little tendency to agglomerate or to adhere to the glass walls of the flask.

A solution of $\text{Fe}(\text{NO}_3)_3 \cdot \text{xN}_2\text{O}_4$ in fuming nitric acid (ca 40 mg/ml) was then dropped into 80 ml dry N_2O_4 , with stirring, at ca 10°C . On the addition of only one drop of the solution a second phase was formed, which did not fully dissolve on stirring, but adhered to the glass, with a small contact angle. This contact angle increased over about 20 minutes, while maintaining stirring, and the second phase still adhered tenaciously to the side of the flask. Several more drops were added, and these showed similar behaviour. After one day the viscosity of the drops had

increased to a maximum (they were no longer moved by the motion of the magnetic stirrer) and were stable under these conditions for over a week. After decantation of the top phase, the lower phase was treated with a slow stream of dry nitrogen until there was no immediately visible NO_2 evolved on allowing to stand. The I.R. spectrum of the resulting clear, pale brown, viscous liquid was then recorded (sample between AgCl plates). The spectrum indicated the presence of HNO_3 , NO^{\pm} (2230 cm^{-1} , broad), and $\text{Fe}(\text{NO}_3)_4^-$. Bands typical of molecular N_2O_4 were absent. Thus, it may be surprised that a solution of $\text{Fe}(\text{NO}_3)_3 \cdot 1.5\text{N}_2\text{O}_4$ in nitric acid had been produced, and that the 'coordinated NO^+ ' species $\text{N}_4\text{O}_6^{2+}$ does not decompose to 'free' NO^+ and N_2O_4 in nitric acid.

On addition of dry liquid N_2O_4 (ca 40 ml) to this viscous liquid (ca 20 mg), complete conversion to a dark brown solid occurred in about 2 hours. The I.R. spectrum (Nujol mull/ AgCl) of the brown solid was consistent with its being $\text{Fe}(\text{NO}_3)_3 \cdot x\text{N}_2\text{O}_4$.

7.3 Spectroscopic studies of $\text{Fe}(\text{NO}_3)_3 \cdot x\text{N}_2\text{O}_4$ in $\text{HNO}_3/\text{N}_2\text{O}_4$ mixtures

On account of the experiments described above, attention was focussed on the denser, nitric acid-rich phase of the $\text{HNO}_3/\text{N}_2\text{O}_4$ system, and solutions of $\text{Fe}(\text{NO}_3)_3 \cdot x\text{N}_2\text{O}_4$ in this mixture. The characteristic I.R. spectrum of solutions of N_2O_4 in HNO_3 (Fig. 7.2) and of solutions of $\text{Fe}(\text{NO}_3)_3 \cdot x\text{N}_2\text{O}_4$ in $\text{HNO}_3/\text{N}_2\text{O}_4$ mixtures (Fig. 7.3) were obtained between 4000 cm^{-1} and 1000 cm^{-1} using a cell which consisted of CaF_2 windows separated by a PTFE spacer. This assembly was filled with the solution in a dry box and was firmly clamped. A solution of $\text{Fe}(\text{NO}_3)_3 \cdot x\text{N}_2\text{O}_4$ in HNO_3 containing some N_2O_4 was obtained

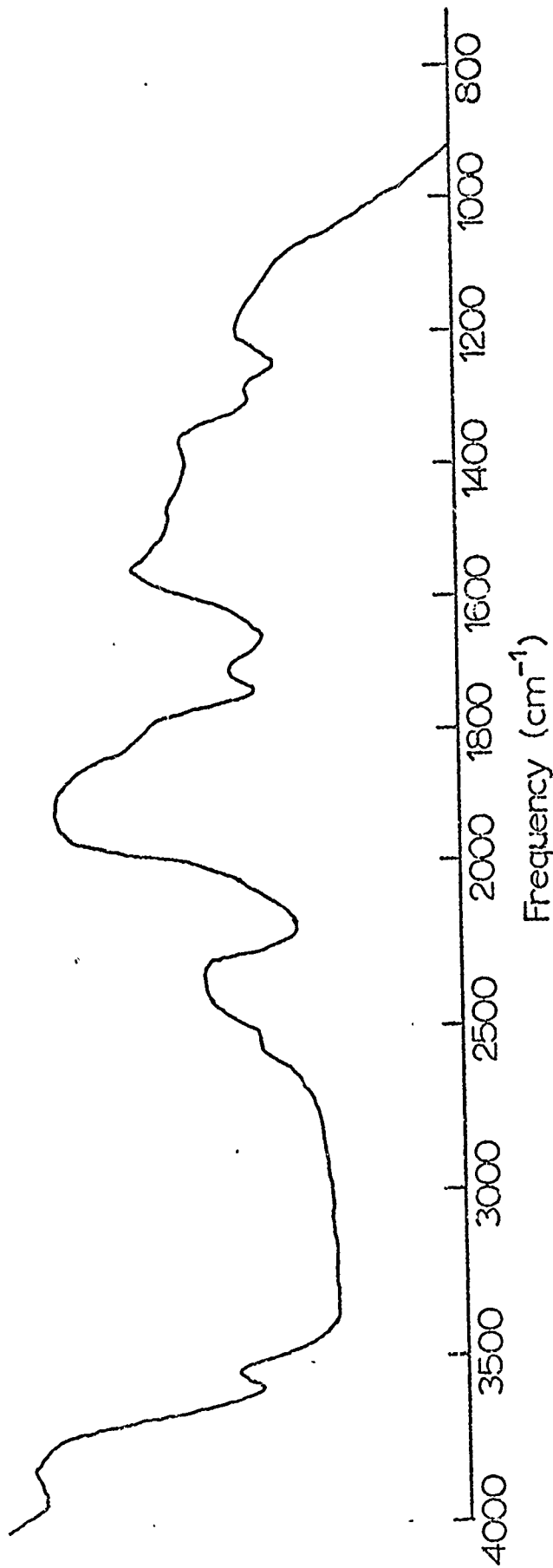


Figure 7.2. I.R. spectrum of solution of N_2O_4 in HNO_3

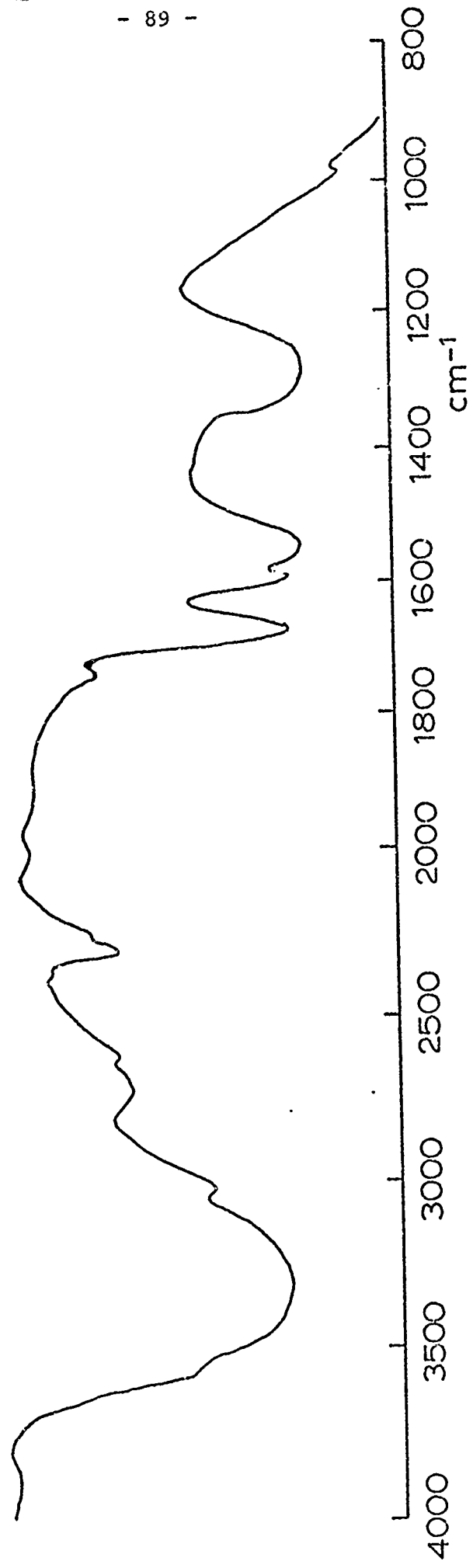


Figure 7.3 Typical I.R. spectrum of $\text{Fe}(\text{NO}_3)_3 \cdot \text{N}_2\text{O}_4$ in HNO_3 containing N_2O_4

by adding $\text{Fe}(\text{NO}_3)_3 \text{xN}_2\text{O}_4$ to the two phase $\text{HNO}_3/\text{N}_2\text{O}_4$ mixture, shaking, and taking a sample of the lower phase. The infrared spectrum of solutions of N_2O_4 in HNO_3 showed bands attributable to HNO_3 (see Section 6) and bands attributable to N_2O_4 ¹². A broad band at about 2220 cm^{-1} was also seen. This has been previously noted in I.R.²³ and Raman^{16, 17} studies on the $\text{N}_2\text{O}_4/\text{HNO}_3$ system and assigned to $\text{NO}^+ \text{NO}_2^-$.

The I.R. spectrum of a solution of $\text{Fe}(\text{NO}_3)_3 \text{xN}_2\text{O}_4$ in HNO_3 containing some N_2O_4 is shown in Fig. 7.3. Bands typical of HNO_3 and N_2O_4 are seen. The remainder of the spectrum shows the characteristic bands of $\text{Fe}(\text{NO}_3)_4^-$ (1600 cm^{-1} , 1550 cm^{-1} , 1000 cm^{-1}), an NO^+ band at 2300 cm^{-1} , and also the broad NO^+ band at 2220 cm^{-1} . The relative intensities of the 2300 cm^{-1} and 2220 cm^{-1} bands varied with the concentration of N_2O_4 in the solution. This behaviour may be contrasted with that above (Section 7.2 (b)) in which it appeared that the coordinated cation producing the band at 2220 cm^{-1} did not dissociate to molecular N_2O_4 and 'free' NO^+ .

7.4 Extraction of solutions of $\text{Fe}(\text{NO}_3)_3 \text{xN}_2\text{O}_4$ in HNO_3 by N_2O_4

The qualitative study described in Section 7.2(b) indicated that a viscous HNO_3 solution of $\text{Fe}(\text{NO}_3)_3 \text{xN}_2\text{O}_4$ was reasonably stable in contact with a large amount of N_2O_4 , and that this HNO_3 phase was, however converted to a solid on further treatment with dry N_2O_4 . In order to place these observations on a more quantitative basis, a series of experiments has been carried out in which solutions of $\text{Fe}(\text{NO}_3)_3 \text{xN}_2\text{O}_4$ in HNO_3 were submitted to progressive extraction of the nitric acid by dry N_2O_4 ,

either batch-wise or continuously in a liquid-liquid extractor designed for this purpose.

a) Batch-wise extraction

0.68 g $\text{Fe}(\text{NO}_3)_3 \cdot \text{N}_2\text{O}_4$ and 14.43 g 97% nitric acid were placed in a Schlenk tube fitted with a PTFE tap. A weighed amount of dry N_2O_4 (ca 50 g) was added to the nitric acid phase against a countercurrent of N_2 and the system allowed to equilibrate (i.e. until the proportions of the two phases did not change). The upper phase was then decanted as completely as possible through the PTFE tap and the remainder was removed by means of a stream of dry N_2 . The lower phase was weighed and its appearance noted. This process was repeated with a further seven portions of N_2O_4 . The results are presented in Table 7.1.

The salient features of these results are:

- I. The presence of ca 0.7 g $\text{Fe}(\text{NO}_3)_3 \cdot \text{N}_2\text{O}_4$ in ca 14 g HNO_3 lowers the solubility of N_2O_4 in the nitric acid from about 14 g to about 8 g.
- II. The second and subsequent extractions progressively decrease the lower phase weight.
- III. The lower phase ultimately solidifies, and the weight of the product is about 15% greater than that of the $\text{Fe}(\text{NO}_3)_3 \cdot \text{N}_2\text{O}_4$ starting material. It may be noted that this weight increase corresponds to that expected if all the $\text{Fe}(\text{NO}_3)_3 \cdot \text{N}_2\text{O}_4$ is converted to $\text{Fe}(\text{NO}_3)_3 \cdot 1.5\text{N}_2\text{O}_4$ and this latter compound has very low solubility in the top, N_2O_4 rich phase.

TABLE 7.1

Batch-wise extraction of $\text{Fe}(\text{NO}_3)_3 \cdot \text{N}_2\text{O}_4$ in HNO_3 by dry N_2O_4

Extraction No.	Approx. time to equilibrate	Wt. of lower phase (g)	Wt. of N_2O_4 last added (g)	Wt. of top phase removed (g)	Appearance of lower phase
1	-	15.11*	-	-	Clear mobile solution
2	5 min.	22.98	58.00	50.13	"
3	20 min.	12.52	55.45	65.91	"
4	40 min.	6.11	55.89	62.30	"
5	16 hr.	1.54	57.79	62.36	Dark red/brown, viscous. Did not adhere strongly to glass.
6	16 hr.	1.32	65.49	65.71	Dark brown, very viscous. Adhered strongly to glass.
7	16 hr.	1.05	56.72	56.99	Dark brown solid.
8	5 days	0.94	67.04	67.15	"
		0.79†	ca 200	-	"

* Initial weight of lower phase.

† N.B. 0.68 g $\text{Fe}(\text{NO}_3)_3 \cdot \text{N}_2\text{O}_4$ \longrightarrow 0.78 g $\text{Fe}(\text{NO}_3)_3 \cdot 1.5\text{N}_2\text{O}_4$

The properties of solids obtained by extraction procedures are discussed below.

b) "Continuous" extraction

A series of experiments carried out with a liquid-liquid extractor (Fig. 7.4) were performed to verify the qualitative results of the batch-wise extraction, to allow intermittent monitoring of the "water" content of the upper (N_2O_4) phase by 1H n.m.r. (Technique described in Appendix 1), and to facilitate the production of solids and viscous liquids in $Fe(NO_3)_3 \cdot N_2O_4 / HNO_3 / N_2O_4$ systems.

$Fe(NO_3)_3 \cdot N_2O_4$ and 100% HNO_3 were weighed into tube A (Fig. 7.4) and the apparatus was assembled as drawn. Distillation of N_2O_4 occurred without heating, but a convenient rate of distillation could be obtained by gentle heating of the flask B. When a sample of the top phase was required for 1H estimation, distillation was discontinued and the top half of the inner funnel C removed to allow the lower phase to achieve equilibrium with a homogeneous upper phase. When the phase boundary in the sample tube A no longer fell, a sample of the top phase was transferred to an n.m.r. tube as rapidly as possible by means of a pipette and the tube was flame sealed. A sample of the viscous lower phase was, in one experiment, removed from the apparatus a short time prior to solidification. On treatment with water it effervesced, evolved NO_2 , and was totally soluble.

In another experiment an attempt was made to isolate a sample of the viscous lower phase. The upper phase (0.07% "water", estimated by 1H n.m.r.) was decanted off, and it was observed with interest that the lower phase immediately solidified.

Methcol
at -10°C

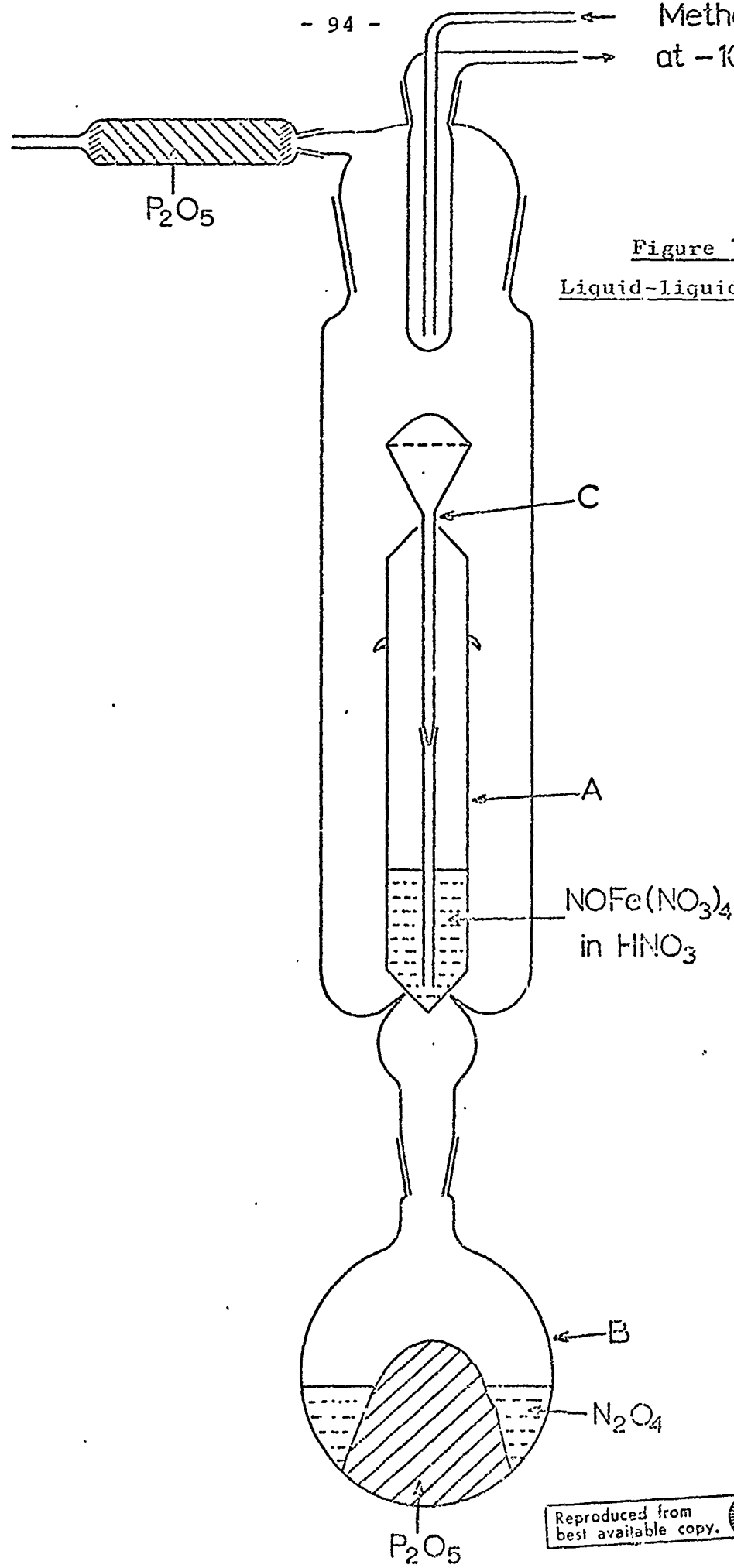


Figure 7.4
Liquid-liquid extractor

In a further experiment the appearance of the lower phase was noted as a function of the "water" content of the upper phase on progressive extraction. The system was allowed 24 hours to come to equilibrium before each sample of the upper phase was taken for quantitative examination by ^1H n.m.r. The results are recorded in Table 7.2.

Table 7.2.

Continuous extraction of $\text{Fe}(\text{NO}_3)_3 \cdot x\text{N}_2\text{O}_4$ in HNO_3 by dry N_2O_4

Sample	% "water" content of upper phase	Lower phase appearance
1	0.6	Clear, red/brown mobile liquid
2	0.24	"
3	0.15	"
4	0.13	"
5	0.19	Increased viscosity
6	0.12	Extremely viscous liquid
7	0.17	Solid

The possibility that equilibrium between a given sample of the upper phase and the lower phase was not achieved in 24 hours must be recognised. It can be seen, however, from Table 7.2 that a progressive diminution in the "water" content of the upper phase was noted as extraction proceeded under the above conditions, with the exception of sample 5 which showed an anomalously high value. This may have been an indication that equilibrium was not being achieved. Furthermore, if equilibrium conditions were achieved, solidification should take place gradually, with the co-occurrence of solid and viscous liquid. This was never observed; during extraction experiments

the solidification of viscous liquids took place rapidly and completely.

A pronounced increase in the "water" content of the upper phase (sample 7) occurred on separation of solid, presumably as a result of expulsion of nitric acid from the liquid phase on solidification. This is a further indication that equilibrium was not being attained, since under equilibrium conditions the "water" content of the upper phase should decrease monotonically with progressive extraction. (See Section 7.6).

It is noteworthy that the solid $\text{Fe}(\text{NO}_3)_3 \cdot x\text{N}_2\text{O}_4$ produced on complete extraction was then stable in contact with N_2O_4 of "water" content as high as 0.17%. Experiments to find the maximum "water" content for solid stability, when equilibrium is achieved, are described in Section 7.6.

7.5 Solids produced from extraction experiments

In every experiment so far performed, the extraction of $\text{Fe}(\text{NO}_3)_3 \cdot x\text{N}_2\text{O}_4$ in HNO_3 with dry N_2O_4 ultimately led to the formation of a solid. The solids were all dark brown, and showed a tendency to evolve NO_2 . Samples which had been treated with a gentle stream of dry N_2 were lighter in colour and showed less tendency to evolve NO_2 than those where the solid was isolated by decantation only. Each solid was completely or almost completely water-soluble.

a) Infra-red spectra

A typical spectrum is shown in Fig. 7.5, obtained as a nujol mull between AgCl plates.

The spectrum is very similar to that for $\text{Fe}(\text{NO}_3)_3 \cdot x\text{N}_2\text{O}_4$, $x > 1$ (See Section 2). The main features of interest are the

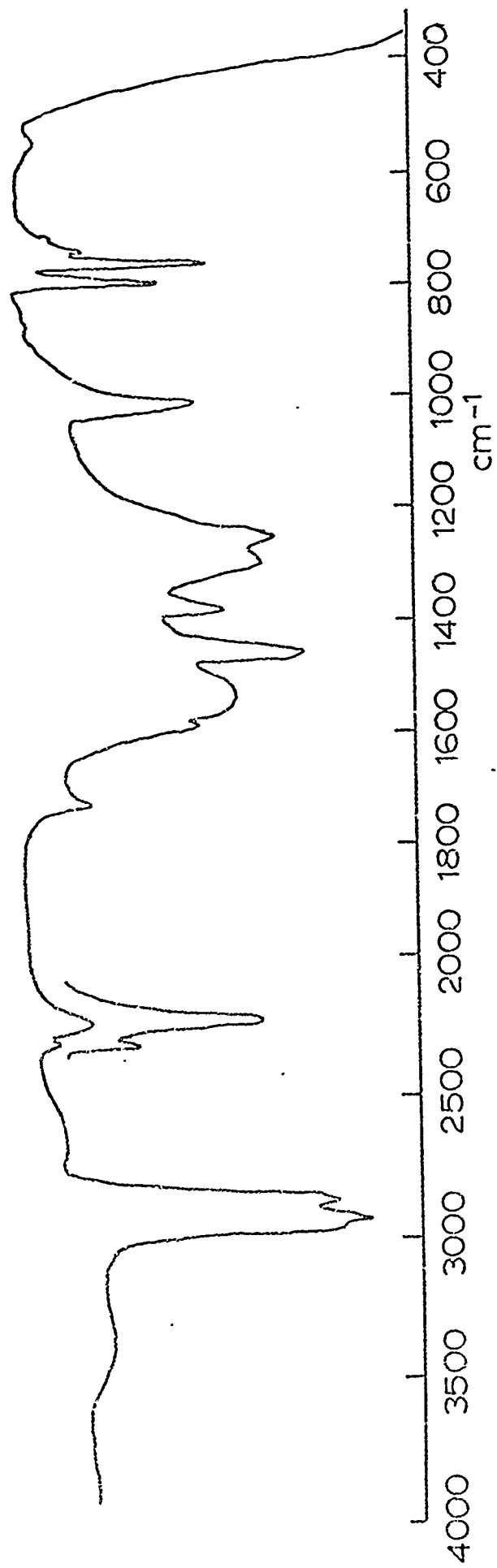


Figure 7.5
Typical I.R. spectrum of solid extraction product of $\text{Fe}(\text{NO}_3)_3 \times \text{N}_2\text{O}_4$ in HNO_3 by N_2O_4

NO^+ region ($2200-2300 \text{ cm}^{-1}$) and the absence of nitric acid. The relative intensities of the band at 2300 cm^{-1} and the broad band centred at 2220 cm^{-1} varied from sample to sample, and in some cases no 2300 cm^{-1} ('free' NO^+) band was observed. No evidence was found for any other iron-containing species than $\text{Fe}(\text{NO}_3)_4^-$.

b) X-ray powder patterns

In two experiments a solid was produced whose X-ray powder pattern was very similar to that for the starting material - i.e. $\text{Fe}(\text{NO}_3)_3 \cdot \text{N}_2\text{O}_4$ produced from $\text{FeCl}_3/\text{EtOAc}/\text{N}_2\text{O}_4$ (see Section 2.6). In two other cases the X-ray powder pattern of the product was very similar to that of $\text{Fe}(\text{NO}_3)_3 \cdot 1.5\text{N}_2\text{O}_4$ produced from $\text{FeCl}_3/\text{EtOAc}/\text{N}_2\text{O}_4$ (see Section 4.6). In one further case, the product had an X-ray powder pattern which appeared to be that of a mixture of $\text{Fe}(\text{NO}_3)_3 \cdot 1.5\text{N}_2\text{O}_4$ and $\text{Fe}(\text{NO}_3)_3 \cdot \text{N}_2\text{O}_4$. However, the film quality was poor because $\text{CuK}\alpha$ radiation, which causes fluorescence with iron compounds, was used, in addition to which the material appeared to be rather amorphous.

c) Analysis

The following analytical methods were employed:-

Fe The atomic absorption method described in Section 2.2(c).

N_2O_4 content Two methods were used to obtain N_2O_4 content, each using the technique of sealed bottle hydrolysis in aqueous alkali (described in Section 2.2), followed by estimation of NO_2^- produced.

Estimation of nitrite by U.V. spectroscopy³³⁷ was attractive, as the method could potentially give a direct

estimation of nitrate, and hence total nitrogen, as well as nitrite. However, very high results for nitrate and nitrite were invariably obtained by this method, and in some cases the solutions were visibly yellow. Both effects were attributed to the presence of soluble hydroxo-iron(III) species, the U.V. absorption of which would augment that due to nitrate and nitrite. The alkali concentration used for the hydrolysis of the solid was therefore varied, in the hope that conditions might be found under which complete precipitation of iron as hydroxide/hydrated oxide would occur. However, no conditions which gave chemically reasonable or reproducible results could be found.

The method eventually used for determination of N_2O_4 content was that described in Section 2.2(b). This was found to be quite satisfactory.

The analytical results for several solids obtained from extraction experiments (Section 7.4) were consistent with compositions $Fe(NO_3)_3 \cdot xN_2O_4$ where $x = 1.0-1.5$. For each solid, the Fe content gave a higher value of x than the NO_2^- determination but the atomic absorption method for Fe was of significantly lower accuracy than the titration of NO_2^- by Ce(IV).

d) Conclusions

All the evidence available at present points to the recovery (i.e. recrystallisation) of $Fe(NO_3)_3 \cdot xN_2O_4$ from HNO_3 by extraction with sufficient dry N_2O_4 to produce a solid. The I.R., X-ray and analytical data all tend to indicate that the 'extra' 0.5 N_2O_4 in $Fe(NO_3)_3 \cdot 1.5N_2O_4$, which appears to be the initial solid product of the extraction experiments, is lost more readily than that from $Fe(NO_3)_3 \cdot 1.5N_2O_4$ obtained

from the $\text{FeCl}_3/\text{EtOAc}/\text{N}_2\text{O}_4$ preparation. This observation is in accord with the fact that the X-ray films of $\text{Fe}(\text{NO}_3)_3 \cdot x\text{N}_2\text{O}_4$ recrystallised from $\text{HNO}_3/\text{N}_2\text{O}_4$ are more diffuse and have a higher background than those of $\text{Fe}(\text{NO}_3)_3 \cdot x\text{N}_2\text{O}_4$ recrystallised from $\text{EtOAc}/\text{N}_2\text{O}_4$. It is concluded that the former are less crystalline. It is also relevant to note at this point that products from the reaction of iron carbonyls with liquid N_2O_4 give diffuse X-ray powder patterns and readily lose "excess" N_2O_4 to yield $\text{Fe}(\text{NO}_3)_3 \cdot \text{N}_2\text{O}_4$.

7.6 The phase behaviour of the $\text{NOFe}(\text{NO}_3)_4/\text{N}_2\text{O}_4/\text{H}_2\text{O}$ system:
a ^1H n.m.r. study.

Attempts to find the maximum "water" content of N_2O_4 in contact with which $\text{Fe}(\text{NO}_3)_3 \cdot x\text{N}_2\text{O}_4$ will remain a solid, described in the extraction experiments (Section 7.4), were rather unsatisfactory. In particular, it was strongly suspected that equilibrium conditions were not attained in these experiments. In the more recent investigations described here, the equilibration process could be monitored, and equilibrium data has been obtained.

a) Experimental
 $\text{Fe}(\text{NO}_3)_3 \cdot x\text{N}_2\text{O}_4$ (ca 0.05 g) was weighed into an n.m.r. tube and N_2O_4 (ca 2g) containing a known small amount of water was syringed onto the solid, and the tube flame sealed. At the same time a sample of this wet N_2O_4 was syringed into another n.m.r. tube in order to estimate its "water" content. Further water was then added to the N_2O_4 and a second pair of tubes filled in a similar fashion. A total of 8 pairs of tubes were filled. The tubes containing solid were allowed to equilibrate for 8 months, while slowly rotating each tube about an axis perpendicular to its length to facilitate this equilibration.

The behaviour of the solid in each tube was noted visually and the ^1H content of the upper (N_2O_4) phase was monitored by ^1H n.m.r. at intervals during the 8 months.

The equilibrium results are shown in Fig. 7.6.

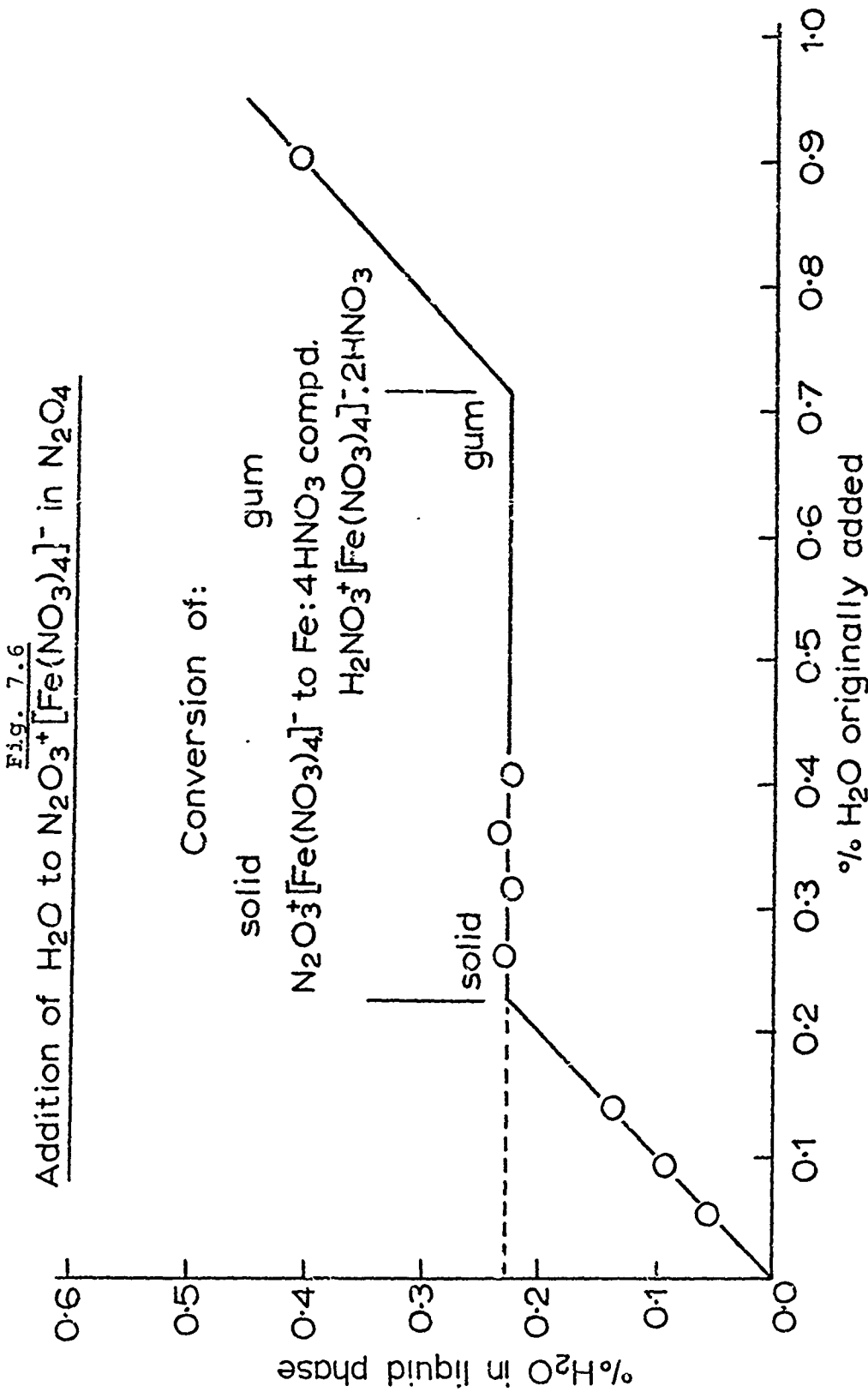
The appearance of the solid in the tubes with N_2O_4 of low "water" content (less than ca 0.2 wt %) did not change, remaining a fine, free-flowing, yellow powder. The solids in the tubes with H_2O content ca 0.2 to ca 0.6 wt% all changed quite markedly in appearance. In the tubes of lower water content in this range, the solid had darkened in colour and there was some agglomeration of the particles of the powder, whereas, in the tubes of higher water content, three phases were present; the N_2O_4 phase, a dark brown gum and particles of a dark brown solid. In the tube with highest original water content (ca 0.9 wt %), the solid changed completely and rapidly (a few days) into a mobile brown gum. This change in appearance was much more rapid than in the tubes of water content 0.2-0.6%, which took several months for equilibration.

b) Results

The salient features of the results presented in Fig. 7.6 are:

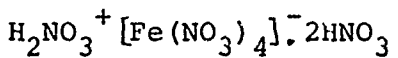
- I. Up to a "water" content of 0.22 wt %, the water content of the top (N_2O_4) phase is the same as the initial "water" content of the N_2O_4 added - i.e. the solid $\text{Fe}(\text{NO}_3)_3 \cdot x\text{N}_2\text{O}_4$ is not combining with any proton containing species.
- II. Above 0.22 wt %, a 4 phase (solid, 2 liquids, vapour) system is obtained: the phase rule requires that for three components at a constant temperature the

Addition of H_2O to $\text{N}_2\text{O}_3^+[\text{Fe}(\text{NO}_3)_4]^-$ in N_2O_4



system should be invariant - ie. the composition of each phase is fixed. This behaviour is completely in accord with the visual observations.

III. On increasing the initial "water" content further, all the $\text{Fe}(\text{NO}_3)_3 \cdot x\text{N}_2\text{O}_4$ becomes converted to a gum, and hence the system is no longer invariant. The added water partitions itself between the N_2O_4^- rich phase and the iron-rich phase: it can thus be seen that the maximum slope of the third portion of the graph (Fig. 7.6) must be unity. This has been assumed in Fig. 7.6, allowing the ratio of Fe:H for the gum to be calculated from the amount of $\text{Fe}(\text{NO}_3)_3 \cdot x\text{N}_2\text{O}_4$ originally present. A maximum estimate of this ratio is approximately 1:4. A reasonable formulation for the gum, consonant with this figure and the known stability of $\text{Fe}(\text{NO}_3)_4^-$ in nitric acid, would be:



c) Conclusions

A. Any flow decay material which separates from N_2O_4 of "water" content less than 0.22% will do so as a solid.

B. Specification "water" content N_2O_4 is 0.1%, but up to 0.2% is considered acceptable for propellant use. The closeness of this figure to that now determined for solid stability and the vagaries of some analytical methods for the "water" content of liquid N_2O_4 imply that gummy or gelatinous iron nitrate phases may well arise in certain instances, in the presence of "specification" N_2O_4 . This may be the explanation of the results

obtained by TRW², in which they encountered flow-decay material as a gelatinous phase.

C. We have found ¹H n.m.r. to be a convenient, accurate and reproducible method for "water" estimation, and consider it likely to be superior to chemical methods of analysis.

7.7 Rationalisation of the behaviour of the $\text{Fe}(\text{NO}_3)_3 \cdot x\text{N}_2\text{O}_4$ / $\text{HNO}_3/\text{N}_2\text{O}_4$ system

In summary, the main features of the work described in Sections 6 and 7 are:

I. $\text{Fe}(\text{NO}_3)_3 \cdot x\text{N}_2\text{O}_4$ dissolves in 100% HNO_3 and $\text{HNO}_3/\text{N}_2\text{O}_4$ mixtures to give NO^+ , a modified NO^+ ion (which is also found in $\text{Fe}(\text{NO}_3)_3 \cdot 1.5\text{N}_2\text{O}_4$), and $\text{Fe}(\text{NO}_3)_4^-$.

II. Treatment of a solution of $\text{Fe}(\text{NO}_3)_3 \cdot x\text{N}_2\text{O}_4$ in HNO_3 with dry N_2O_4 leads ultimately to the recovery of solid $\text{Fe}(\text{NO}_3)_3 \cdot x\text{N}_2\text{O}_4$ from the solution.

III. Solutions of HNO_3 in N_2O_4 have been prepared where the concentration of HNO_3 is too small for the $\text{Fe}(\text{NO}_3)_3 \cdot x\text{N}_2\text{O}_4$ to separate out a liquid, HNO_3 -rich phase. In the analogous system in which water replaces nitric acid, the maximum "water" content is 0.22%.

IV. $\text{Fe}(\text{NO}_3)_3 \cdot x\text{N}_2\text{O}_4$ is stable in contact with N_2O_4 containing a small amount of HNO_3 or "H₂O" and is not converted, for instance, into a hydrated nitrate or hydroxy species.

It appears most fruitful to interpret the properties of the $\text{Fe}(\text{NO}_3)_3 \cdot x\text{N}_2\text{O}_4/\text{HNO}_3/\text{N}_2\text{O}_4$ system in terms of a gross modification of the $\text{HNO}_3/\text{N}_2\text{O}_4$ phase diagram by the $\text{Fe}(\text{NO}_3)_3 \cdot x\text{N}_2\text{O}_4$. The observed behaviour is qualitatively that expected for any ionic

salt in the $\text{HNO}_3/\text{N}_2\text{O}_4$ system. The ionisation to NO^+ and $\text{Fe}(\text{NO}_3)_4^-$ (I) and the lack of chemical reaction except for strong ligation of NO^+ is consistent with this idea. Points II, III and IV above are also comprehensible, since at a suitably low HNO_3 content in the $\text{HNO}_3/\text{N}_2\text{O}_4$ system only one liquid phase is obtained and it is likewise expected that below some critical HNO_3 content in a $\text{Fe}(\text{NO}_3)_3 \cdot x\text{N}_2\text{O}_4/\text{HNO}_3/\text{N}_2\text{O}_4$ system, only one liquid phase would again be obtained - i.e. $\text{Fe}(\text{NO}_3)_3 \cdot x\text{N}_2\text{O}_4$ would remain a solid.

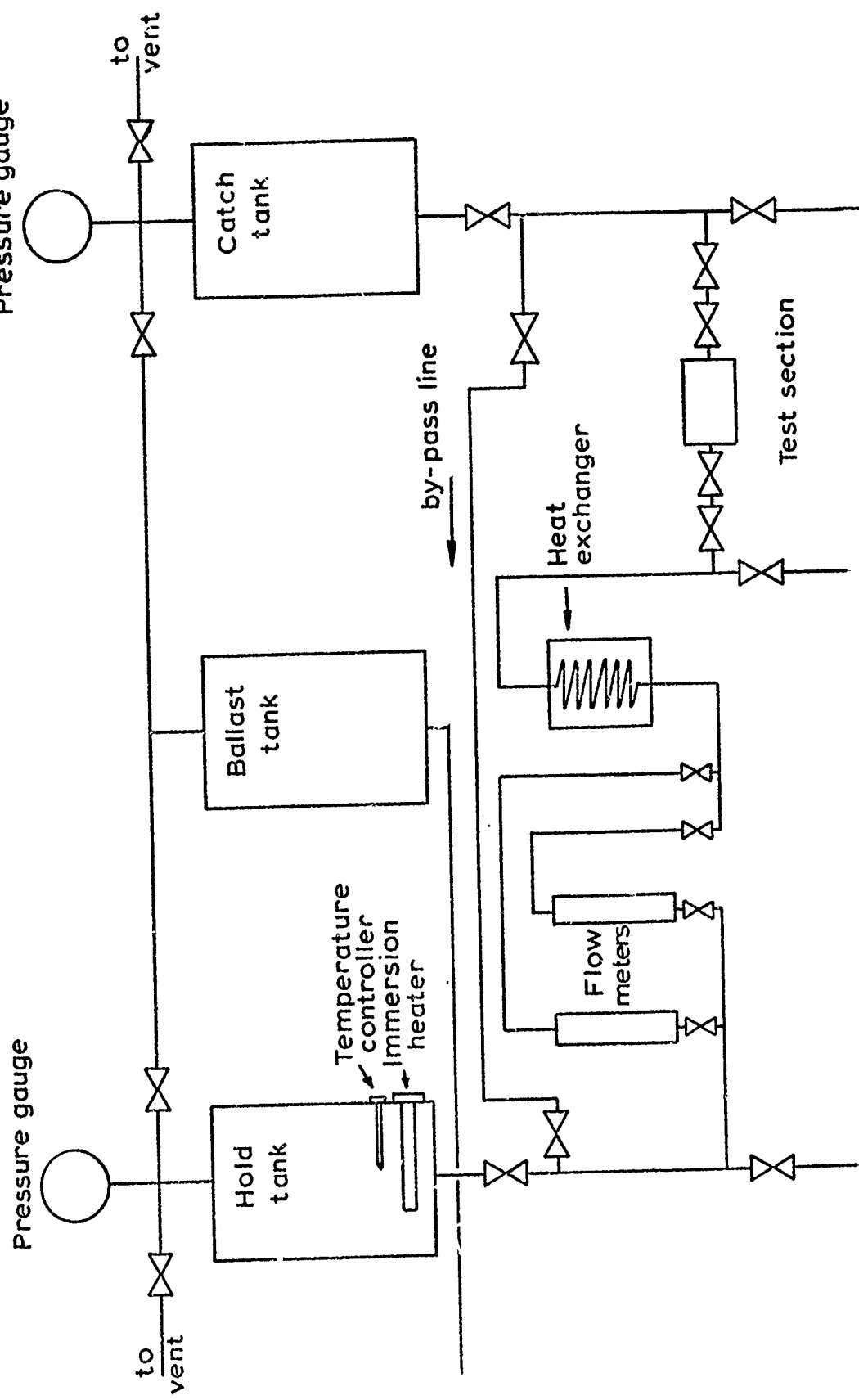
6 THE FLOW APPARATUS AND EXPERIMENTS.

6.1 Construction

The design of the flow apparatus was based upon a system which has been used by previous workers² to demonstrate flow-decay. A schematic diagram of the flow apparatus is presented in Fig. 8.1. Glass and fluorinated plastics were unsuitable for fabrication of tanks and pipework because of fragility and contructional difficulties. Also, if the apparatus was built in glass or plastic, it would have been necessary to saturate N_2O_4 used for flow runs with iron in order to induce flow-decay. It was thought at this time that inclusion of metals other than iron in the system should be avoided, and to this end mild steel was used in preference to stainless steel in the construction. Since our workshop staff had considerable experience in the machining of Teflon cone valves for use in fluorine systems, valves of this type were at first adapted for incorporation into the apparatus. The quantity of glass in the system was reduced to a minimum and was eventually used only in the construction of the hold tank level indicator and in the flowmeters. This glass had been tested to pressures far in excess of those to be used in flow experiments.

Pressurisation of the system was effected by means of a cylinder of high purity nitrogen. The gas was passed through a Negretti and Zambra pressure regulating valve into a 5 gallon ballast tank. N_2O_4 was held in a 5 gallon hold tank and was passed under pressure through one of two flowmeters (depending upon the flow-rate required) and through the heat exchanger, which comprised a 20 ft. mild steel coil inside a cooling jacket supplied

Figure 8.1
Schematic diagram of the flow apparatus



with coolant from an Ultra-Kryomat TK30D circulating refrigerant unit. From here, the cooled liquid N_2O_4 was passed through a test section (See Section 8.2) and into a catch tank. Both the hold and catch tanks were fitted with relief valves so that a constant predetermined pressure could be maintained during flow experiments. Each tank was also fitted with a pressure gauge. A by-pass line was constructed between the two tanks, allowing N_2O_4 to be passed directly from tank to tank ie. circumventing the test section, heat exchanger and flowmeters if necessary.

A cylinder of N_2O_4 was connected to the apparatus by means of steel tubing and the hold tank was filled using the internal cylinder pressure to force the liquid into the system. Several of the Teflon valves showed signs of leakage, necessitating tightening of pipe connections and valve stems and upon manipulation, most of the remaining valves showed seepage of N_2O_4 . The valves immediately on each side of the test section leaked persistently and defied all efforts to arrest this by tightening. These valves were therefore replaced by steel valves. During the time used for commissioning the apparatus, most of the Teflon valves gave further trouble and these were replaced by steel ball valves with Teflon seats. Other workers³⁸ have found Teflon to be porous to N_2O_4 . However, since installation of the steel ball valves no further trouble has been experienced.

8.2 Test sections and flow experiments.

a) Gauze filters. Previous workers² observed viscous gel formation on this type of test section and an attempt was made to reproduce this effect. The test section comprised a

thimble of stainless steel gauze (100 or 400 mesh or 10μ) contained in a thick glass envelope. The steel end-flanges were connected through a Neoprene gasket carrying a Teflon insert so placed that the Neoprene made no contact with N_2O_4 . Flow runs using various pressure and temperature differentials and flow rates were performed using a 100 mesh gauze. The test section was illuminated using both transmitted and reflected light and the gauze was observed using a microscope, but at no time was any flow-decay material observed. Trouble was experienced with the Teflon gasket material, since it was apparently porous towards N_2O_4 and allowed attack of the Neoprene portion and subsequent major leakage. It was then decided to change to needle valve test sections in further attempts to induce flow decay.

b) Needle valves. The use of needle valves was prompted by the observation of a brown solid deposit on a needle control-valve adjacent to the gauze test section. The quantity of material was too small to allow any characterisation but it was thought likely that more of this solid might be accumulated by using a needle valve test section. While a suitable steel needle valve was being modified for use as a test section, a Teflon-in-glass stopcock was temporarily fitted and some experiments were performed with this. However, using a full range of variables, no flow-decay material was observed in the test section. Perhaps this is not surprising, since adherence to a Teflon surface is probably difficult.

A stainless steel needle valve was fitted with glass windows so that the needle could be viewed directly, using a microscope. Using the apparatus as described above (without a temperature differential) no accumulation of flow-decay material on the needle was observed. The N_2O_4 in the flow apparatus

was found by H.N.M.R. (Appendix 1) to contain 0.12% "water" which compared closely with the usual specification of propellant N_2O_4 and should have been sufficient to cause flow-decay if the presence of HNO_3 was a governing factor. Previous workers¹ observed that if the hold tank was "conditioned" with N_2O_4 by warming to ca $35^{\circ}C$, flow-decay could be induced with relative ease. It was decided therefore to modify the flow apparatus to incorporate heating equipment in the hold tank.

8.3 Modification of the flow apparatus.

The flow apparatus was reconstructed using 316 stainless steel tubing and during this reconstruction certain modifications were made. Before assembly, all components were scrupulously cleaned and degreased. The hold tank was fitted with a 500 watt stainless steel immersion heater to facilitate heating and conditioning of N_2O_4 . The temperature of the N_2O_4 was monitored using a British Rototherm vapour pressure thermometer which also controlled the output of the heater. The N_2O_4 was still stored in the original mild steel vessels but the level-indicator was replaced by a glass indicator of more robust construction which was fitted at either end with shut-off valves. Thus, in the event of breakage the valves could be closed and major leakage prevented. A similar indicator and set of valves was fitted to the catch tank.

8.4 Further flow experiments

a) Stainless steel needle valve test section

The N_2O_4 in the hold tank was heated at $35^{\circ}C$ for two days

to allow it to condition. The stainless steel sight glass needle valve described earlier (Section 8.2(b)) was used without modification as the test section in this set of flow experiments. In the first set of runs the conditions were as follows:-

	Pressure (psi)	Temperature (°C)
Hold tank	39	35
Catch tank	3	
Heat exchanger		24.8

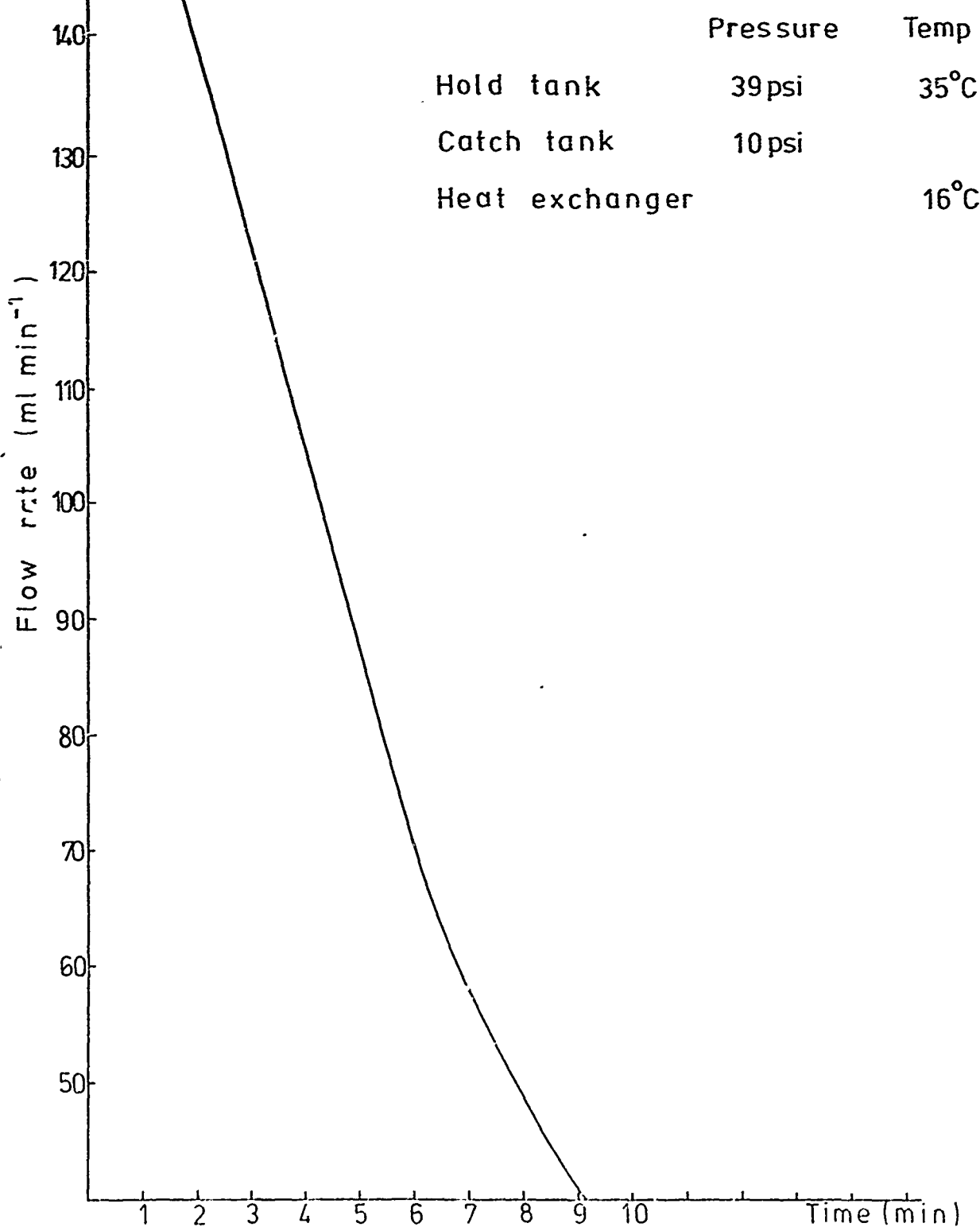
During the run time of ca 1 hr. the hold tank was emptied through the test section and into the catch tank, but no indication of a fall in flow rate was observed. It was considered that the temperature of the heat exchanger might have been too high to induce any dissolved nitrate-iron species to precipitate from the N_2O_4 if indeed a process akin to precipitation occurs. Accordingly, the temperature of the heat exchanger was lowered to $20.1^{\circ}C$ and a second flow run commenced. During this experiment the flow rate of N_2O_4 was observed to fall from 170 ml min^{-1} to 66 ml min^{-1} over a period of ca 3 hr. On further lowering of the heat exchanger temperature to $15^{\circ}C$ the flow rate fell from 170 ml min^{-1} to 40 ml min^{-1} in a time interval of 11 to 30 minutes. The value 40 ml min^{-1} corresponded to a scale reading of zero on the particular flow meter in use, whilst 170 ml min^{-1} was the maximum of this scale. A decrease in flow rate from 170 to 40 ml min^{-1} is subsequently referred to as "full scale decay". Several flow experiments were conducted under these conditions and the flow decay observed was consistent and

reproducible.

Although the main purpose of these flow experiments was to isolate and study the flow decay material, graphs of flow rate against time were plotted. These graphs showed that flow rate decayed smoothly with time and a typical plot is illustrated in Figure 8.2. A number of flow runs were then completed in order to accumulate material on the valve needle. At no stage was an obvious deposit visible on the valve needle on looking through the sight glass. Near the end of this series a large and almost instantaneous increase in flow-rate occurred during an otherwise normal run. It seemed likely that some of the flow-decay compound had become dislodged. The test section was drained and dismantled as follows. Valves 1 and 2 (Figure 8.3) were closed, thus isolating the test section from the remainder of the system. A 250 ml two-necked flask was fitted to the stainless steel ground joint A, and valves 3,4 and 7 were opened. The second neck of the flask was fitted with a phosphoric oxide guard tube to act as a vent and to prevent ingress of moisture. When all of the liquid N_2O_4 had drained into the flask, valve 7 was closed and the flask transferred to joint B. Valves 5,6 and 8 were opened and the remaining N_2O_4 was drained. Valve 8 was closed and the flask was replaced by a phosphoric oxide guard tube. A supply of dry nitrogen was connected to joint A and valves 7 and 8 were opened. The system was flushed with dry nitrogen to remove the bulk of the remaining N_2O_4 . Valves 4 and 5 were closed, the couplings were separated and the test section removed to a dry box.

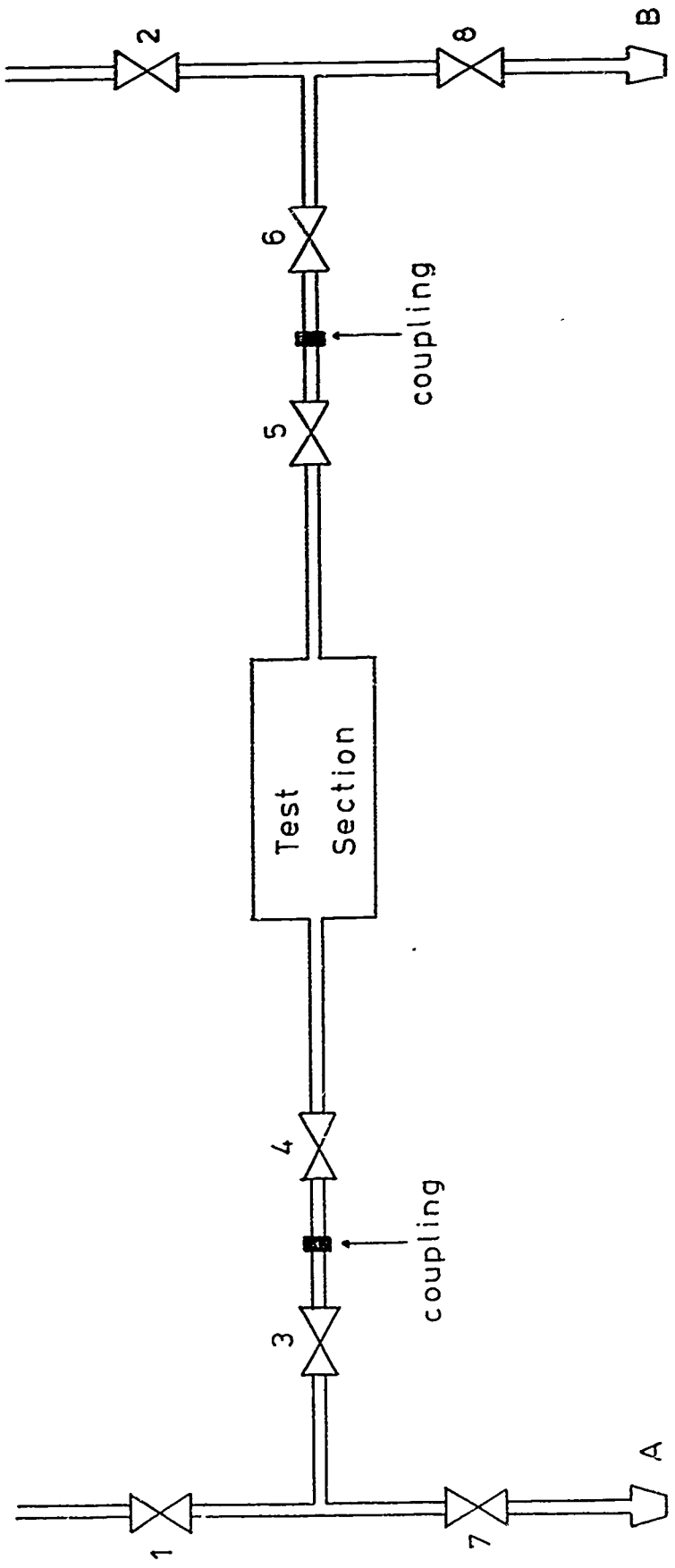
Figure 8.2

Stainless Steel Needle Valve



	Pressure	Temp
Hold tank	39 psi	35°C
Catch tank	10 psi	
Heat exchanger		16°C

Figure 8.3. Valves operative in dismantling test section



On dismantling the valve, the needle was found to be coated with a very thin film of a white material and only a minute ring of a brown substance had been deposited at a point on the needle where some scoring of the metal surface was apparent i.e. at the point of contact with the valve seat. Insufficient material was available for study but it was obvious that no gelatinous material had been deposited.

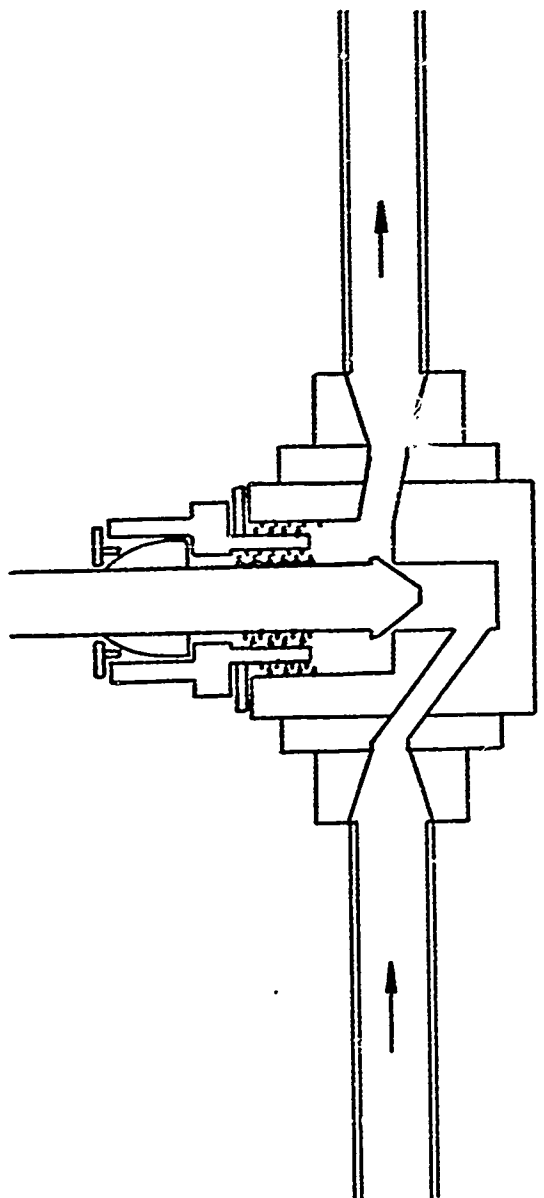
Another 30 runs were performed under similar conditions to those mentioned above. After these, the test section was dismantled and the main deposit on the valve needle was again a white plastic material. Although insufficient of this was available for infra-red spectroscopy it was apparent that the material was Teflon in the form of shavings from the valve packing. A small ring of an off-white substance was observed on the needle seat and this was examined by infra-red spectroscopy. The spectrum was of poor quality because of the small quantity of solid available but bands assignable to the $\text{Fe}(\text{NO}_3)_4^-$ ion were clearly visible. The N_2O_4 used was found by ¹H n.m.r. (see Appendix 1) to contain 0.12% "water".

In order to remove the contamination of the system by Teflon and assist the deposition of flow-decay compound a new mild steel test section was designed. This was a needle valve (Figure 8.4) with a packing of harder Teflon, which also incorporated a needle of larger cross-sectional area than that used previously. The valve needle was lightly abraded before assembly to provide a "key" for the deposition of flow-decay compound.

b) Mild steel needle valve test section

The hold tank was replenished with fresh N_2O_4 which

Figure 8.4.
Test Section Valve
(mild steel)



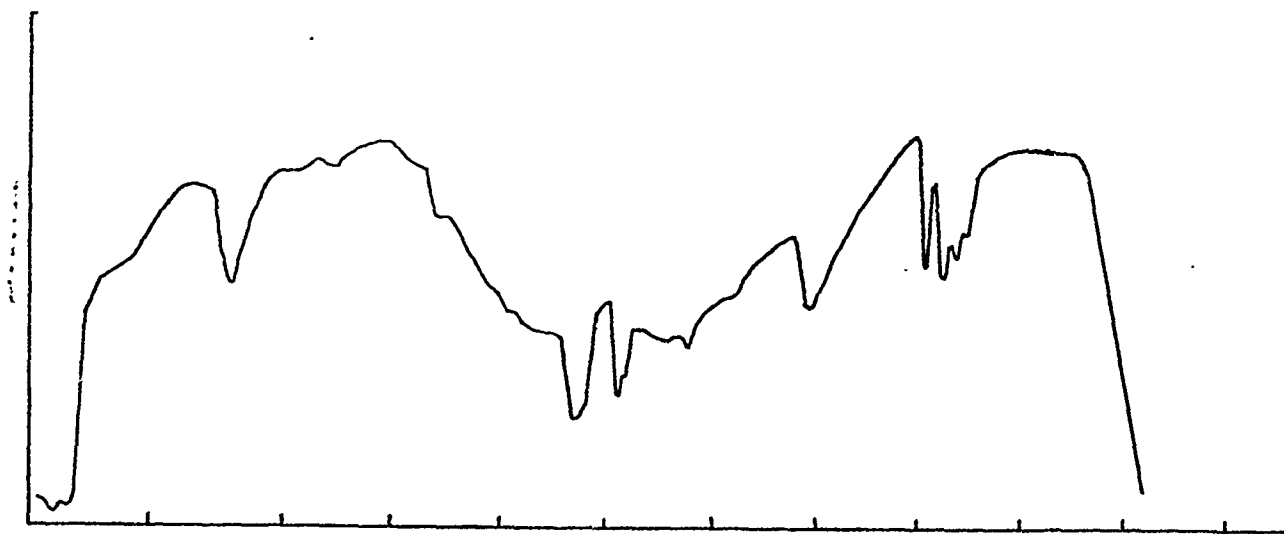
was conditioned at 35° for two days. At the beginning of this new series of experiments the conditions were as follows:-

	Pressure (psi)	Temperature °C
Hold tank	39	35
Catch tank	4	
Heat exchanger		11.3

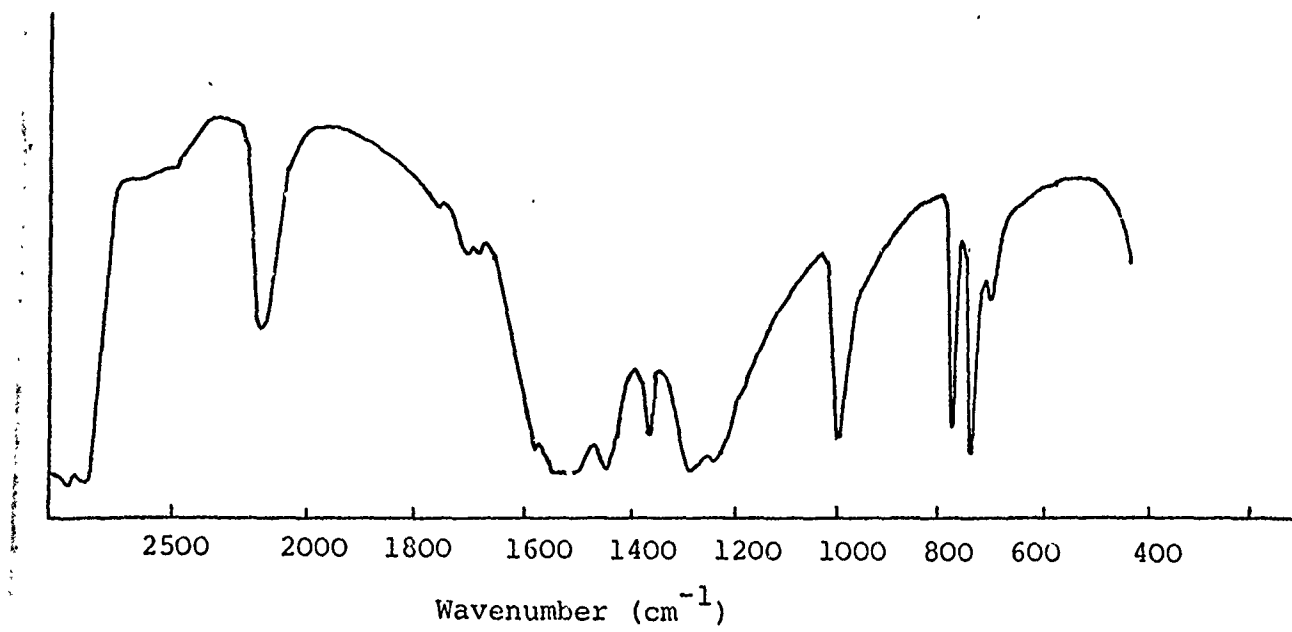
Under these conditions a rapid (full-scale) decay (from 170 ml min⁻¹ to 40 ml min⁻¹) occurred. A total of 68 flow runs were performed and in 52 of these the flow had decayed to 40 ml min⁻¹ within 2½ min. In no case did the full-scale decay process require longer than 8 minutes and the sudden increase in flow observed in a previous experiment (Section 8.4(a)) did not occur.

At the end of this series of flow experiments the test section was drained and flushed as before and removed to a dry box. On dismantling the valve, the originally clean and lustrous valve needle was found to be coated with a brown solid. A ring of a yellow-white solid had accumulated around the needle at the point of contact with the valve body, (Fig. 8.4). It was thought likely, however, that these solids were of identical composition, the yellow form being a more finely divided modification of the brown form. It proved impossible to separate these components, but the infra-red spectrum of the mixed solids was recorded and found to be identical to that of $\text{Fe}(\text{NO}_3)_3 \cdot x\text{N}_2\text{O}_4$ (x ca 1.5) (Figure 8.5). Insufficient material was available for X-ray powder photography and a further series of runs was initiated to produce more flow-decay compound. During this further series of experiments an attempt was

Figure 8.5 a) I.R. spectrum (nujol mull) of material isolated from valve needle.



b) I.R. spectrum (nujol mull) of $\text{Fe}(\text{NO}_3)_3 \cdot 1.5\text{N}_2\text{O}_4$



made to establish the dependence of flow-decay upon temperature. These runs were divided into seven groups, using conditions outlined in Table 8.1.

Flow series 1

Prior to the initial run of this series the heater in the hold tank was switched off, allowing the temperature of the tank to fall. During early runs when ΔT was still close to 10°C , the time for "full-scale decay" was ca $2\frac{1}{2}$ minutes but as ΔT fell to 3° this time increased to ca 7 minutes. Graphs of flow rate against time were plotted and some of these are illustrated in Figure 8.6.

Flow series 2

After series 1 the N_2O_4 was returned to the hold tank where it was re-conditioned for 15 hrs. at 35°C . The heat exchanger was held at a temperature of 29° whilst the hold tank was again allowed to cool down. Results were essentially similar to those of the previous series although it was interesting to note that the flow rate decayed slowly even at zero temperature differential.

Flow series 3

30 runs were completed in this series, under conditions known to produce rapid flow decay, in order to accumulate flow decay material on the valve needle, thereby removing as much as possible of this from the N_2O_4 .

Flow series 4

The N_2O_4 used in the previous series was re-conditioned for $19\frac{1}{2}$ hrs. and a further 20 runs were completed. During these runs the time for "full-scale decay" varied somewhat

TABLE 8.1

Conditions used for flow experiments with mild steel needle valve test section

Series	N ₂ O ₄ conditioning time (hr.)	Pressure differential (psi)	Hold tank temp. °C Initially	Hold tank temp. °C Finally	Heat exchanger temp. °C Finally
1	164	35	35.0	28.0	25.2
2	1.5	31	35.0	29.5	29.0
3	93	33	35.0	35.0	11.5
4	19.5	32	35.0	35.0	11.1
5	0	38	33.0	35.0	11.5
6	21	33	23.0	23.0	10.0
7	97.5	38	35.0	35.0	-5.2
					15.1

Figure 8.6

Mild Steel Needle Valve

H_2O content $0.12 \pm 0.01\%$

Flow Series 1

Pressure

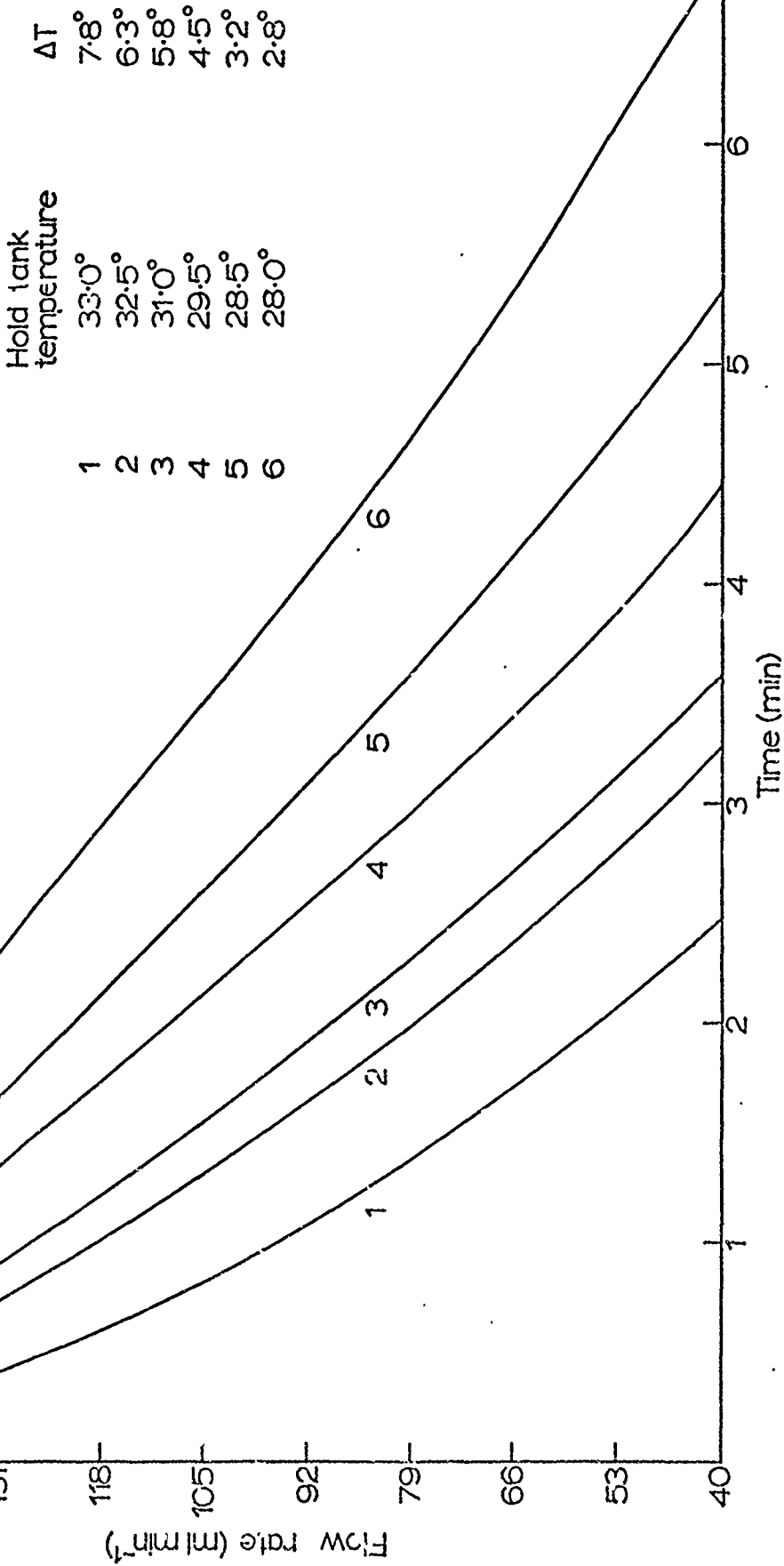
39 psi

Hold tank

Catch tank

Flow rate (ml min^{-1})

- 121 -



erratically. Although this could be interpreted in terms of rapid re-conditioning but poor mixing within the hold tank, such a conclusion would be contrary to the findings of Series 2 where the N_2O_4 was conditioned for only 15 hrs. and erratic behaviour was not observed.

Flow series 5

After series 4, the N_2O_4 was returned to the hold tank and a new series of flow runs was commenced immediately. The time for "full-scale decay" was long at the start of this series (170 to 40 ml min^{-1} in ca 20 minutes) but became appreciably shorter (ca 4 min.) in later runs. This behaviour is illustrated in Figure 8.7, which provides evidence for the rapid restoration of iron content of N_2O_4 at 33° (ca 1 hr.).

Flow series 6

The N_2O_4 was conditioned for 21 hrs. at 35° and then cooled to room temperature (23°). The temperature of the heat exchanger was increased from ca 10° to ca 20° in 5° steps. Flow decay was very slow under these conditions and had almost stopped when the heat exchanger temperature had reached 20° .

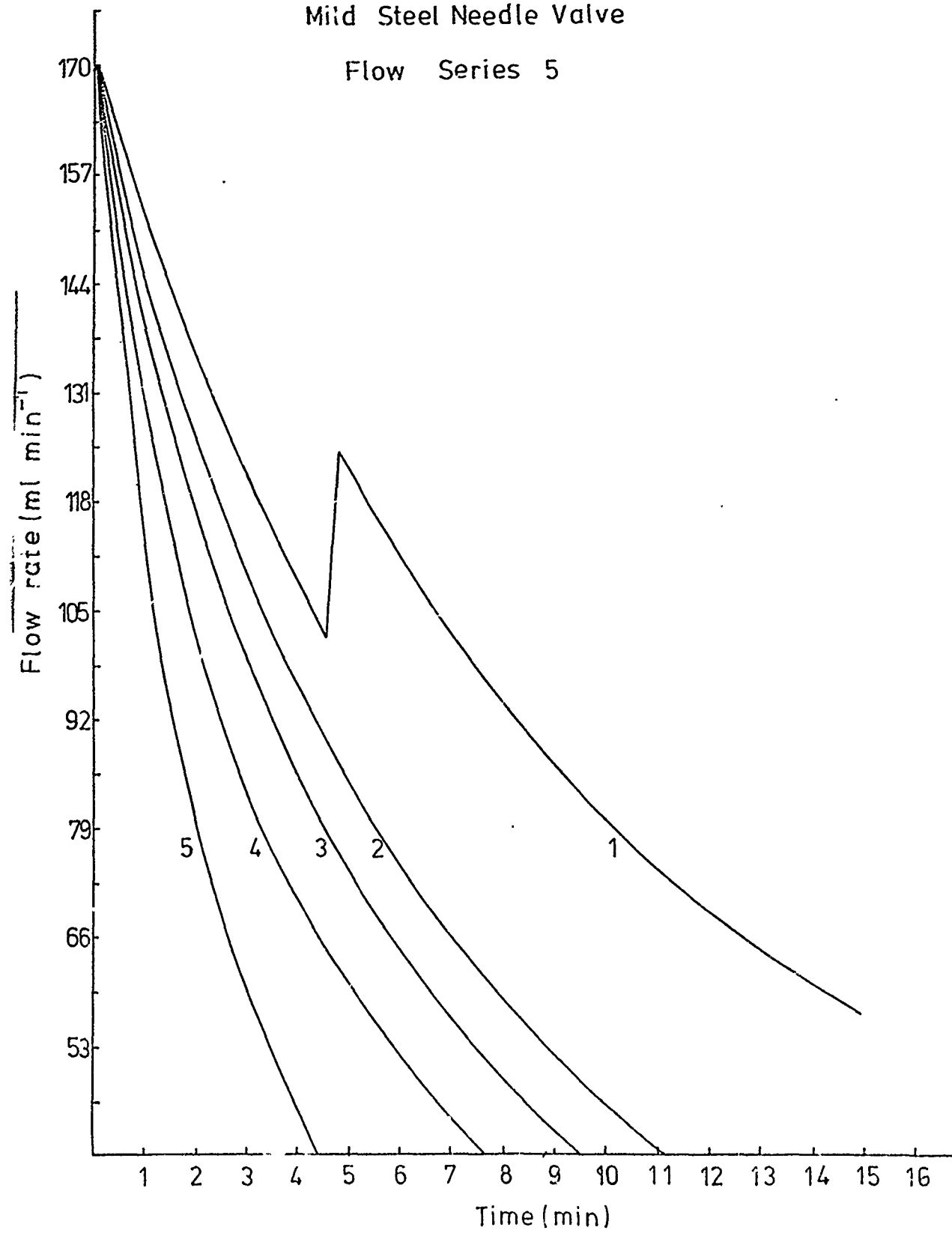
Flow series 7

The hold tank was again held at 35° and the temperature of the heat exchanger was raised in 5° steps from -5° to $+15^\circ$ during the course of the series. At low heat exchanger temperatures (-5°) the decrease in flow rate was relatively slow, possibly due to premature deposition of flow decay compound in parts of the system other than the needle valve (e.g. in the heat exchanger).

Figure 8.7

Mild Steel Needle Valve

Flow Series 5



At $+5^{\circ}$ and $+10^{\circ}$ flow rate decreased more rapidly, then again more slowly as the temperature was raised to $+15^{\circ}$. After this series of flow experiments the test section was drained and flushed with dry nitrogen and transferred to a dry box. On dismantling the valve, a distinct ring of a yellow solid was observed on the needle, together with a corresponding ring on the valve seat. After removal and collection of this small amount of solid, it was evident that once again there was insufficient to allow both infra-red and X-ray examination. The solid was therefore examined by X-ray powder diffraction, since the earlier sample from the same needle valve had been investigated using infra-red spectroscopy. The film obtained was measured and d-values calculated. These values are presented in Table 8.2 together with d-values for $\text{Fe}(\text{NO}_3)_3 \cdot 1.5\text{N}_2\text{O}_4$, $\text{Fe}(\text{NO}_3)_3 \cdot 2\text{H}_2\text{O}$ and also the solid isolated by previous workers¹ from their flow apparatus. On inspection of the data (Table 8.2) it can be seen that the powder pattern of the flow decay material is virtually identical with that of $\text{Fe}(\text{NO}_3)_3 \cdot 1.5\text{N}_2\text{O}_4$ with the exception of a small number of lines which increase in intensity with time. These lines can be assigned with confidence to the compound $\text{Fe}(\text{NO}_3)_3 \cdot 2\text{H}_2\text{O}$ by comparison with those for a synthetic sample prepared from anhydrous FeCl_3 and 100% HNO_3 ²⁴. This hydrate is evidently produced slowly due to imperfect sealing of the X-ray tube. It is also worthy of note that an X-ray powder photograph obtained by previous workers¹ for their flow decay compound is very similar to that obtained in these experiments.

8.5 Summary of results

1. No flow-decay was observed using gauze filter test sections (100 mesh).

TABLE 8.2.

d-spacings (Å) of flow-decay compound compared with those of
 $\text{Fe}(\text{NO}_3)_3 \cdot 1.5\text{H}_2\text{O}_4$, $\text{Fe}(\text{NO}_3)_3 \cdot 2\text{H}_2\text{O}$ and flow-decay compound isolated by
Rocketdyne workers¹.

Flow-decay compound (present work)	$\text{Fe}(\text{NO}_3)_3 \cdot 1.5\text{H}_2\text{O}_4$		$\text{Fe}(\text{NO}_3)_3 \cdot 2\text{H}_2\text{O}^{24}$		Rocketdyne com- pound		
d	I	d	I	d	I	d	I
9.99	2	9.95	5				
9.21	10	9.28	20				
8.11	2	8.23	10				
7.56	50	7.56	40			7.51	s
7.15	80	7.20	70			7.17	vs
6.78	2	6.81	20				
*6.55	50			6.56	80		
6.31	50	6.31	90			6.28	vs
*6.04	50			6.10	80		
5.63	30	5.65	30			5.61	s
5.39	10	5.45	5				
5.14	30	5.20	15			5.16	m
4.90	5	4.86	5				
4.59	100	4.61	100			4.58	v.v.s.
4.41	40	4.42	30				
4.23	40	4.27	30				
*4.09	70	4.10	40	4.08	40		
3.75	50	3.77	60				
3.58	50	3.60	50				
3.44	40	3.44	60				
*3.34	90	3.36	10	3.35	100		
3.27	30	3.28	40				
3.20	20	3.18	30				

* lines observed to increase in intensity with time.

2. No flow-decay was observed using needle valves (mild and stainless steel), without conditioning of N_2O_4 .
3. Flow-decay was observed with both stainless and mild steel needle valve test sections after conditioning N_2O_4 at $35^{\circ}C$.
4. The flow rate decays smoothly with time.
5. As the temperature differential ΔT (T hold tank - T heat exchanger) decreases, so the time for "full-scale decay" increases.
6. Some flow decay is still observed when $\Delta T = 0$.
7. At $35^{\circ}C$, the N_2O_4 re-conditions rapidly (ca 1 hr).
8. Flow-decay compound has been conclusively identified by infra-red spectroscopy and X-ray powder diffraction as $Fe(NO_3)_3 \cdot 1.5N_2O_4$.
9. Optimum conditions for producing flow decay were:

Pressure differential 35 psi

Hold tank temperature $35^{\circ}C$

Heat exchanger temperature $+5^{\circ}$ to $+10^{\circ}C$

9 CORROSION STUDIES BY SCANNING ELECTRON MICROSCOPY

Studies have been carried out on the effects of pure liquid N_2O_4 , and liquid N_2O_4 containing small, known amounts of the most common impurities present in propellant grade N_2O_4 , on mild steel and 316 stainless steel samples. These corrosion studies were conducted in sealed vessels at ambient temperature.

9.1 Experimental

The N_2O_4 used in these experiments was prepared by the thermal decomposition of analytical reagent grade $Pb(NO_3)_2$ and was dried by passage through a column packed with phosphoric oxide. N_2O_4 prepared by this method contains less than 35 p.p.m. $NOCl$ and will hereafter be referred to as 'pure' N_2O_4 .

Metal samples were treated with one of the following reagents A-D:

- (A) pure N_2O_4
- (B) pure N_2O_4 containing $NOCl$, obtained directly from a cylinder (British Drug Houses Laboratory Gas Service) and dried by passage through a column packed with anhydrous $CaCl_2$
- (C) Pure N_2O_4 containing 100% HNO_3 , the latter prepared in the manner described in Section 6.2
- (D) Pure N_2O_4 containing NO obtained from a cylinder (Air Products) and not further purified.

The metal surfaces were prepared by abrasion with emery paper followed by treatment on a polishing wheel, using initially 8 micron, and finally 1 micron diamond paste.

A series of photographs (magnification 2,500) of the polished metal surface of both mild and stainless steel samples were taken to establish a characteristic surface micrograph. A typical mild steel surface was generally featureless except for fine scratch-marks and a large number of small black marks, assumed to be pits in the surface. A typical stainless steel surface appeared to be almost featureless, with only very fine scratch marks and very few pits.

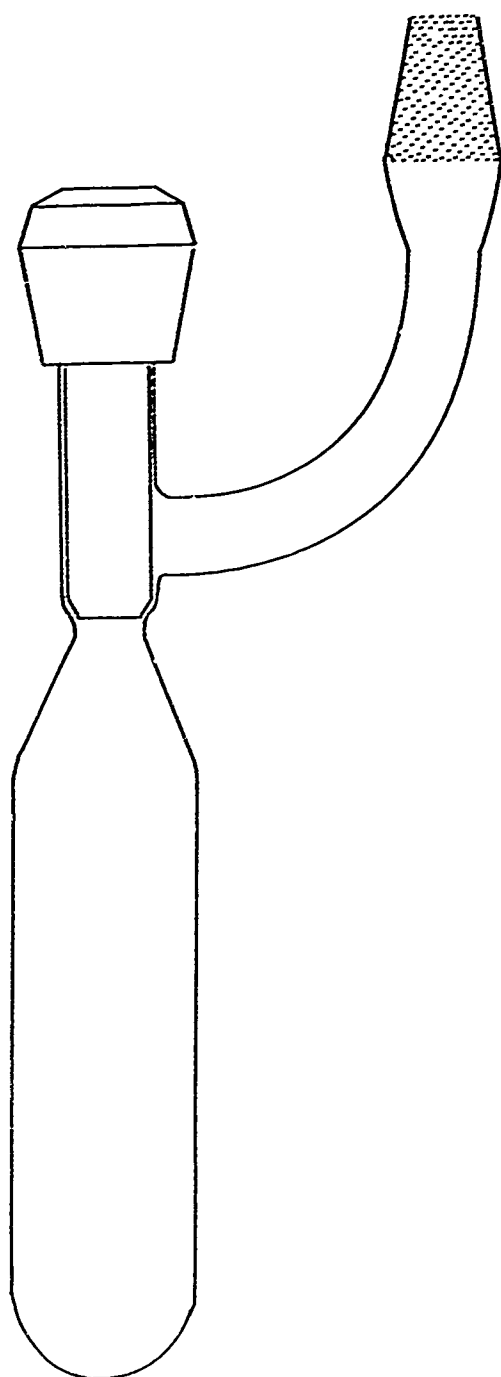
Metal samples were degreased and placed in a specially thickened glass vessel sealed by a PTFE tap (Fig. 9.1). Removal of the PTFE plug allowed the small steel samples of suitable geometry and dimensions for scanning electron microscopy to be inserted through the barrel of this tap.

(A) Pure N₂O₄

About 25 g of pure N₂O₄ was distilled onto each steel sample and the vessels were sealed and left for the requisite period of time.

The N₂O₄ was removed by evacuation and initially the surface of the metal was examined on the Scanning Electron Microscope. On some samples there appeared to be a surface film. It appeared possible that this might be due to a small amount of impurity remaining on the metal surface after evacuation. It was decided that more meaningful results could be obtained by washing any film from the surface, using de-ionised water and analytical reagent grade acetone before microscopic examination. If this film was in fact a reaction product there should be evidence of attack on the surface of the metal, whereas if the film was solely due to impurity the surface of the metal should remain unchanged.

Fig. 9.1. Vessel used in corrosion studies



(B) NOCl in N₂O₄

Solutions of NOCl in N₂O₄ were prepared by distillation of known weights of NOCl and N₂O₄ into the reaction vessels. Concentrations of 5.0, 1.0, 0.4 and 0.1 wt % NOCl were used. The solutions were then frozen in liquid nitrogen and the steel samples were added to the vessels against a counter current of dry nitrogen.

(C) 100% HNO₃ in N₂O₄

Weighed amounts of 100% HNO₃ were pipetted into the reaction vessels in a dry atmosphere and the requisite amounts of N₂O₄ were distilled into the vessels to give 0.1 and 0.4 wt % HNO₃ solutions. These solutions were then frozen in liquid nitrogen and the steel samples were added against a counter current of dry nitrogen.

(D) NO in N₂O₄

5.0, 2.0 and 1.0 wt % solutions of NO were prepared by collection of the calculated volume of gas at 1 atmosphere in a dry bulb of the correct volume, followed by distillation of this gas and the requisite weight of N₂O₄ into the vessel. The steel samples were again added against a counter-current of dry nitrogen.

9.2 Results

(a) Mild Steel

(A) Pure N₂O₄

Pure N₂O₄ had no detectable effect on the surface of mild steel over a period of 24 days.

(B) NOCl in N₂O₄

The mild steel sample in 5% NOCl solution showed

signs of corrosion within 24 hours and after 1 week a heavy deposit of brown powder had formed on the surface (the first sign of attack appeared to be the formation of very small droplets of a second liquid phase, which solidified after 1-2 days). An infrared spectrum of this brown deposit was obtained and all the features expected for $\text{Fe}(\text{NO}_3)_3 \cdot x\text{N}_2\text{O}_4$ were clearly discernable.

The surface of the mild steel sample in 1% NOCl showed tarnishing after 1 day but even after 1 week no deposit was visible to the naked eye. When examined under the scanning electron microscope, however, a deposit was clearly visible and when this was removed by washing the surface of the metal showed clear evidence of attack.

After immersion in solutions containing 0.1 and 0.4 % NOCl for 6 days a small amount of attack was discernible on the mild steel samples when viewed with the scanning electron microscope. The amount of corrosion was comparable in both cases. After only 3 days immersion, attack could not be detected with certainty.

The attack on these mild steel samples appeared to be very localised i.e., there was considerable "pitting". It therefore appears likely that the attack is initiated at the small holes present in the polished surface.

(C) HNO_3 in N_2O_4

The samples were immersed for 24 days. Upon examination by scanning electron microscopy no sample showed any sign of attack.

(D) NO in N₂O₄

The steel samples were immersed for 14 days. Upon examination at the end of this period there were definite signs of corrosion of the mild steel sample which had been in contact with the 5% NO solution. The attack appeared to be more widespread than in the case of the NOCl solutions, and there were very many small pits in the surface.

(b) Stainless Steel

In the parallel series of experiments using stainless steel samples the only sign of attack appeared on the surface of the sample which had been immersed in 5% NOCl for 3 weeks, and even in this experiment the amount of attack was very small.

9.3 Conclusions

I.. It is clear that whenever NOCl is present in N₂O₄ in concentrations > 0.1 wt% there will be attack on any mild steel present in the system, and stainless steel will also be attacked but at a much slower rate.

II. The fact that nitric acid impurity has no corrosive effect is not surprising in view of the essentially covalent nature of the HNO₃ molecule in N₂O₄ solution.

III. The corrosive effect of dissolved NO has particular interest, and could be significant. When a metal reacts with liquid N₂O₄ the first stage is the transfer of electrons from NO⁺ to the metal atom in the metal surface. The second stage involves removal of that metal ion (eg. Feⁿ⁺) so formed, from

the metal lattice into solution. With N_2O_4 this second stage does not occur for the naked ion, which must be coordinated in some way before transfer from the metal surface to solution can take place. Of all the transition metals, iron is the only case in which a simple metal nitrosyl ($Fe(NO)_4$) has been identified and many other complexes are known in which the NO group is coordinated to iron.

- 104 -

stability in contact with N_2O_4 of potential additives for flow decay prevention.

Earlier workers¹ demonstrated that the addition of selected organic solvents to liquid N_2O_4 can substantially overcome flow-decay. They expressed concern, however, as to the desirability of long term contact of the liquid in view of possible reactions between N_2O_4 and these solvents.

To study these long term effects a series of sealed n.m.r. tubes was set up, each tube containing dry liquid N_2O_4 (< 0.01% H_2O) and a distilled organic solvent in the ratio of ca 3:1 v/v. The ¹H n.m.r. spectrum of these mixtures was recorded periodically over nine months, together with the visual appearance. The results are presented in Table 10.1.

The solvents chosen for study were generally those which are known to bring about ready dissolution of $NO^+(Fe(NO_3)_4)^-$.

TABLE 10.1

Organic Solvent	Observations	¹ H n.m.r. spectrum
Ethyl Acetate	a	a
Nitromethane	a	a
Acetonitrile	a	a
Propanediol-1,2-carbonate	c	a
Benzonitrile	c	a
Nitrobenzene	c	b
Sulpholane	c	b
Tictran	d	-
	d	d
Diethyl	d	-
a no change	b slight change over 9 months	
c green colour	d evidence of reaction	

The ^1H n.m.r. spectrum of diethyl ether/ N_2O_4 was not obtained because the sealed tube exploded. On addition of N_2O_4 to 1,4-dioxan, a white solid phase formed. This solid was stable in contact with N_2O_4 but dissolved on agitation. The resulting solution transformed to a gel on standing at room temperature, but became mobile on slight warming. N_2O_4 and 1,4-dioxan are known to form a 1:1 molecular addition compound which is a white crystalline solid⁴¹.

The ^1H n.m.r. spectrum of pure sulpholane shows basically a doublet (with each peak slightly split). The only modification to the ^1H n.m.r. spectrum of sulpholane in N_2O_4 was a slight change in the splitting of the doublet. There was also a solid deposit in the tube, (sulpholane is itself a solid at room temperature).

The ^1H n.m.r. spectrum of nitrobenzene was largely unchanged except for the appearance of a very small peak at about 4.5 p.p.m. downfield of the main signal.

The green colour which developed immediately on mixing propanediol-1,2-carbonate or benzonitrile with N_2O_4 , may have arisen from relatively weak molecular interactions between the components of the mixtures, since the ^1H n.m.r. spectra were unchanged, even after 9 months contact and the solvents had been carefully dried before use.

It is therefore confirmed by ^1H n.m.r. that two of the additives known¹ to be effective in the elimination of flow-decay (i.e. acetonitrile and ethyl acetate) are substantially inert to N_2O_4 over long periods of time. Nitromethane has also been shown to fall into this category, contrary to the findings of the Rocketdyne workers¹ who also reported the insolubility

of $\text{NOFe}(\text{NO}_3)_4$ in nitromethane. This again is contrary to observations in these laboratories, where the suitability of nitromethane for the recrystallisation of $\text{NOFe}(\text{NO}_3)_4$ was investigated (Section 2.1(d)) .

APPENDIX

Determination of the "water" content of liquid N₂O₄ by ¹H n.m.r.

At the commencement of the present research program, the necessity for a rapid and convenient method of determining the "water" content of samples of liquid N₂O₄ used in the flow apparatus and in other laboratory investigations was immediately recognised. The use of proton n.m.r. for this purpose has been reported previously^{39,40}. Initial experiments in these laboratories were conducted using a Varian HA100 (100 MHz) n.m.r. spectrometer, on account of its higher sensitivity than the 60 MHz Perkin-Elmer R.10 spectrometer, also available in this Department. However, it is necessary with the 100 MHz instrument to incorporate with the sample a standard proton containing material to provide a suitable locking signal. Benzene and chloroform (dissolved in the N₂O₄) were tried as internal standards, and tetramethylsilane as an external standard (i.e. not dissolved in the N₂O₄, but placed in the sample tube in a small glass capillary). However, none of these was entirely satisfactory; benzene because of nitration (and hence increase in proton content of the N₂O₄) in samples with high "water" content; chloroform because of the proximity of the "water" and chloroform resonances, which produced attendant difficulties in locking and integration of signals, and tetramethyl silane because of the diminution of the sample volume (and hence "water" signal) by displacement insertion of the glass capillary. For these reasons, subsequent estimations were carried out on the Perkin-Elmer R10 (60 MHz) spectrometer, which operates in a non-locked mode, and hence needs no reference standard.

A series of calibration standards was prepared from small weighed amounts of water (5 figure balance) and weighed amounts of dry N_2O_4 (distilled from phosphoric oxide). N.m.r. samples in 0.7 mm wall-thickness soda glass tubes were frozen in liquid N_2 , evacuated and sealed. These tubes were found to be quite safe under the conditions used; each sealed sample was heated to $40^{\circ}C$ before estimation (n.m.r. probe temperature $31^{\circ}C$), but no tube exploded. Within experimental error a linear calibration graph of signal integral against % "water" content was obtained. N_2O_4 distilled from phosphoric oxide was shown in this manner to have a very low "water" content which was difficult to measure accurately, but was certainly less than 0.01%. N_2O_4 distilled in this way is described throughout this report as "dry N_2O_4 ".

REFERENCES

1. Methods for elimination of corrosion products of nitrogen tetroxide, Rocketdyne, Final Report AFRPL-TR-67-277, (July 1967).
2. Investigation of the formation and behaviour of clogging material in earth and space storable propellants, TRW, Interim Report 08113-5007-RO00, (October 1967).
3. Engineering parameters study of nitrogen tetroxide flow decay, Rocketdyne, Final Report AFRPL-TR-72-38 (June 1972).
4. Addison, C. C., Boorman, P. M. and Logan, N., J. Chem. Soc., 4978 (1965).
5. Addison, C. C., Johnson, B. F. G. and Logan, N., J. Chem. Soc., 4490 (1965).
6. Addison, C. C., Hathaway, B. J. and Logan, N., Proc. Chem. Soc., 51 (1958).
7. Sudborough, J. J., J. Chem. Soc., 655 (1891); Partington, J. R. and Whynes, A. L., J. Chem. Soc., 1952 (1948); 3135 (1949).
8. Addison, C. C. and Lewis, J., J. Chem. Soc., 2843 (1951).
9. King, T. J., Logan, N., Morris, A. and Wallwork, S. C., Chem. Comm., 554 (1971).
10. Addison, C. C., Logan, N., Wallwork, S. C. and Garner C. D., Quart. Revs., 25, 289 (1971).
11. Morris, A., Ph.D. thesis, Nottingham, 1970.
12. Snyder, R. G. and Hisatsune, I. C., J. Mol. Spectroscopy 57, 139 (1957).
13. Addison, C. C. and Conduit, C. P., J. Chem. Soc., 1390 (1952).
14. Addison, C. C., Hodge, N. and Sheldon, J. C., Chem. and Ind., 133 (1953).
15. Flow decay, University of Nottingham, U.K., Department of Chemistry, Annual Scientific Report, (June 1971).
16. Coulden, J. D. S. and Millen, D. J., J. Chem. Soc., 2620 (1950).

17. Goulden, J. D. S., Millen, D. J. and Ingold, C. K., *Nature*, 165, 565 (1950).
18. Burg, A. B. and McKenzie, D. E., *J. Amer. Chem. Soc.*, 74, 3143 (1952).
19. Giauque, W. F. and Kemp, J. D., *J. Chem. Phys.*, 6, 40 (1938).
20. Verhoek, F. H. and Daniels, F., *J. Amer. Chem. Soc.*, 53, 1250 (1931).
21. Vosper, A. J., *J. Chem. Soc. (A)*, 625 (1970).
22. Addison, C. C., Boorman, P. M. and Logan, N., *J. Chem. Soc.*, 5146 (1965).
23. Millen, D. J. and Watson, D., *J. Chem. Soc.*, 1369 (1957).
24. Hathaway, B. J. and Underhill, A. E., *J. Chem. Soc.*, 648 (1960).
25. Burg, A. B. and Campbell, D. E., *J. Amer. Chem. Soc.*, 70, 1964 (1948).
26. Addison, C. C. and Lewis, J., *Quart Rev.* IX, 115 (1955).
27. Woodward, L. A. and Taylor M. J., *J. Chem. Soc.*, 3557 (1963).
28. Landau, L and Fletcher, W. H., *J. Mol. Spec.* 4, 276 (1960).
29. Hisatsune, I. C. and Devlin, J. P., *Spectrochim. Acta*. 16, 401 (1960).
30. King, T. J., Logan, N., Morris, A. and Wallwork, S. C., *Chem. Comm.*, 554 (1971).
31. Lee, W. H., "Nitric Acid", Chapter 4, The Chemistry of Non-Aqueous Solvents, Volume 2, Academic Press, New York (1967), p. 159.
32. Addison, C. C., Brownlee, G. S., and Logan, N., *J. Chem. Soc. (Dalton)* 1440 (1972).
33. Marcus, R. A. and Fresco, J. M., *J. Chem. Phys.*, 27, 564 (1957).
34. Ingold, C. K. and Millen, D. J., *J. Chem. Soc.*, 2612 (1950).

35. Klemenc, A. and Speiss, T., *Monatsch*, 77, 216 (1947).
36. Corcoran, W. H., Reamer, H. H. and Sage, B. H., *Ind. Eng. Chem.*, 46, 2541 (1954).
37. Addison, C. C., Gamlan, R. and Thompson, R., *J. Chem. Soc.*, 338 (1952).
38. Advanced Valve Technology for Spacecraft Engines,
Space Technology Laboratories, Inc., Final Report
8651-6016-RU-000 (March 1967).
39. Sutton, N. V., Dubb, H. E., Bell, R. E., Lysyj, I.
and Neale, B. C., *Adv. Chem. Series. (Amer. Chem. Soc.)*,
54, 231 (1966).
40. Ward, G. A., *International Laboratory*, 1, 72 (1971).
41. Rubin, B., Sisler, H. H. and Schechter, H., *J. Amer. Chem. Soc.*, 74, 877 (1952).
42. Sharp, D. W. A. and Thorley, J., *J. Chem. Soc.*, 3557 (1963).